LATE PLEISTOCENE PALEOENVIRONMENTAL CHANGES IN THE LOWER NEUSE RIVER BASIN, NORTH CAROLINA, AND IMPLICATIONS FOR RELATIVE SEA LEVEL AND COASTAL EVOLUTION

by:

Jessica Lynn King

August 2024

Directors of Thesis: Dr. D.J. Mallinson and Dr. S.J. Culver

Department: Geological Sciences

Abstract

The coastal plain of eastern North Carolina evolved through the changes associated with late Pleistocene rapid relative sea-level oscillations during Marine Isotope Stages 5 to 2. The sea-level highstand deposits of MIS 5 and MIS 3 have been previously studied in eastern North Carolina; however, certain regions have had little to no data collected, which makes determining the areal extent of facies and associated depositional environments challenging. To overcome these limitations and better understand the spatial and temporal variation of sea-level fluctuations, geophysical and geological data from the lower Neuse River Basin have been analyzed. These data reveal the presence of multiple paleoenvironments with distinctive sequences corresponding to MIS 5e, MIS 5a, and MIS 4. The chronological framework, determined using optically stimulated luminescence dating, provides sediment age estimates ranging from 123.5 (± 7.2) ka to > 56.8 (± 4.1) ka. DS-5e is composed of eastward thickening shelly sand lithofacies. This sequence contains two distinct foraminiferal assemblages. Samples dominated by *Elphidium excavatum, Ammonia parkinsoniana,* and *Elphidium mexicanum* are

overlain by samples also containing *Buccella inusitata, Nonionella atlantica,* and *Rosalina* sp. Additionally, pollen samples collected within DS-5e show a trend of cooler conditions in the lowermost sample of the core to likely warmer than modern conditions in the uppermost collected sample. This transition from low to higher diversity foraminifera assemblages, warming climate conditions, and shelly marine deposits is indicative of a transgressive environment, interpreted as a high salinity estuary becoming an inner shelf environment. DS-5a is characterized by burrowed laminated sand, as well as sandy mud and is barren of foraminifera, with the exception of one sample. Lithofacies show an upward-fining succession transitioning from flaser to wavy tidal bedding. One pollen sample from DS-5a suggests conditions ranging from modern to slightly warmer than present. With apparent tidal bedding, the absence of foraminifera, and warm climate conditions DS-5a is potentially indicative of coastal tidal flat deposits. The lithofacies of DS-4 are characterized by medium to fine-grained burrowed laminated sand and sandy mud, with all samples being barren of foraminifera. Regression during MIS 4 likely exposed sediment from a shallow marine shoal in cores south of the river, where aeolian forces likely reworked the sand into dunes. Comparing these facies across the Neuse River Basin with similar studies in the region offers valuable insights into how coastal North Carolina's geomorphology responded to changes in relative sea-level during the late Pleistocene.

LATE PLEISTOCENE PALEOENVIRONMENTAL CHANGES IN THE LOWER NEUSE RIVER BASIN, NORTH CAROLINA, AND IMPLICATIONS FOR RELATIVE SEA LEVEL AND COASTAL EVOLUTION

A Thesis

Presented to

The Faculty of the Department of Geological Sciences

East Carolina University

In Partial Fulfillment

of the Requirements for the Degree

Master of Science

by

Jessica King

2024

Acknowledgments

I would like to express my heartfelt gratitude to my family and friends for their unwavering support throughout this journey. I am deeply thankful to my advisors for their guidance and numerous revisions. Special thanks to my committee members, Drs. R. DeWitt and E. Leorri, for their assistance and advice. I am also grateful to Scott Rose, Cody Brown, Collin Earls, and Eric Teabo for their help in the field. A sincere thank you to Debra Willard from the USGS for analyzing my pollen samples. Lastly, I would like to thank the NSF grant (OCE-1841835) and the Department of Geological Sciences at ECU for providing the funding for this research.

Table of Contents

List of Tables

List of Figures

LiDAR map (D). The lower stratigraphic cross-section (B) displays interpreted lithofacies, depositional sequences, and OSL ages. Panel (C) highlights the locations of two OSL samples and their sediment characteristics. From Parham et al. (2013).

Figure 26. Adapted from Scott (2010), an estimated glacioisostatic curve is depicted alongside the δ18O SPECMAP composite and eustatic sea-level curves from the Huon Peninsula in Papua New Guinea. Forebulge subsidence during MIS-5 and extending into MIS-3 likely facilitated shoreline deposition in Virginia during MIS-3.

Figure 27. A shaded relief map depicting terraces and paleoshoreline positions in southeastern Virginia and northeastern North Carolina, adapted from Parham et al. (2009).

Figure 28. Generalized model of two fundamental types of depositional coasts. Panel A illustrates wave-dominated coasts, typically microtidal with a tidal range less than 6 feet, exemplified by the modern North Carolina Coast. Panel B represents mixed-energy coasts, usually mesotidal with a tidal range of 6-12 feet, showcasing the modern Georgia Coastline. In Panel A, red lines denote nearshore, subtidal wave-formed sand bars, while in Panel B, they indicate sand deposits.

LATE PLEISTOCENE PALEOENVIRONMENTAL CHANGES IN THE LOWER NEUSE RIVER BASIN, NORTH CAROLINA, AND IMPLICATIONS FOR COASTAL EVOLUTION

1.0 Introduction

Coastal areas around the world are experiencing high rates of erosion and inundation which impact their increasing human population, economic investments, and infrastructure. Global sea-level rise is accelerating and is projected to rise 0.5 meters to 1.0 meters above 1900 levels by 2100 (IPCC, 2023). Along the world's open ocean coasts, there are more than 20,000 km of barrier islands with associated back barrier estuaries or lagoons (Stutz and Pilkey, 2011). These low-gradient coastal systems are especially susceptible to the effects of sea-level change. Thus, it is important to have a clear understanding of the potential rates and magnitudes of sea-level rise that will affect coastal systems globally.

In coastal environments, the relationship between oceanic and geologic processes is dynamic and complex. Many factors affect how a low gradient coastal system will be influenced by sea-level rise. Storm activity, glacio-isostatic adjustments (GIA), sediment flux, sea-level rise rate, and antecedent topography are regional factors that complicate the understanding of how coastlines will be impacted by sea-level rise (Komar, 1998; Mallinson et al., 2008; Scott et al., 2009; Zaremba, 2016). Sea-level rise has been shown to increase the erosion rate of coastal geomorphology and affect the hydrologic characteristics (salinity distribution and hydrologic stratification) of barrier islands and their adjacent estuarine systems (Grand Pre et al., 2011; Chua and Ming, 2014; Masterson et al., 2014; Zaremba et al., 2016; Shmorhun et al., 2022).

Due to its large areal extent and the variety of its geologic, geomorphic, hydrodynamic and biologic characteristics, the Albemarle–Pamlico estuarine system (APES) of eastern North Carolina is an ideal environment to investigate low gradient coastal responses to sea-level rise.

The dynamic interactions between coastal processes and adjacent mainland areas are recorded within the well-preserved Quaternary stratigraphic record of sediment cores from the Albemarle-Pamlico estuarine system (Culver et al., 2008; Mallinson et al., 2008; Grand Pre et al., 2011; Parham et al., 2013). Specifically, the late Pleistocene had multiple episodes of rapid sea-level rise and fall that occurred during Marine Isotope Stage 5 (MIS 5; 130 to 71 ka) and Marine Isotope Stage 3 (MIS 3; 55 to 29 ka*).* Previous research (Culver et al., 2008; Culver et al., 2016; Mallinson et al., 2005; Mallinson et al., 2008; Parham et al., 2013, Gudmunson, 2022) suggests that future transgressions associated with projected sea-level rise may be comparable to transgressions during the late Pleistocene. To make accurate predictions about how this low gradient coastal system will respond to future sea-level rise, it is important to define the geological framework and represented paleoenvironments of late Pleistocene deposits.

1.1 Objectives

This study's purpose is to understand the evolution of a low gradient coastal system in response to rapid sea-level change. Since the coast of North Carolina has been inundated multiple times throughout the Quaternary, deposits from previous highstands can be analyzed to address this objective. Specific objectives are:

1. To use geophysical data and cores to define and characterize the stratigraphy and facies (litho-, bio-, geophysical).
2. To use optically stimulated luminescence (OSL) to place age constraints on the deposits using siliciclastic sediments from the cores to establish geochronology.
3. To correlate facies, stratigraphic surfaces, and depositional environments for early and late MIS 5 and MIS 3 units.

1.2 Study Area

The study area for this project, the Lower Neuse River Basin, is located on a ~90 m thick wedge of well-preserved Quaternary sediments (Riggs et al., 1992; Mallinson et al., 2005; Mallinson et al., 2010; Culver et al., 2011). The Suffolk Shoreline, a paleoshoreline feature formed during the highstand of MIS 5 (Mallinson et al., 2008; Scott et al., 2010; Parham et al. 2013) intersects the Neuse River (Figure 1). The Lower Neuse River Basin is an ideal study area to investigate paleo sea-level cycles because of its well-preserved stratigraphic record and proximity to the Suffolk Shoreline.

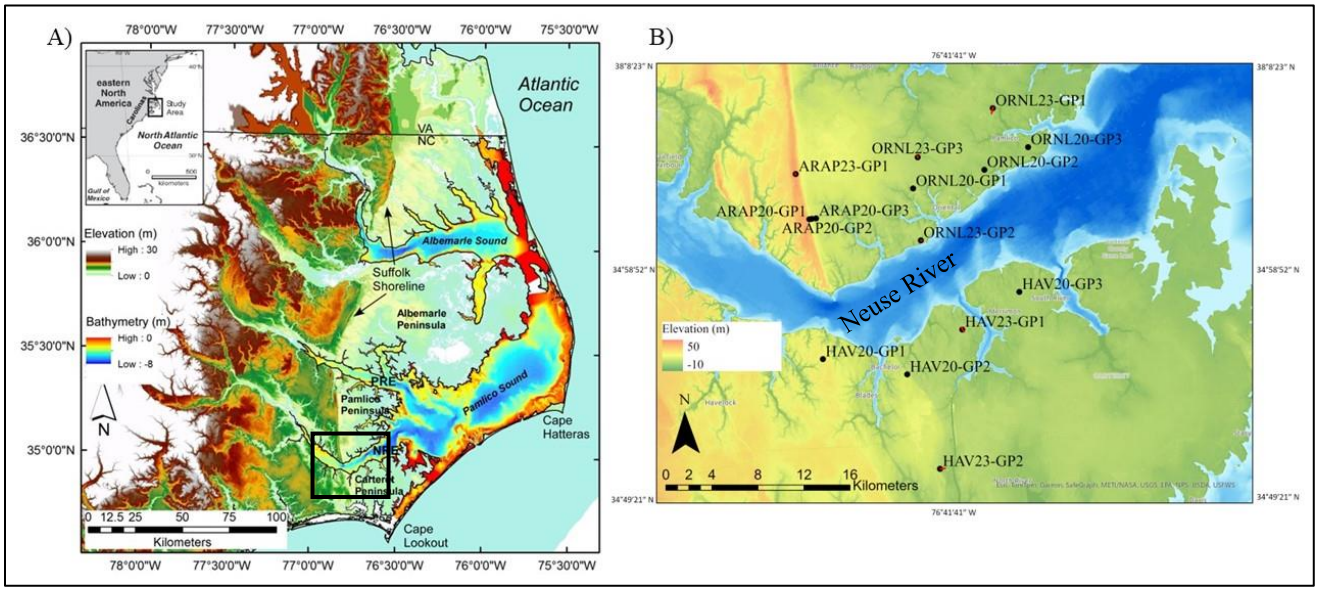

Figure 2. A) LiDAR map showing topography of eastern North Carolina (North Carolina Spatial Data Download). The Suffolk Shoreline is expressed as a prominent topographic break. The black box represents the study area. B) LiDAR map of the study area. The black circles represent Geoprobe core locations.

1.2.1 Geologic Setting

The coast of North Carolina is characterized as a microtidal, wave energy-dominated, low gradient coastal system (Mallinson et al., 2008). The study area lies within the Albemarle

Embayment. This Cenozoic basin-like feature contains dipping and seaward-thickening Neogene and Quaternary strata (Ward and Strickland, 1985; Riggs et al., 1992). Records of sea-level fluctuations during the Quaternary can be found in the depositional sequences located within the top 85 meters of sediments within the Albemarle Embayment (Riggs et al., 1992; Mallinson et al., 2005; Parham et al., 2007; Mallinson et al., 2010).

The alternating glacial and interglacial periods in Earth's Quaternary climate history are represented by marine isotope stages. Odd numbered stages are interglacials, which are warm periods of glacial retreat, and even numbered stages are glacials, or cool periods of glacial advance (Emiliani, 1955). MIS 1 (Marine Isotope Stage 1) corresponds to the Holocene interglacial, which started at 11.7 ka and is still ongoing today. Marine isotope stages are determined using oxygen isotope data taken from benthic foraminifera in deep sea cores (Lisiecki and Raymo, 2005; Siddal, 2008). The cyclical waxing and waning of global ice volume over long periods is influenced by Milankovitch cycles, which affect summer insolation at 65 degrees latitude, where the large northern hemisphere ice sheets are located (Siddal et al., 2008). When global ice volume decreases, global sea levels rise, and conversely, when global ice volume increases, eustatic sea levels fall. Milankovitch cycles are caused by variability in orbital eccentricity (400, 125, and 95 ka), axil tilt (41 ka), and precession (24, 22, and 19 ka) (Siddal et al., 2008). Marine isotope stages are divided into smaller substages by oscillations in climate and sea level related to precession (Siddal, 2008).

Eustatic sea level was as much as 6 to 9 m higher than it is today during the MIS 5 interglacial period, which lasted between 130 ka and 71 ka (Chappell et al., 1996). Based on alternating warm and cool periods, MIS 5 is further divided into smaller substages a through e. The roughly north-south paleoshoreline, known as the Suffolk Shoreline (Figure 1), was

deposited during the various MIS 5 highstands forming a topographic high in the coastal plain. Based on the preserved stratigraphy, it is suggested that the shoreline was formed by several highstand events from small-scale sea-level oscillations during MIS 5e, MIS 5c, and MIS 5a (Mallinson et al., 2008; Parham et al., 2013). Deposits collected along the Suffolk Shoreline appear to be tidal estuarine grading up to eolian sands and are part of the Sedgefield Member of the Tabb Formation (Mallinson et al., 2008; Parham et al., 2013).

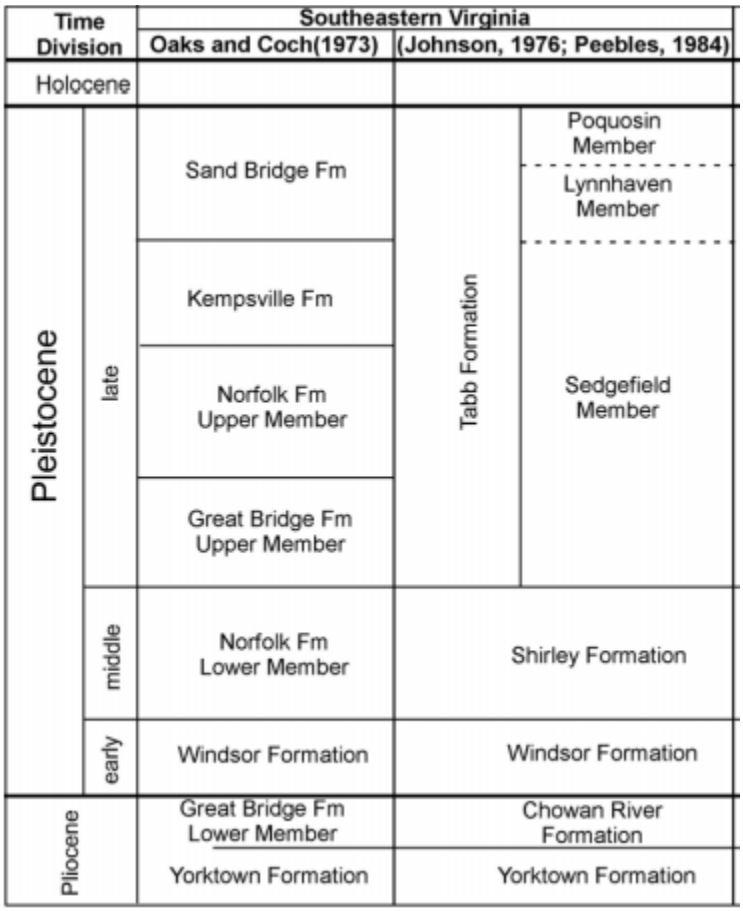

Figure 2. Time intervals and geological formations in southeastern Virginia. From Parham et al. (2013).

MIS 3 occurred between 57 ka and 29 ka (Emiliani, 1955; Lisiecki and Raymo, 2005). Due to significant climate change during MIS 3, sea-level rose quickly, similar to what is

expected in the future (Siddall, 2008). According to Parham et al. (2013), during MIS 3 the shoreline transgressed to meet and partially occupy the Suffolk Shoreline. Located east of the Suffolk Shoreline are the MIS 3 transgressive and highstand deposits. The Land of Promise Ridge and the Lynnhaven Member ridges in northeast North Carolina correspond with the Lynnhaven Member in southeast Virginia (Figure 2). These features, along with the Powell's Point Ridge and Hickory Scarp in northeastern North Carolina were determined through OSL dating to be deposited approximately 60—40 ka, during early MIS 3 (Figure 3) (Mallinson et al., 2008; Scott et al., 2010These deposits reveal a transgressive coastal system characterized by a basal peat layer that grades upward to washover deposits, topped by eolian sands (Mallinson et al., 2008). During MIS 3, eustatic sea level was lower than present day, but the shoreline deposits are -1 to 12 m above the current mean sea level in North Carolina and Virginia (Mallinson et al., 2008; Scott et al., 2010).

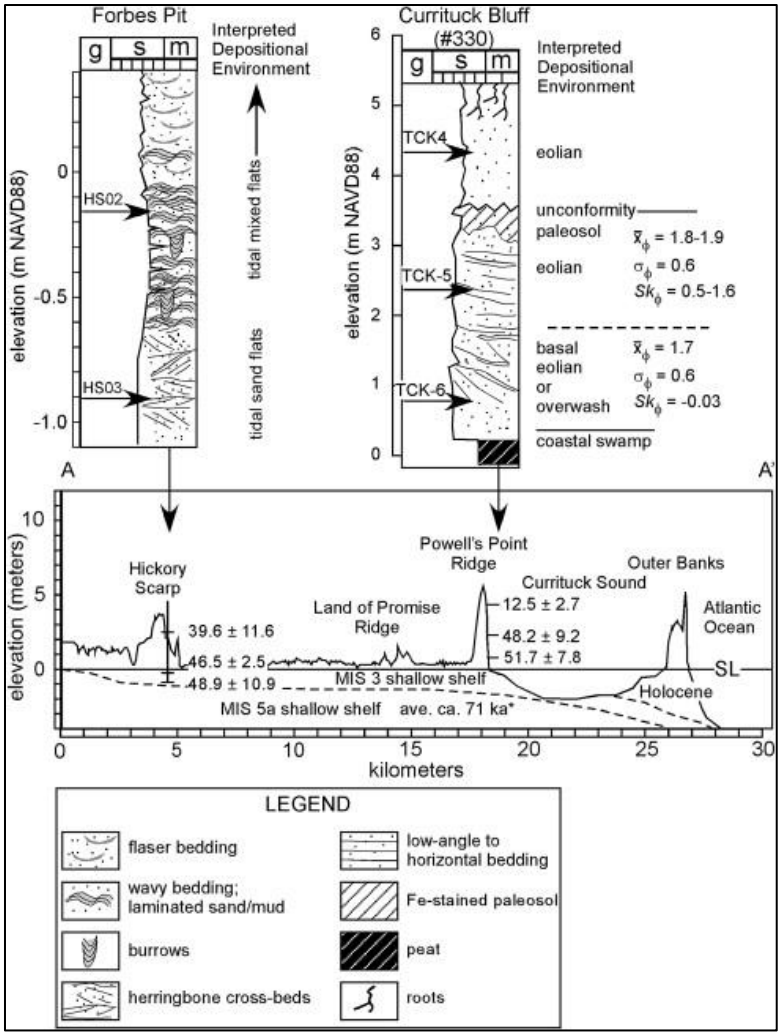

Figure 3. Topographic profile of sampled exposures at both the Hickory Shoreline and Powell's Point Ridge (Mallinson et al., 2008). The profile includes OSL ages for reference. Grain-size statistics (mean, sorting, and skewness) are provided for the Powell's Point site.

Subsidence and glacioisostatic adjustment (GIA) account for this discrepancy. Isostatic conditions across the region reached a state of near equilibrium during MIS 3 following uplift of a glacial forebulge during the MIS 6 glaciation and subsequent subsidence for the majority of MIS 5 (Figure 4) (Potter and Lambeck, 2003; Mallinson et al., 2008; Scott et al., 20010; DeJong et al., 2015). To improve our understanding of North Carolina's coastal response to sea-level

rise and GIA, a more complete understanding of the dates and elevations of Pleistocene deposits are needed. Currently, there is a gap in the research, as there are no data collected along the Neuse River where it intersects the Suffolk Shoreline. This investigation is intended to fill that data gap.

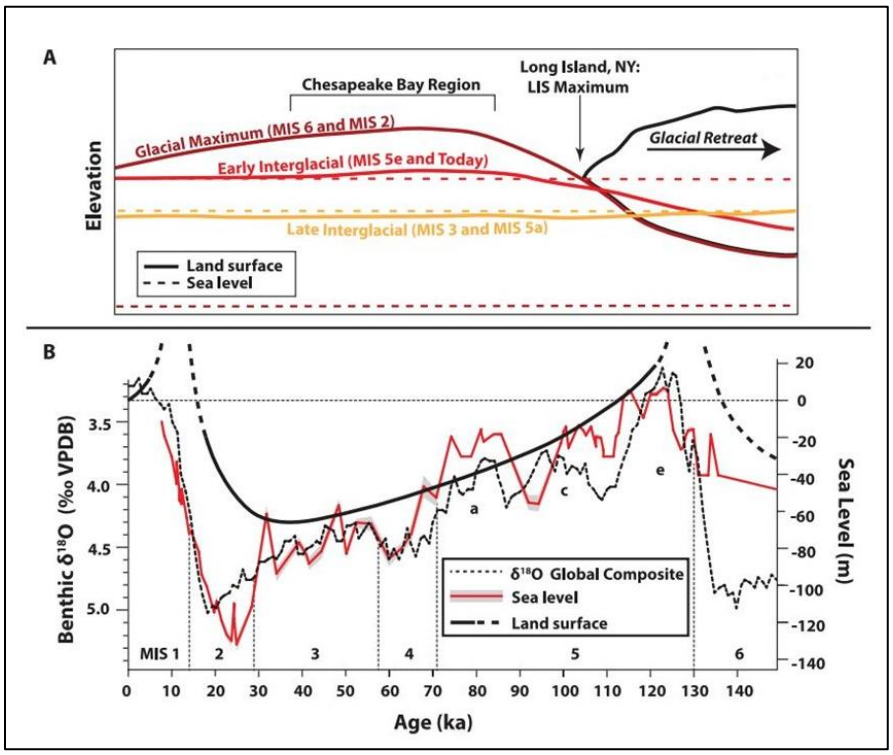

Figure 4. A) Cross section illustrating how the land surface relates to the changing sea level at specific points in glacial cycles based on the distance from the Laurentide ice sheet. B) Oxygen isotope and sea-level data spanning the past 150,000 years. The glacioisostatic curve illustrates land surface changes based on ages of shoreline deposits in the mid-Atlantic region. This curve demonstrates how adjustments in land-surface elevation due to glacio-hydro-isostatic processes could lead to the submergence of the Chesapeake Bay region during periods of significantly lower eustatic sea levels. VPDB refers to Vienna Pee Dee Belemnite. Adapted from DeJong et al. (2015).

2.0 Methods

2.1 Core collection and analysis

Fifteen Geoprobe core samples were collected in Pamlico, Craven, and Carteret County. Core collection sites were based on geophysical data and accessibility. The latitude, longitude and elevation relative to NAVD88 of each core were recorded. All cores were photographed and graphically logged following the methods outlined by Farrell et al. (2013). Cores were sampled for foraminiferal analysis, sediment grain-size analysis, and optically stimulated luminescence dating (OSL).

2.2 Grain-Size Analysis

Sediment samples were collected from the cores and dried for 24 hours. The dry weight of each sample was recorded. Muddy samples were disaggregated in sodium hexametaphosphate, then placed in a sonicator for 15 minutes. The samples were washed over a 63 µm sieve and dried at 60^{o} C; the dry weight was recorded. Based on the weight difference before and after sieving, the sand and mud percentages were calculated. Dried samples were processed for 15 minutes in a RO-TAP machine in nested sieve stacks with half-phi sieves ranging from -2 to 4 phi (Folk, 1974). Specific grain-size statistical analysis was performed using GRADISTAT spreadsheet (Blott and Pye, 2001).

2.3 Foraminiferal Analysis

Forty-seven samples from the fifteen cores were processed for foraminifera. The samples were oven-dried, weighed and disaggregated in a weak solution of sodium hydroxide, sodium hexametaphosphate, and water. To remove coarse sand, gravel, clay and silt, samples were washed over 710 µm and 63 µm nested sieves. Where necessary foraminifera in the 63—710 µm

fraction of sediment were separated from quartz grains by floating in sodium polytungstate (Munsterman and Kerstholt, 1996). Approximately 100 foraminifera were picked (using a random numbers table to select specimens) from each sample and identified by comparison with illustrations in the published literature. Modern foraminiferal distribution data in Schniker (1971), Culver and Buzas (1980), Vance et al. (2006), Robinson and McBride (2006), Grand Pre et al. (2011) were used as a basis for identification and defining paleoenvironments represented by cored sediments.

2.4 Palynology (D. Willard, Personal Communication)

Nine sediment samples were isolated for pollen using standard palynological techniques (Willard et al., 2003). To determine percent abundance and pollen concentration, at least 300 pollen grains were counted from each sample. Pollen data were compared to a modern pollen database from marine and estuarine surface samples collected in Mississippi Sound (Edwards and Willard, 2001), Chesapeake Bay (Willard et al., 2003), the western Atlantic Ocean (Litwin and Andrie, 1992, Willard et al., 2005), and the eastern Canada Shelf (Mudie, 1980, Mudie, 1982) to determine paleoenvironmental conditions. Using the modern analogue technique and chord distance (SCD) measure (Overpeck et al., 1985), samples with SCD values ≤ 0.15 were considered to be analogous to modern samples.

2.5 Optically Stimulated Luminescence Dating

Eleven sediment samples were taken from opaque Geoprobe cores and cut under safe (red) light conditions in the ECU Department of Physics OSL laboratory. Samples were removed from the cores in 10 cm sections, avoiding sediment against the core casing. Samples underwent wet sieving to isolate the 90—150 μm fraction used for processing. To dissolve carbonates and organics, the samples underwent a 10% HCl and 29% H_2O_2 bath. Subsequently they were etched

for 40 minutes with 48% HF to remove outer shell of quartz grains (approx. 20 µm) that had been affected by alpha radiation and to dissolve feldspars. Following the completion of chemical treatment, density separation was performed using lithium polytungstate (2.75 and 2.62 g/cm^3) to separate quartz grains from heavier minerals and the lighter feldspars. To determine the equivalent dose (D_e) (Murray and Wintle, 2000; Wintle and Murray, 2006) samples were measured using the single-aliquot regenerative dose (SAR) protocol. High resolution gamma spectrometry was used to determine the activity of uranium, 232Th and potassium in the excess material from each sample to determine the dose rate. OSL ages are calculated by dividing the D_e by the dose rate. OSL ages are reported in years before 2020.

2.6 Ground Penetrating Radar (GPR)

GPR surveys were collected at the coring sites in Pamlico, Craven, and Carteret County, North Carolina using a GSSI SIR-3000 GPR with a 200 MHz antenna. A WAAS-enabled Garmin 76Csx GPS was used to collect waypoint positions. GPR data were filtered, stacked, and gain-enhanced using Radan v. 7 software by Geophysical Survey Systems, Inc. GPR data were interpreted using Canvas X graphics software to define the contacts, characteristics, and geometries of the buried stratigraphic units.

3.0 Results

3.1 Lithofacies Descriptions

Sixteen lithofacies were identified in 15 cores based on observed characteristics and grain size analysis of fifty-six sediment samples (Appendix B). The lithofacies and characteristics are listed in Table 1. The most common lithofacies identified within the cores are muddy sands and sandy muds.

Table 1: Lithofacies and characteristics identified in 15 cores.

Lithofacies	Code	Description and Sedimentary Features
Organic-rich sand	S-org	Fine-grained sand with plant fragments
Burrowed laminated muddy sand	mS-b-lam	Moderately well sorted, fine-grained sand with mud, burrows, and laminations
Burrowed sand	S-b	Moderately to well sorted, fine-grained sand with burrows
Burrowed muddy sand	mS-b	Well to poorly sorted, fine-grained sand with mud and burrows
Sand	S	Well to very well sorted, fine-grained sand
Laminated muddy sand	mS-lam	Moderately well sorted, fine grained sand with mud laminations
Burrowed laminated organic-rich muddy sand	mS-b-lam-org	Fine-grained sand with mud, burrows, plant fragments, and laminations
Organic rich muddy sand	mS-org	Fine-grained sand with mud, plant fragments and shell fragments common
Muddy sand	mS	Well sorted, fine-grained sand with mud
Sandy mud	sM	Mud with moderately to poorly sorted fine-grained sand
Burrowed laminated sandy mud	sM-b-lam	Mud with poorly sorted fine-grained sand, burrows, and laminations
Laminated sandy mud	sM-lam	Mud with moderately sorted, fine to medium-grained sand, and laminations
Mud	M	Mud with well sorted very fine-grained sand
Burrowed sandy mud	sM-b	Mud with poorly sorted medium-grained sand and burrows
Plant roots sandy mud	sM-rt	Mud with well sorted fine-grained sand, plant fragments common
Mixed muddy sandy gravel	msG-mxd	Gravel with poorly sorted coarse sand, 30 – 70% broken shells, plant fragments, and mud

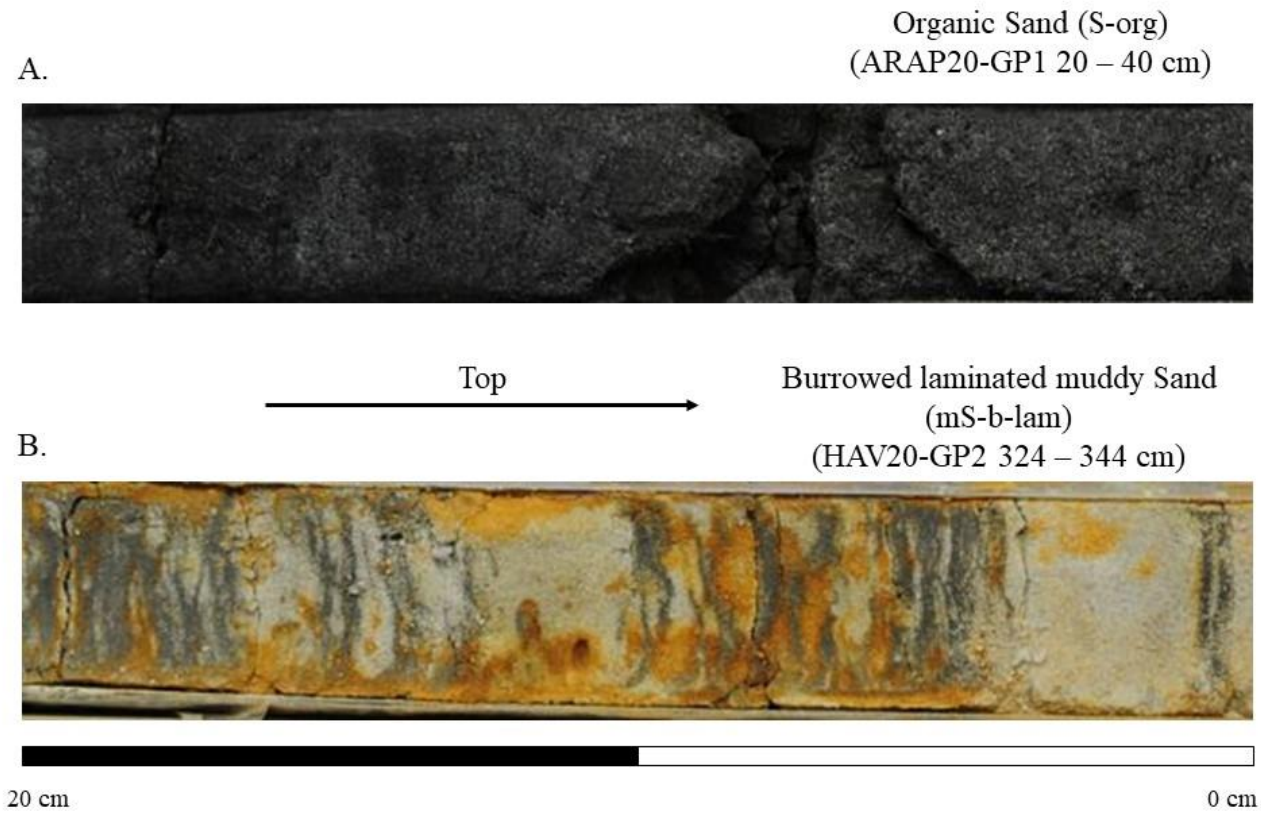

Figure 5. Panel A is a photograph of ARAP20-GP1 that shows the typical sediment of the Organic-rich Sand (S-org) lithofacies. Panel B is a photograph of HAV20-GP2 that shows the typical sediment of the burrowed laminated muddy Sand (mS-b-lam) lithofacies.

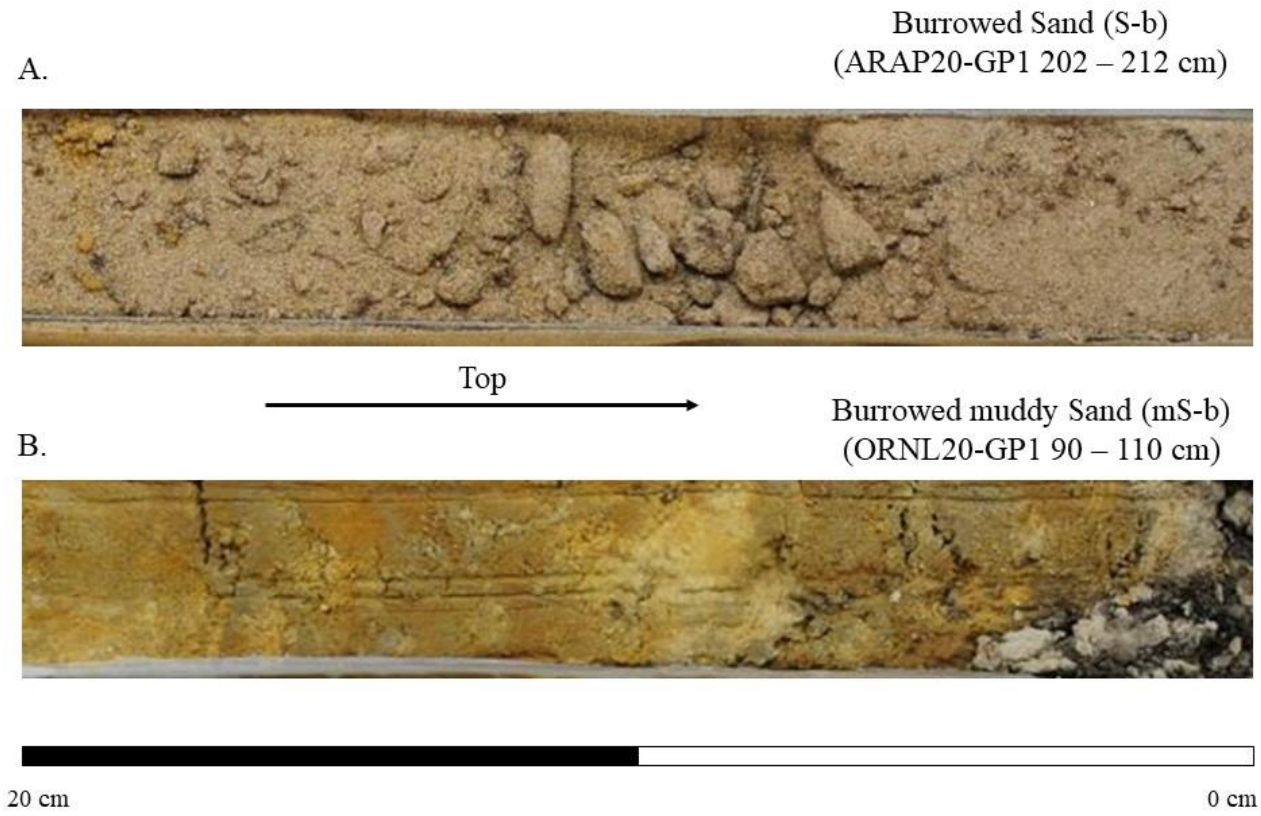

Figure 6. Panel A is a photograph of ARAP20-GP1 that shows the typical sediment of the Burrowed Sand (S-b) lithofacies. Panel B is a photograph of ORNL20-GP1 that shows the typical sediment of the burrowed muddy Sand (mS-b) lithofacies.

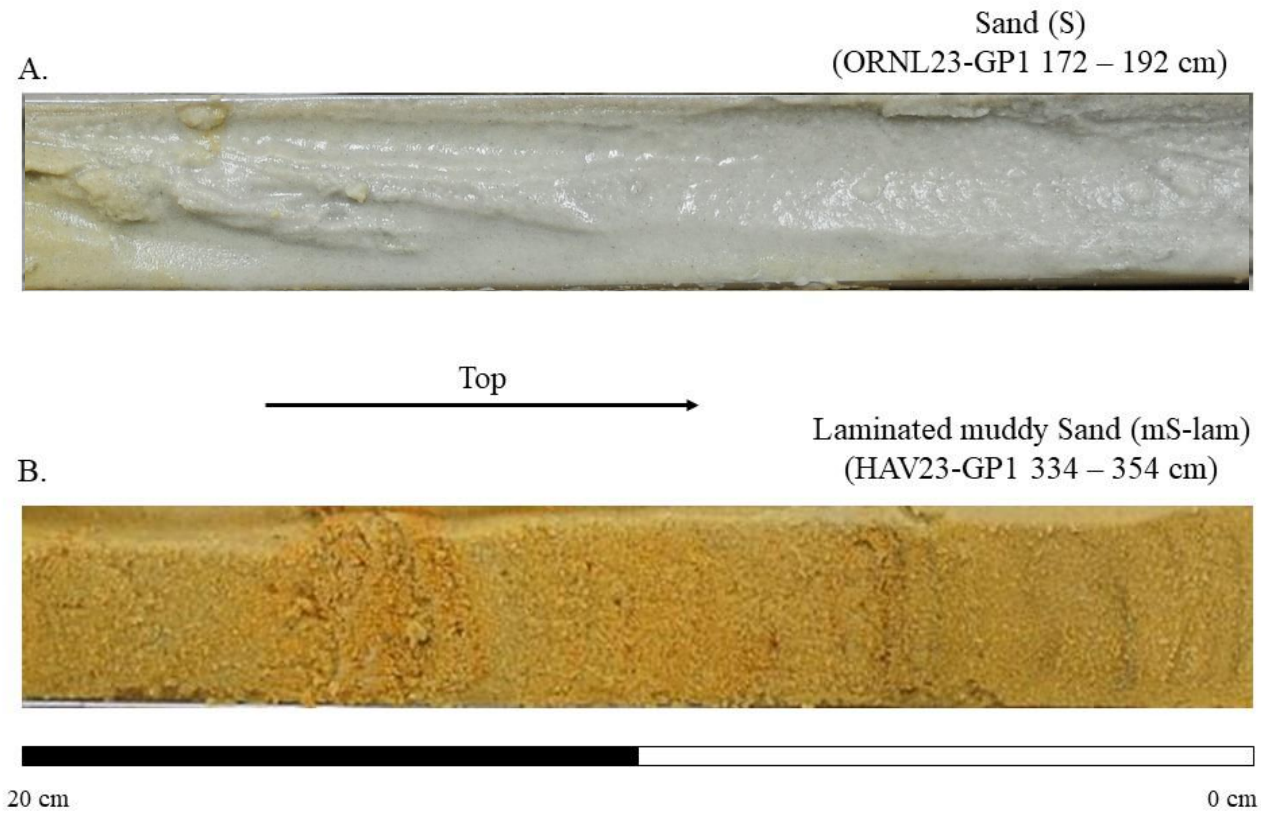

Figure 7. Panel A is a photograph of ORNL23-GP1 that shows the typical sediment of the Sand (S) lithofacies. Panel B is a photograph of HAV23-GP1 that shows the typical sediment of the laminated muddy Sand (mS-lam) lithofacies. Laminations are composed of mud.

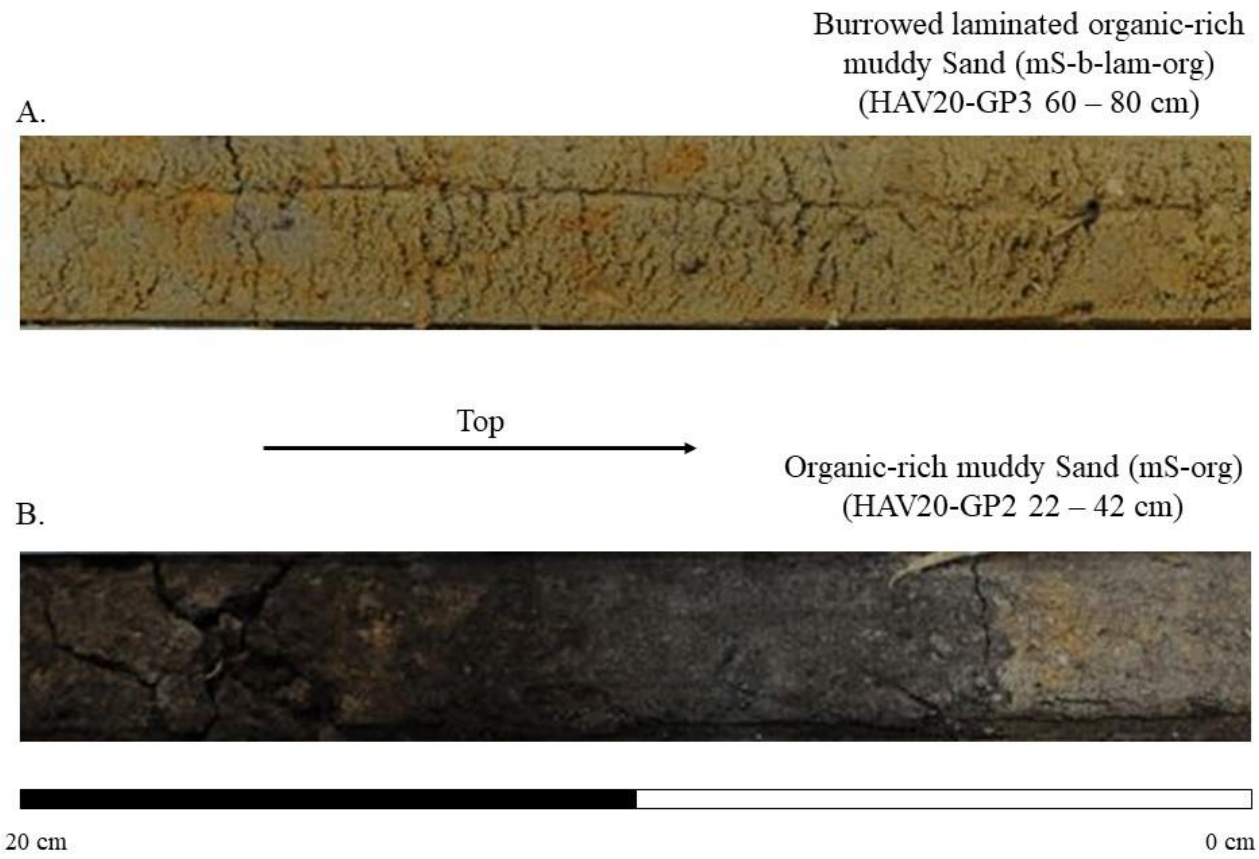

Figure 8. Panel A is a photograph of HAV20-GP3 that shows the typical sediment of the burrowed laminated organic-rich muddy Sand (mS-b-lam-org) lithofacies. Panel B is a photograph of HAV20-GP2 that shows the typical sediment of the organic-rich muddy Sand (mS-org) lithofacies.

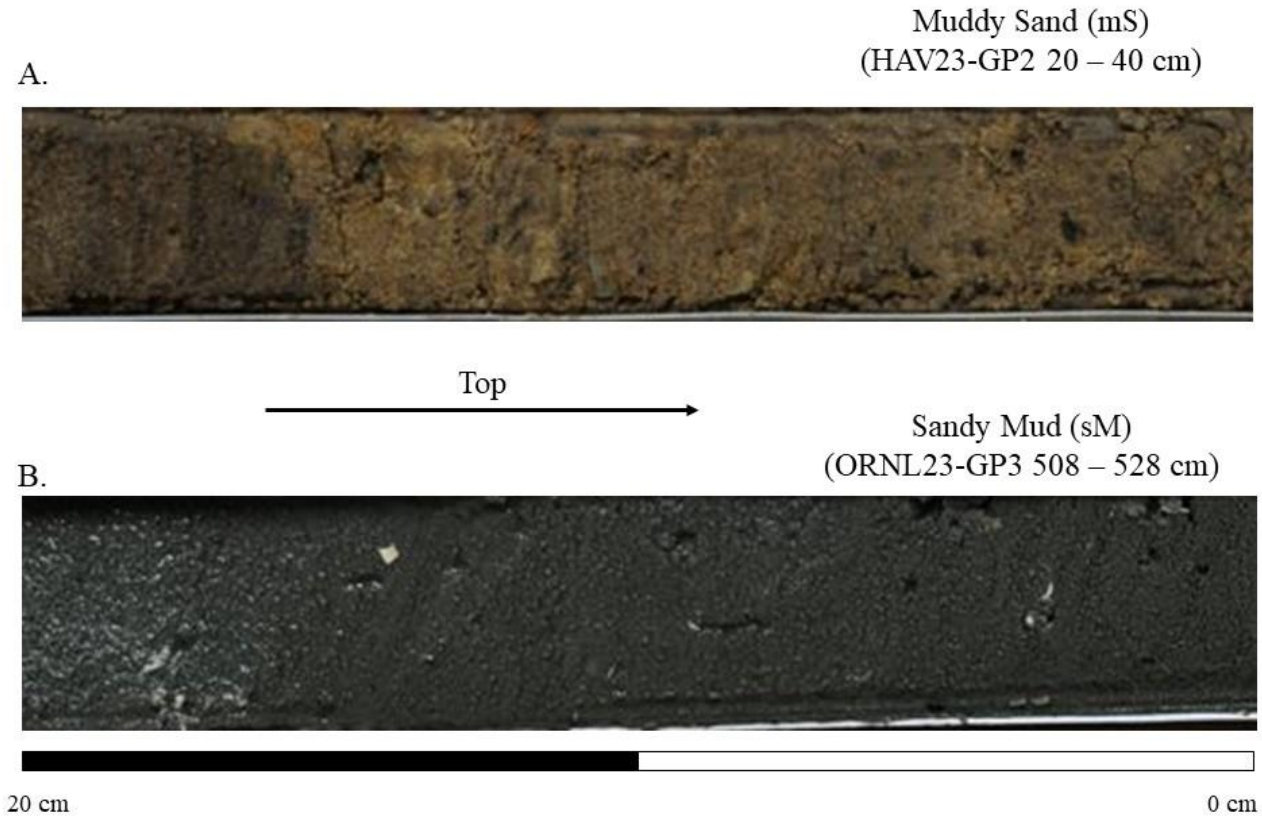

Figure 9. Panel A is a photograph of HAV23-GP2 that shows the typical sediment of the muddy Sand (mS) lithofacies. Panel B is a photograph of ORNL23-GP3 that shows the typical sediment of the sandy Mud (sM) lithofacies.

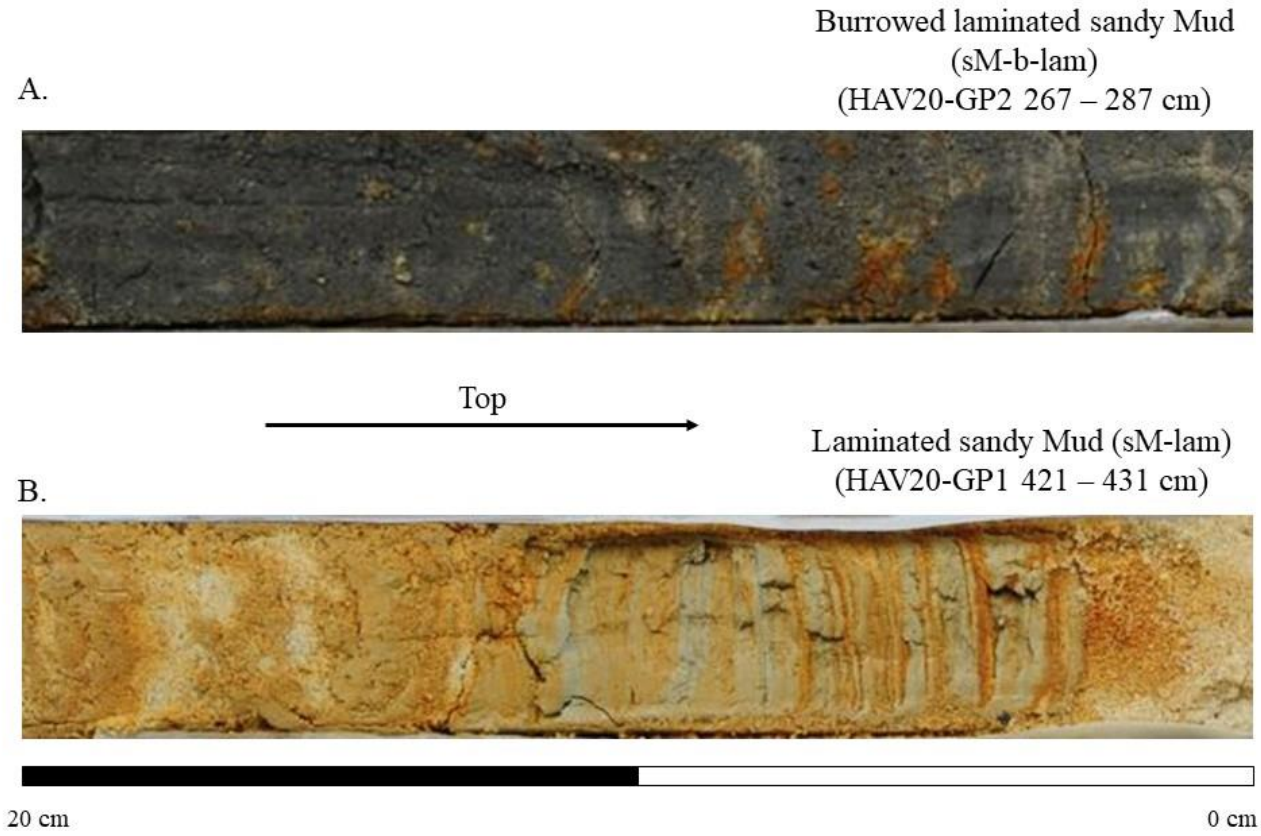

Figure 10. Panel A is a photograph of HAV20-GP2 that shows the typical sediment of the burrowed laminated sandy Mud (sM-b-lam) lithofacies. Panel B is a photograph of HAV20-GP1 that shows the typical sediment of the laminated sandy mud (sM-lam) lithofacies.

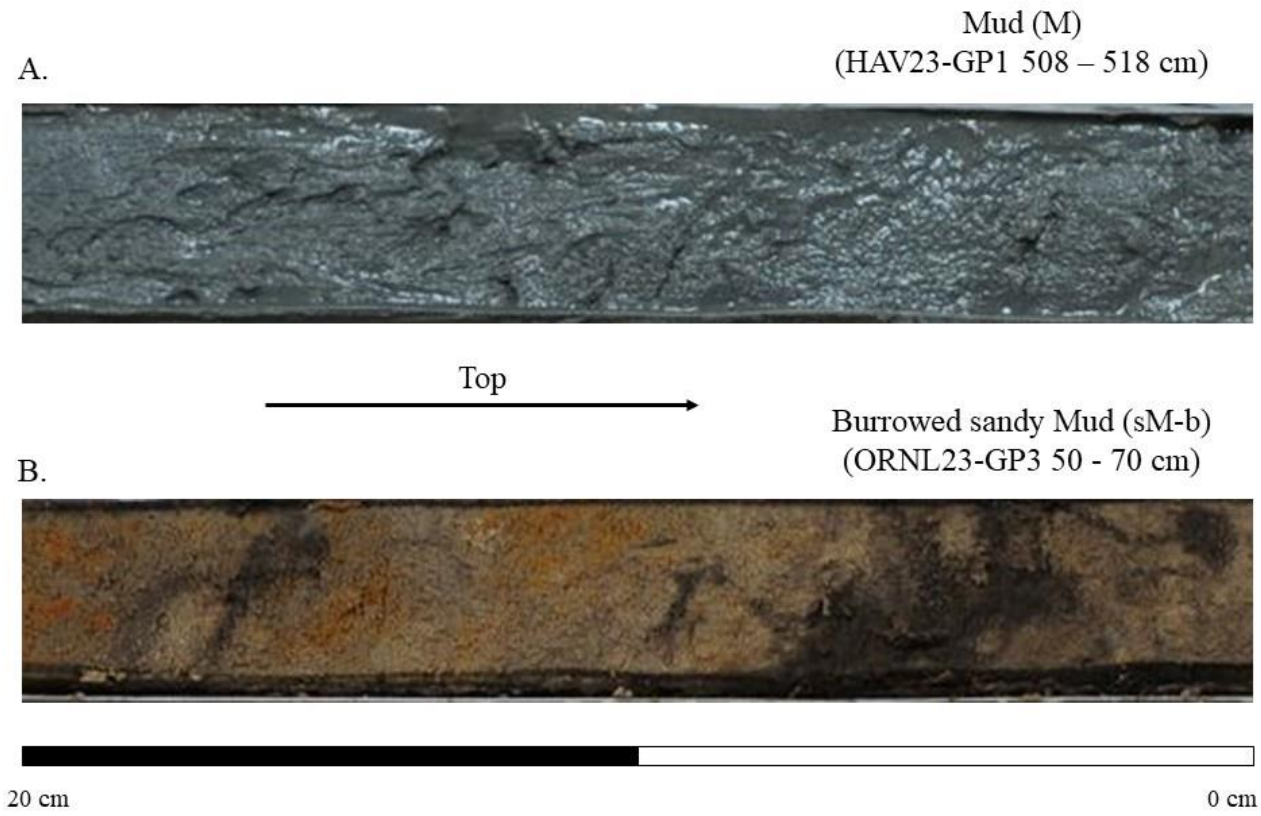

Figure 11. Panel A is a photograph of HAV23-GP1 that shows the typical sediment of the Mud (M) lithofacies. Panel B is a photograph of ORNL23-GP3 that shows the typical sediment of the burrowed sandy Mud (sM-b) lithofacies.

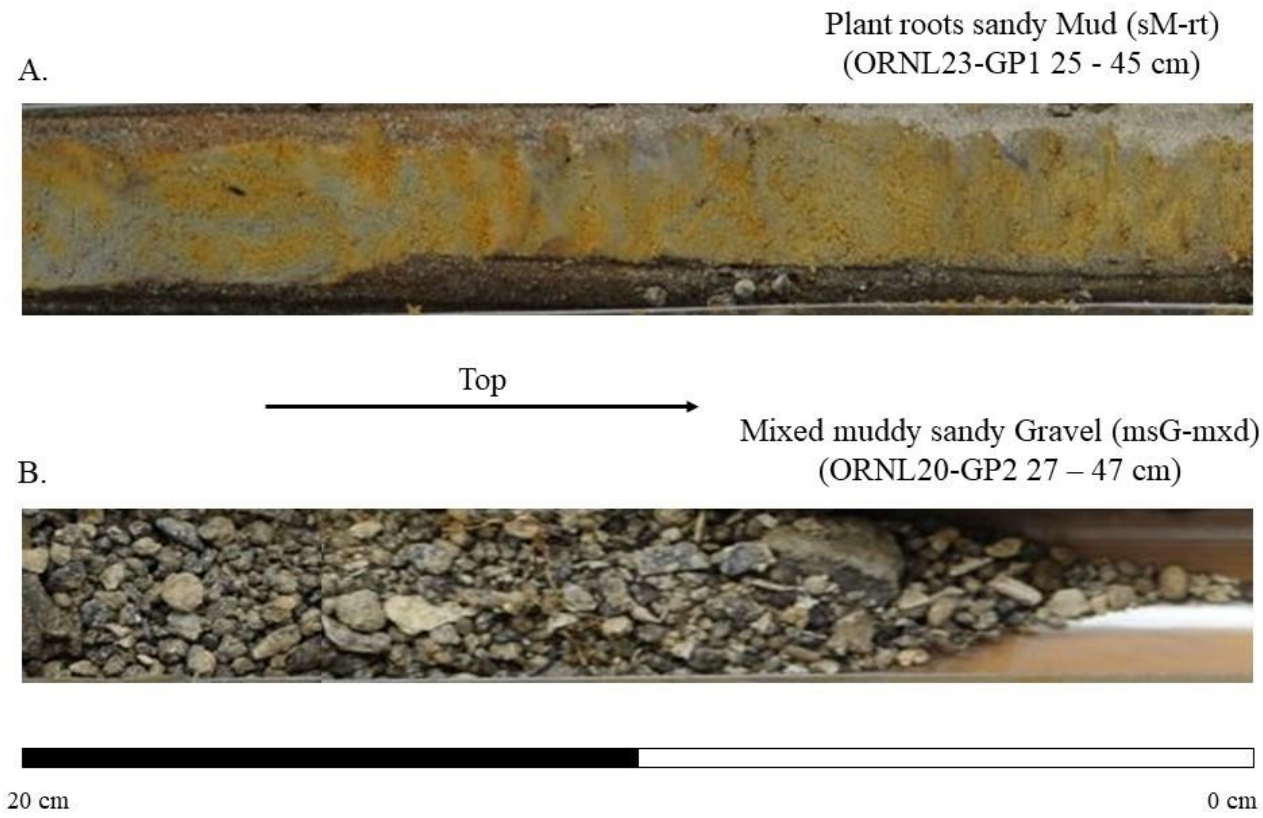

Figure 12. Panel A is a photograph of ORNL23-GP1 that shows the typical sediment of the plant roots sandy mud (sM-rt) lithofacies. Panel B is a photograph of ORNL20-GP2 that shows the typical sediment of the mixed muddy sandy Gravel (msG-mxd) lithofacies.

3.2 Sedimentology

The sedimentological analysis of 56 samples reveals varied grain-size patterns across the cores (Table 2). For samples with <5% mud, mud fractions were disregarded in grain-size analysis, focusing on sand to gravel sediment fractions (Blott and Pye, 2001). The mud fraction percentages in samples with >5% mud ranged from 37.36% to 9.99% (Appendix G). Sediments are predominantly fine to very fine sand and exhibit moderate to good sorting. Skewness results varied, ranging from very coarse to symmetrically skewed.

The sand-dominated lithofacies, comprising sand and muddy sand, exhibit sorting (phi) values ranging from 0.35 to 1.87, varying from well to poorly sorted (Table 2). These values indicate slightly better sorting compared to the sand within the mud-dominated lithofacies (mud and sandy mud), which yielded sorting (phi) values ranging from 0.61 to 1.31. On average, grain-size results from the sand-dominated lithofacies exhibited a more coarsely skewed distribution compared to those calculated for mud-dominated lithofacies.

Grain-size data from samples collected south of the river indicate moderate to well sorting and predominantly coarse to very coarse skewness. In contrast, samples collected north of the river reveal more varied results, ranging from poorly to well sorted and symmetrical to very coarse skewed distributions.

Table 2. Grain-size analysis results for 56 samples collected in 15 cores.

Core Sample	Depth below ground surface (cm)	Sorting Φ	Skewness Φ	Mean Φ	Sediment Type
ORNL 20-GP1	205	0.38	-0.02	2.66	Well Sorted Fine Sand
ORNL 20-GP1	336	0.41	-0.60	2.94	Well Sorted Fine Sand
ORNL 20-GP2	176	0.43	-1.33	3.05	Well Sorted Very Fine Sand
ORNL 20-GP2	270	0.42	-0.79	2.98	Well Sorted Fine Sand
ORNL 20-GP2	428	1.83	-0.97	1.63	Poorly Sorted Medium Sand
ORNL 20-GP2	551	1.29	-0.89	2.08	Poorly Sorted Fine Sand
ORNL 20-GP3	186	0.51	-1.47	2.90	Moderately Well Sorted Fine Sand
ORNL 20-GP3	260	0.47	-1.62	3.27	Well Sorted Very Fine Sand
ORNL 20-GP3	304	0.52	-3.23	2.84	Moderately Well Sorted Fine Sand
ORNL 20-GP3	450	1.53	-1.94	2.68	Poorly Sorted Fine Sand
ORNL 20-GP3	476	0.99	-1.17	2.57	Moderately Sorted Fine Sand
ORNL 20-GP3	546	1.66	-0.80	1.52	Poorly Sorted Medium Sand
ARAP 20-GP1	87-89	0.51	-1.25	2.38	Moderately Well Sorted Fine Sand
ARAP 20-GP1	290	0.70	-1.14	2.37	Moderately Well Sorted Fine Sand
ARAP 20-GP1	330	1.43	-0.19	1.30	Poorly Sorted Medium Sand
ARAP 20-GP2	190	1.31	-0.89	2.15	Poorly Sorted Fine Sand
ARAP 20-GP2	300	1.28	-2.54	2.67	Poorly Sorted Fine Sand
ARAP 20-GP2	470	1.64	-1.35	2.03	Poorly Sorted Fine Sand

ARAP 20-GP3	390	1.87	-1.52	2.17	Poorly Sorted Fine Sand
HAV 20-GP1	294	0.35	-2.00	2.74	Well Sorted Fine Sand
HAV 20-GP2	110	0.84	-0.17	0.86	Moderately Sorted Coarse Sand
HAV 20-GP2	384	0.84	-2.61	2.55	Moderately Sorted Fine Sand
HAV 20-GP2	415	1.0	-1.92	2.36	Moderately Sorted Fine Sand
HAV20-GP2	540	0.91	-2.48	2.46	Moderately Sorted Fine Sand
HAV 20-GP3	276	0.37	-0.90	2.97	Well Sorted Fine Sand
HAV 20-GP3	455	0.36	-0.55	2.90	Well Sorted Fine Sand
ORNL23-GP1	100	0.47	-0.52	2.75	Well Sorted Fine Sand
ORNL23-GP1	222	0.41	-2.25	2.48	Well Sorted Fine Sand
ORNL23-GP1	294	0.42	-1.23	2.79	Well Sorted Fine Sand
ORNL23-GP2	100	0.44	0.32	2.72	Well Sorted Fine Sand
ORNL23-GP2	182	0.70	-4.26	2.84	Moderately Well Sorted Fine Sand
ORNL23-GP2	304	0.35	0.33	2.37	Very Well Sorted Fine Sand
ORNL23-GP2	456	0.46	-0.35	2.17	Well Sorted Fine Sand
ORNL23-GP2	548	0.80	0.40	1.15	Moderately Sorted Medium Sand
ORNL23-GP3	80	0.41	0.38	2.67	Well Sorted Fine Sand
ORNL23-GP3	324	0.57	-1.52	2.79	Moderately Well Sorted Fine Sand
ORNL23-GP3	391	0.74	-2.86	2.70	Moderately Sorted Fine Sand
ORNL23-GP3	476	0.97	-1.95	2.84	Moderately Sorted Fine Sand
ORNL23-GP3	533	1.14	-2.09	2.61	Poorly Sorted Fine Sand

ARAP23-GP1	60	0.43	-0.45	2.41	Well Sorted Fine Sand
ARAP23-GP1	202	0.44	0.003	2.42	Well Sorted Fine Sand
ARAP23- GP1	284	0.43	-0.45	2.31	Well Sorted Fine Sand
ARAP23- GP1	334	0.44	-0.29	2.31	Well Sorted Fine Sand
ARAP23-GP1	446	0.45	-0.75	2.34	Well Sorted Fine Sand
HAV23-GP1	100	0.67	-0.94	2.48	Moderately Well Sorted Fine Sand
HAV23- GP1	222	0.51	-2.04	2.53	Moderately Well Sorted Fine Sand
HAV23-GP1	304	0.48	-2.73	2.66	Well Sorted Fine Sand
HAV23- GP1	446	0.61	-1.61	2.58	Moderately Well Sorted Fine Sand
HAV23-GP1	528	0.48	-0.38	3.12	Well Sorted Very Fine Sand
HAV23- GP1	588	0.87	-1.09	1.89	Moderately Sorted Medium Sand
HAV23- GP2	90	0.78	-0.21	1.83	Moderately Sorted Medium Sand
HAV23-GP2	167	0.70	0.01	2.07	Moderately Well Sorted Fine Sand
HAV23-GP2	207	0.60	-0.42	1.86	Moderately Well Sorted Medium Sand
HAV23-GP2	297	0.37	0.63	2.55	Well Sorted Fine Sand
HAV23-GP2	344	0.60	-2.74	2.55	Moderately Well Sorted Fine Sand
HAV23-GP2	461	0.48	0.42	2.70	Well Sorted Fine Sand

3.3 Foraminifera Data

Twenty-eight of the 47 samples were barren of foraminifera. In the remaining 19 samples, 17 species were identified (Appendix D). Samples dominated by *Elphidium excavatum, Ammonia parkinsoniana* and *Elphidium mexicanum* were found at 466 cm—610 cm core depth. Twelve samples, also dominated by *Elphidium excavatum, Ammonia parkinsoniana* and *Elphidium mexicanum* but also containing *Buccella inusitata, Nonionella atlantica,* and *Rosalina* sp., occurred from 264 cm—466 cm core depth. Samples taken above 264 cm in the cores were barren of foraminifera. Samples collected in cores ARAP20-GP1, ORNL20-GP1, HAV20-GP1, HAV20-GP2, HAV20-GP3, and HAV23-GP2 at varying depths were also barren of foraminifera.

3.4 Pollen Data (D. Willard, Personal Communication)

Nine pollen samples were analyzed against a marine surface sample database and a terrestrial surface sample database from across North America (Table 3). The mean annual temperatures and dissimilarity values were reconstructed. The relative temperature reconstructions as well as the abundance of arboreal and non-arboreal for each sample can be found in Appendix E. Sample ORNL20-GP2 157—162 cm was barren of palynomorphs.

Table 3. Pollen analysis of samples collected in the Lower Neuse River Basin.

Core Sample	Depth below ground surface (cm)	Comments/interpretations
ARAP20-GP2	185—189	Possibly warmer than today, based on similarity to Gulf Coast assemblages.
ARAP20-GP2	314—319	Similar to modern conditions - intermediate between other two samples from this core.

ARAP20-GP2	466—473	Modern to slightly cooler than modern temperatures, based on lack of close analogs from the Gulf Coast
ORNL20-GP2	294—299	Modern to warmer than modern conditions, based on analogs from Florida and the Gulf Coast
ORNL20-GP2	451—456	Cooler than sample above based on existence of modern analogs as far north as Chesapeake and the presence of hemlock. Likely near modern conditions.
ORNL20-GP3	182—187	Modern to slightly warmer than modern conditions.
ORNL20-GP3	264—269	Probably cooler than today but warmer than underlying sample.
ORNL20-GP3	426—431	Likely represent cooler than modern conditions. May have forested wetlands nearby, based on occurrence of cypress and tupelo pollen.

3.5 OSL Age Estimates

Luminescence dating analysis was conducted on eleven sand samples extracted from eight Geoprobe cores. The Pleistocene luminescence ages obtained from these samples span a range from 123.5 (± 7.2) ka to > 56.8 (± 4.1) ka (refer to Table 4). Ages with the (>) symbol are interpreted as older than the calculated date.

Five of the 11 samples yielded a luminescence age consistent with Marine Isotope Stage (MIS) 5e (OSL 3, 8, 9, 14, and 15). One sample yielded MIS 5d age (OSL 7). Three samples were determined to be from MIS 5a (OSL 5, 6, and 13). Notably, two samples collected south of the Neuse River revealed an age indicative of MIS 4 (OSL 1 and 2).

Table 4. OSL age estimates and equivalent dose data of samples from the Lower Neuse River Basin. Sample depths (under Sample ID) are measured from the core top.

Sample	Sample ID	Sample Depth (m)	Dose (Gy)	Dose Rate (Gy/ka)	Age (ka)	Interpreted MIS
OSL 1	HAV23-GP1	2.02 to 2.12	74.2 ± 4.6	1.086 ± 0.026	68.3 ± 4.5	4
OSL 2	HAV23-GP1	4.26 to 4.36	73.1 ± 4.9	1.030 ± 0.027	71.0 ± 5.1	4
OSL 3	HAV23-GP1	5.58 to 5.66	>95.1 ± 5.5	1.259 ± 0.034	>75.6 ± 4.8	5e
OSL 5	ORNL23-GP1	1.82 to 1.92	80.1 ± 4.9	0.944 ± 0.028	84.9 ± 5.7	5a
OSL 6	ORNL23-GP2	2.02 to 2.12	>101.1 ± 7.0	1.782 ± 0.042	> 56.8 ± 4.1	5a
OSL 7	ORNL23-GP2	4.36 to 4.46	43.6 ± 2.6	0.407 ± 0.012	107.0 ± 7.0	5d
OSL 8	ORNL23-GP3	2.09 to 2.19	>107.5 ± 6.6	1.827 ± 0.045	>58.9 ± 3.9	5e
OSL 9	ORNL23-GP3	4.46 to 4.56	>133 ± 12	1.581 ± 0.041	>83.9 ± 8.1	5e
OSL 13	ORNL-20-GP2	4.16 to 4.66	82.6 ± 4.2	0.963 ± 0.036	85.7 ± 5.3	5a
OSL 14	ARAP-20-GP2	1.72 to 1.82	227 ± 14	1.949 ± 0.074	116.4 ± 8.2	5e
OSL 15	ORNL-20-GP3	4.26 to 4.36	179.4 ± 9.8	1.282 ± 0.049	123.5 ± 7.2	5e

3.6 Ground Penetrating Radar Data

Approximately 2.3 kilometers of GPR data were collected across the lower Neuse River Basin at the coring sites. Correlations of these data to litho/biofacies serve to enhance our understanding of the subsurface geological framework of the region and the factors influencing the modern morphology of the study area. The data collected experienced signal attenuation likely due to saline pore water in the shallow subsurface, making interpretation challenging to nearly impossible. GPR survey lines 010, 011, and 012 are not presented within this study due to signal attenuation.

3.6.1 Line 013

Line 013, approximately 0.55 km in length, was acquired at core HAV23-GP1 (Figure 13). The survey reveals continuous, medium to high amplitude horizontal bedding across its extent. Shallow channel structures, incised to approximately 2 meters below the surface and approximately 20 meters wide, are evident in both the northern and southern sections of the

survey area. These channels exhibit discontinuous, medium to high amplitude, V-shaped reflectors.

3.6.2 Line 014

Line 014, extending approximately 0.5 km along core HAV23-GP2, reveals discontinuous, high amplitude, eastward dipping reflectors, indicative of channel structures in this area (Figure 14). The largest channel structure, located at depths of 1 to 4 meters, spans approximately 80 meters along the survey. A smaller channel structure, located at depths of 1 to 3 meters, is approximately 12 meters wide.

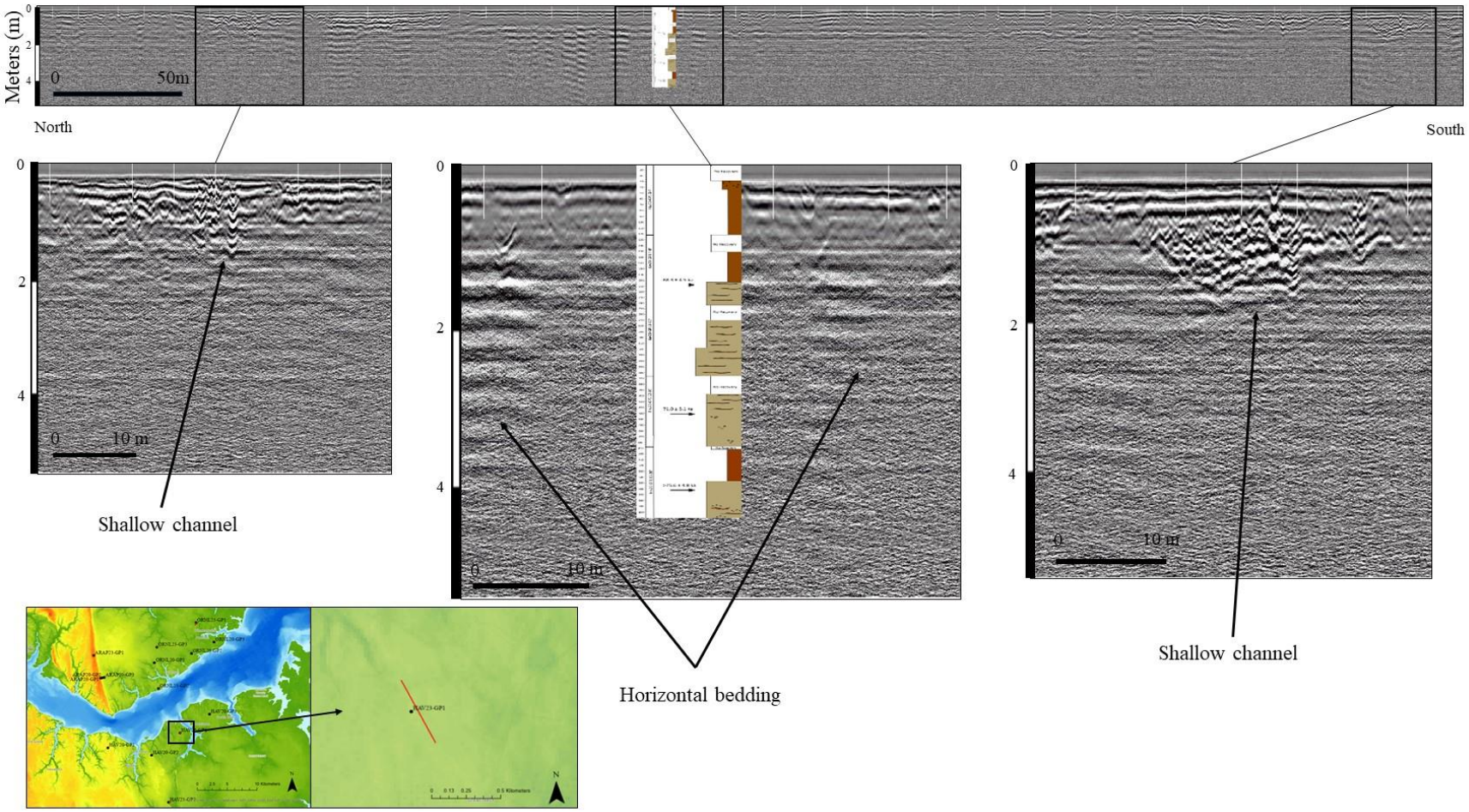

Figure 13. GPR data Line 013 with corresponding Geoprobe core (HAV23-GP1). The figure comprises original data with interpreted features and reference location. The red line on the LiDAR map indicates the survey location.

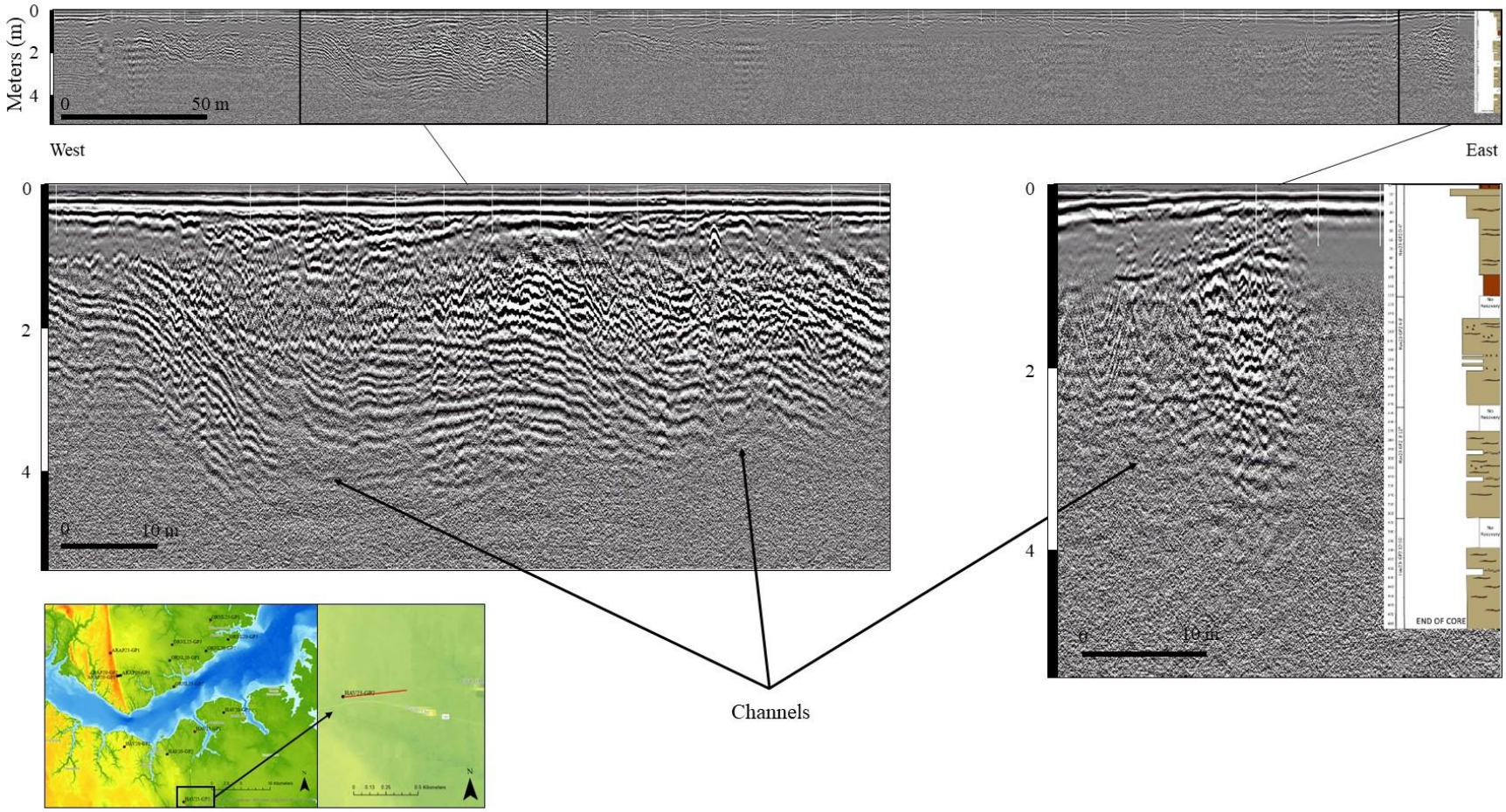

Figure 14. GPR data Line 014 with corresponding Geoprobe core (HAV23-GP2). The figure comprises original data with interpreted features and reference location. The red line on the LiDAR map indicates the survey location.

3.6.3 Line 015

Line 015, measuring approximately 0.29 km along core ORNL23-GP3, exhibits considerable signal attenuation at depth (Figure 15). Notably, road fill is preserved within the 0 to 1 meter depth interval along this survey, but few reflectors are discerned below the road fill.

3.6.4 Line 016

Line 016, covering approximately 0.225 km along core ARAP23-GP1, displays semi-continuous, sub-horizontal, medium to high amplitude reflections. Four units are defined by high-amplitude reflectors, with the upper unit also exhibiting U-shaped channel structures. (Figure 16).

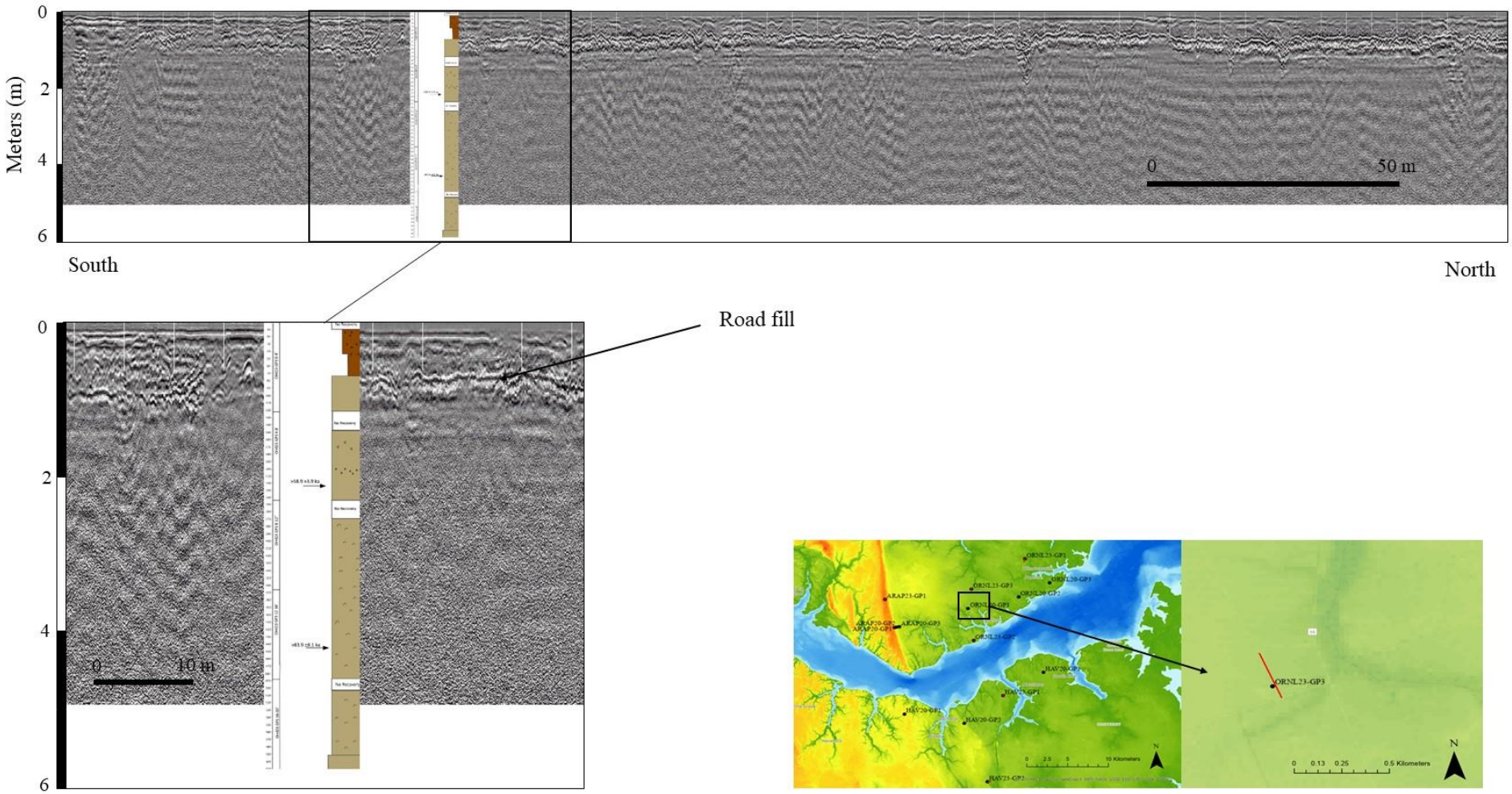

Figure 15. GPR data Line 015 with corresponding Geoprobe core (ORNL23-GP3). The figure comprises original data with interpreted features and reference location. The red line on the LiDAR map indicates the survey location.

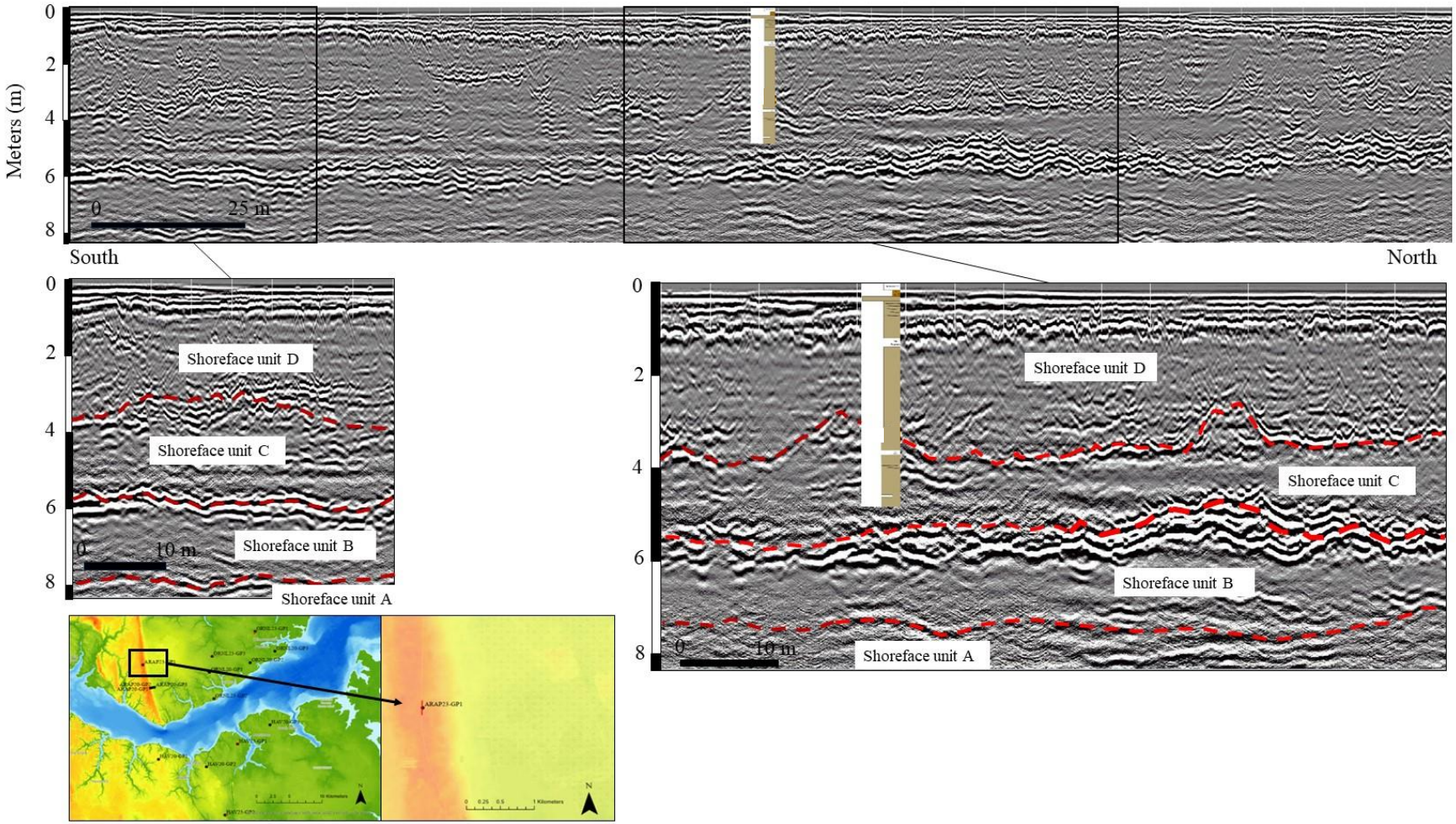

Figure 16. GPR data Line 016 with corresponding Geoprobe core (ARAP23-GP1). The figure comprises original data with interpreted features and reference location. The red line on the LiDAR map indicates the survey location, while the red dashed lines on the survey images denote historical shorelines.

4.0 Discussion

4.1 Defining the lithostratigraphy and chronostratigraphy

A depositional sequence is a stratigraphic unit that is defined by subaerial unconformities or their corresponding conformities (Catuneanu, 2015). The observed depositional sequences (DS) are delineated by correlating grain-size analysis, foraminiferal analysis, and pollen analysis with their respective lithologies. Sequence boundaries are marked by burrowed or erosional surfaces, as well as changes in grain size, color, mineralogy, or structure within the core. Four cross sections illustrate the lateral correlations of these depositional sequences. Each depositional sequence comprises a vertical succession of lithostratigraphic layers, representing a series of paleoenvironments that evolved in response to sea-level changes and shifting environments from MIS 5e to MIS 4. OSL ages establish the chronostratigraphic framework and offer further support for lateral facies correlations. Based on the data, three Pleistocene chronostratigraphic units were identified.

4.1.1 Depositional Sequence 5e

Age constraints for DS-5e are determined from six OSL samples, indicating a MIS 5e age (>58.9 ± 3.9 to 123.5 ± 7.2 ka) (Table 4). DS-5e is composed of eastward thickening shelly sand lithofacies. Parham at el. (2013) similarly characterized MIS 5e deposits as shelly laminated mud and shelly sand extending from the Suffolk Shoreline eastward to Pamlico Sound on the Albemarle-Pamlico Peninsula. Sediment samples collected within DS-5e (ORNL20-GP2 551cm, ORNL20-GP3 450 cm, and ORNL23-GP3 598) show poorly sorted, strongly coarse skewed sand with shell material present (Figures 17 and 18).

The lowermost foraminifera samples exhibit low diversity, dominated by *Elphidium excavatum*, *Ammonia parkinsoniana,* and *Elphidium mexicanum*. These species likely indicate a high salinity estuarine environment, as low salinity estuary assemblages typically contain agglutinated species (Vance et al., 2006; Abbene et al., 2016). However, species diversity increases upwards in the sequence, with the same three species being predominant along with open shelf species such as *Buccella inusitata*, *Nonionella atlantica*, and *Rosalina*

sp. This increase in diversity forming assemblages are similar to those found in modern shoreface and inner shelf environments with typical marine salinity (~34) off the Outer Banks (Workman, 1981).

Additionally, pollen samples collected within DS-5e show a trend of cooler conditions in the lowermost sample of the core to likely warmer than modern conditions in the uppermost collected sample. Cooler climate conditions are supported by the presence of *Pinus* (pine), *Quercus* (oak), *Tsuga* (hemlock), *Nyssa* (tupelo), and Cupressaceae (cypress) pollen in samples ARAP20-GP2 (466 cm), ORNL20-GP2 (451 cm), and ORNL20-GP3 (426 and 264 cm) which are abundant in modern tundra and forest vegetation zones (Davis and Webb, 1975; Willard et al., 2003). Warmer climates typically foster greater tree diversity, with vegetation zones including conifer/hardwood forests, deciduous forests, and southeastern forests (Davis and Webb, 1975). The presence of *Pinus* (pine), *Quercus* (oak), *Liquidambar* (sweetgum), and *Carya* (hickory) pollen in samples ARAP20-GP2 (314 cm and 190 cm) and ORNL20-GP3 (182 cm) suggest conditions ranging from modern to slightly warmer than modern conditions, based on comparisons with modern analogs. This transition from low to higher diversity foraminifera assemblages, warming climate conditions, and shelly marine deposits is indicative of a transgressive environment, interpreted as a high salinity estuary becoming an inner shelf environment (Murray, 1969; Schnitker, 1971; Workman, 1981).

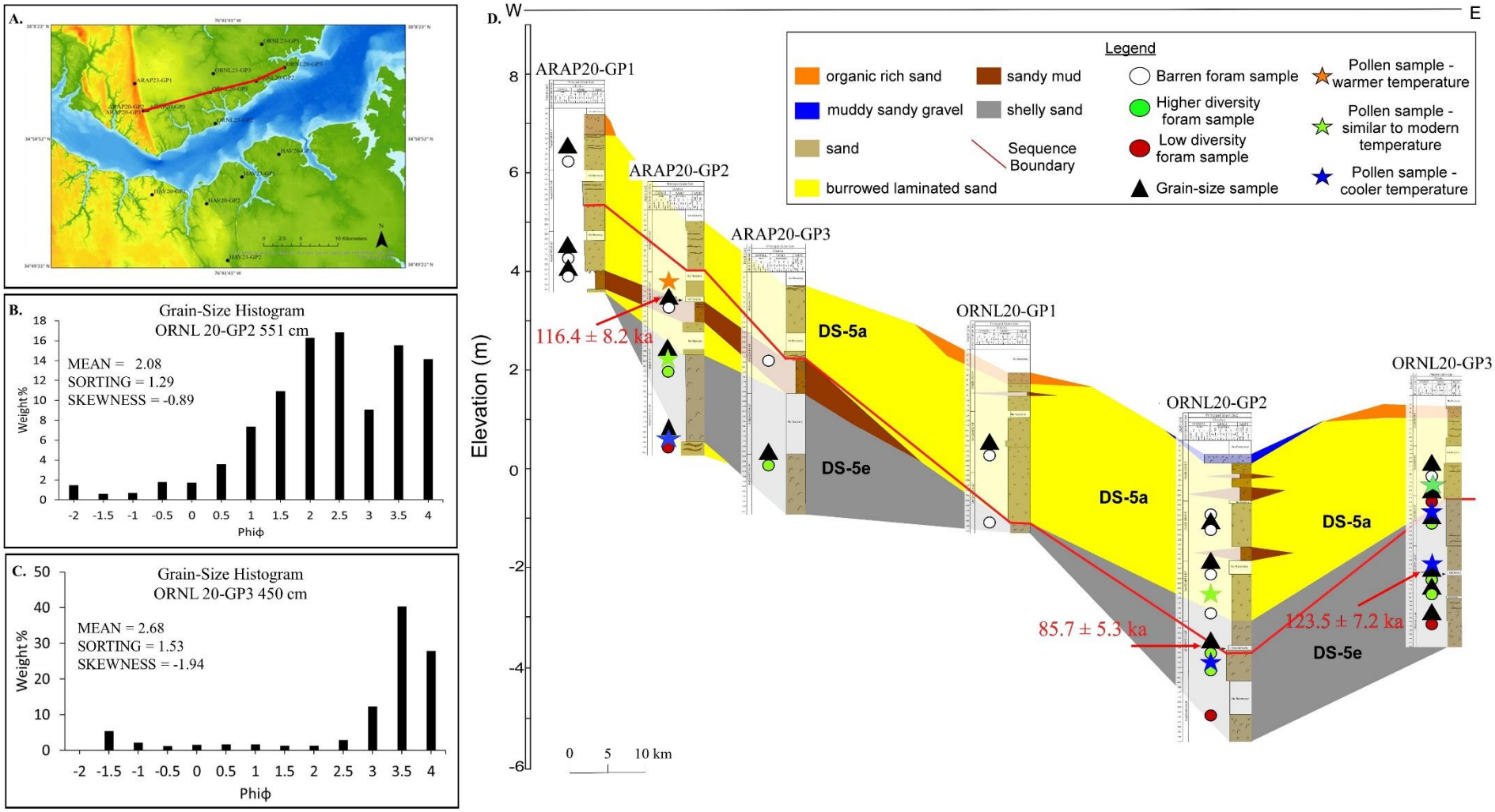

Figure 17. Stratigraphic cross section across the Suffolk Shoreline complex, north of the lower Neuse River, showing lithostratigraphy, depositional sequences, and sequence boundaries.

4.1.2 Depositional Sequence 5a

DS-5a consists of deposits of MIS 5a age (Figure 17 and 18). Samples within this sequence are mostly barren of foraminifera, except for one low diversity sample. This is likely due to dissolution, as no other calcareous shell material was found in the study area. The lithofacies associated with DS-5a are characterized by burrowed laminated sand, as well as sandy mud. Lithofacies show an upward-fining succession transitioning from flaser to wavy tidal bedding. Parham (2007) similarly described non-shelly tidal deposits as interlaminated sand and mud, featuring flaser and wavy tidal bedding, and commonly containing burrows. Grain-size histograms for sediment samples (ARAP23-GP1 at 406 cm and ORNL23-GP1 at 416 cm) within DS-5a consist primarily of well to moderately sorted, negatively skewed, fine to medium burrowed laminated sands (Figures 19 and 21). One pollen sample (ORNL20-GP2 at 294 cm) from DS-5a suggests conditions ranging from modern to slightly warmer than present. Pollen and diatom data collected in Baffin Bay support a climate warmer than the Holocene during MIS 5a (Miller et al., 1999; Wolfe et al., 2000). Figure 16 displays GPR data for core ARAP23-GP1, which penetrates the upper two units, D and C. The interpreted 5a/5e boundary for this core is approximately 4 meters below the surface, corresponding to the transition between units C and D. This suggests that unit D represents DS-5a, while unit C represents DS-5e. The significant beach deposition and probable washover, indicated by channel-like reflections, imply that the shoreline during 5a extended to this area. With apparent tidal bedding, the absence of foraminifera, and warm climate conditions DS-5a is potentially indicative of coastal tidal flat deposits (Parham, 2007; Daidu et al., 2013).

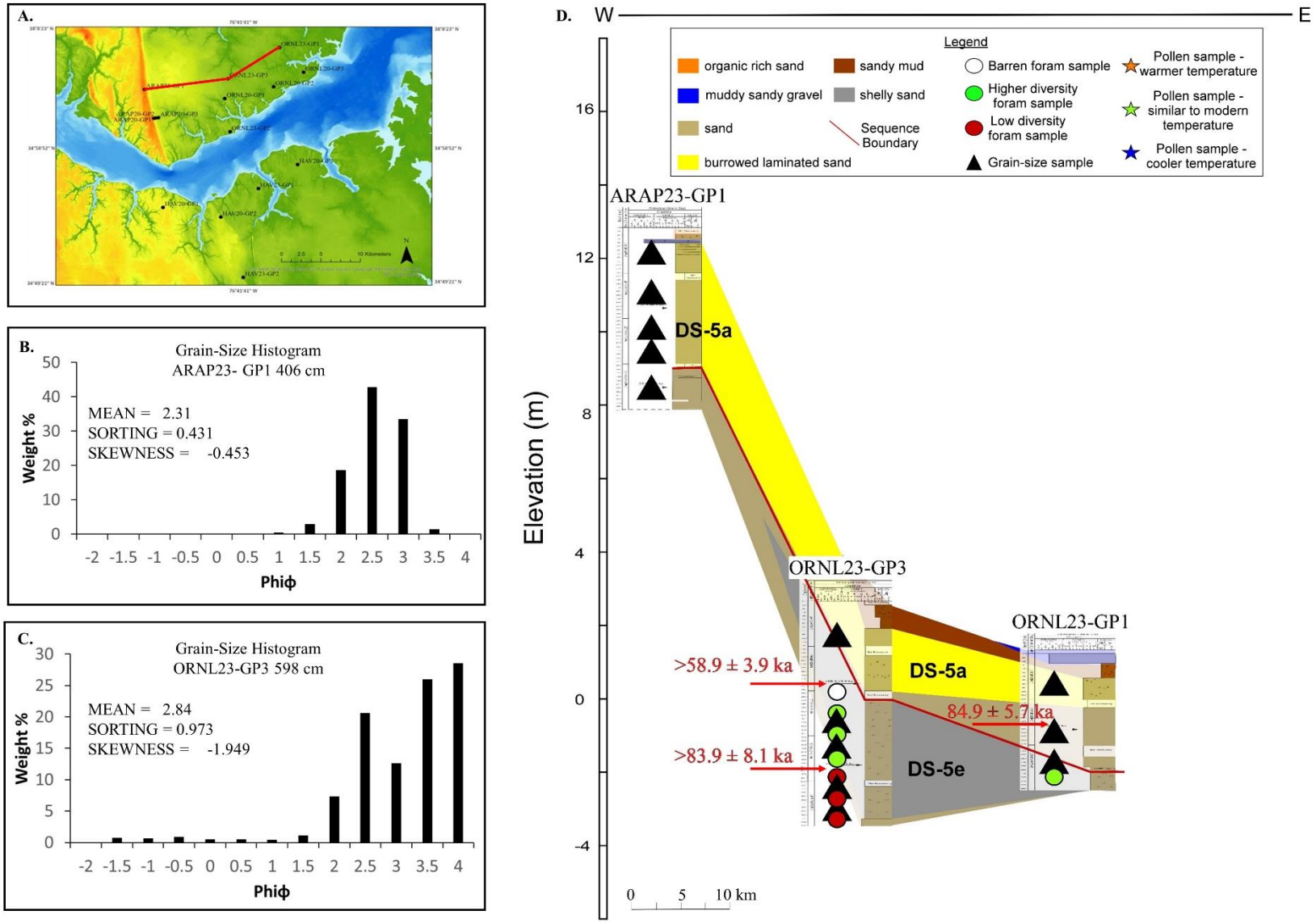

Figure 18. Stratigraphic cross section across the Suffolk Shoreline complex, north of the Lower Neuse River, showing lithostratigraphy, depositional sequences, and sequence boundaries.

4.1.3 Depositional Sequence 4

DS-4 is characterized by OSL ages suggesting deposition during MIS 4 and is predominantly found in cores situated south of the Neuse River (Figures 19 and 20). The lithofacies of DS-4 contain medium to fine-grained burrowed laminated sand and sandy mud. Sediment samples collected within DS-4 (HAV23-GP1 at 100 cm, HAV23-GP1 at 650 cm, and HAV23-GP2 at 289 cm) display well-sorted, near symmetrical to coarsely skewed sand in grain-size histograms found in Figures 19 and 20. All samples retrieved from DS-4 were barren of foraminifera. Regression during MIS 4 likely led to the incision of the Neuse River Channel into MIS 5 marine deposits, exposing sediment from a shallow marine shoal in cores south of the river. As these sand facies were exposed at the land surface, aeolian forces likely reworked the sand into dunes (Burdette and Mallinson, 2008; Parham et al., 2013). Similar medium to fine-grained sand facies were recovered by Gudmunson (2022) north of the Albemarle Sound, with an OSL age of 68.8 ± 5.4 ka. DS-4 is interpreted as an environment transitioning between fluvial and aeolian processes based on grain-size, sorting, and bedding structure.

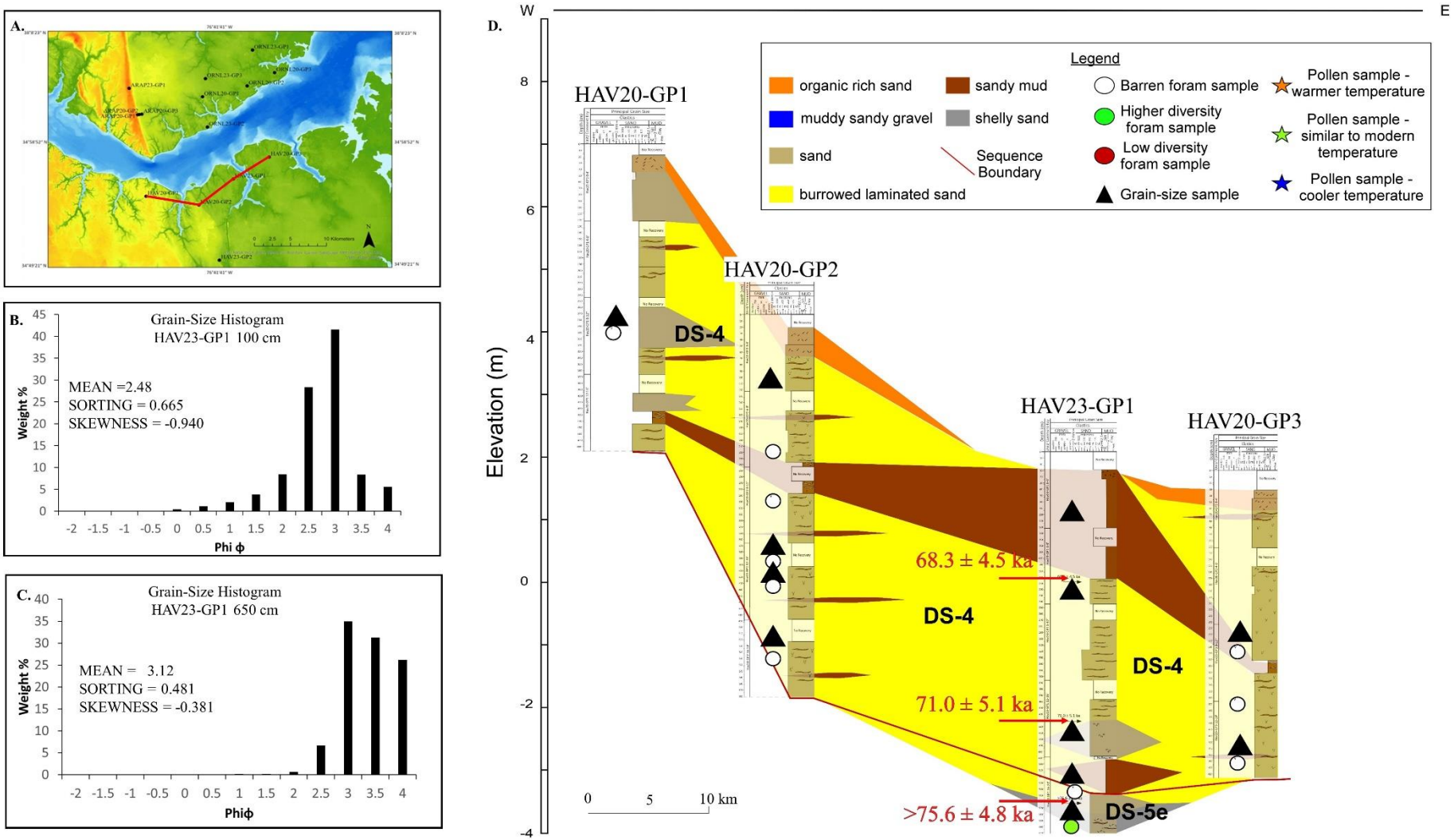

Figure 19. Stratigraphic cross section across the Suffolk Shoreline complex, south of the Lower Neuse River, showing lithostratigraphy, depositional sequences, and sequence boundaries.

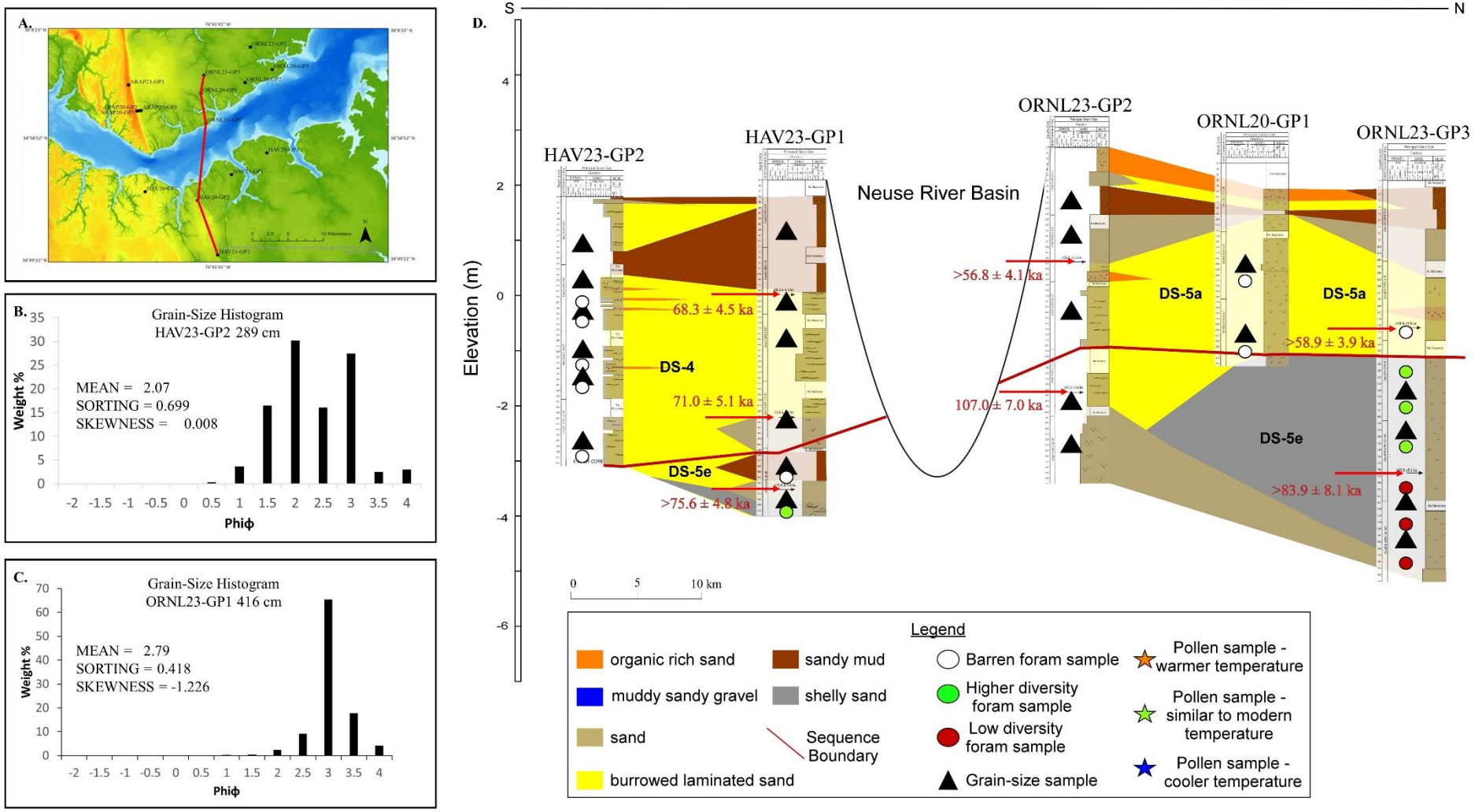

Figure 20. South to north stratigraphic cross section across the Lower Neuse River, showing lithostratigraphy, depositional sequences, and sequence boundaries.

4.2 Development of Late Quaternary Deposits

The Earth's climate throughout the Quaternary period has been characterized by successive glacial and interglacial cycles. The duration of these cycles increased from 41,000 years to 100,000 years starting from the Middle Pleistocene, around 780,000 years ago (Pisias and Moore, 1981; Railsback et al., 2015) (Figure 21). Notably, the presence of terrestrial glaciers in North America, specifically the Laurentide Ice Sheet during the Quaternary, significantly influenced regional sea-level fluctuations along the western Atlantic coast through glacio-isostatic adjustment (GIA) (Potter and Lambeck, 2003; Peltier, 2004; Scott et al., 2010; DeJong et al., 2015).

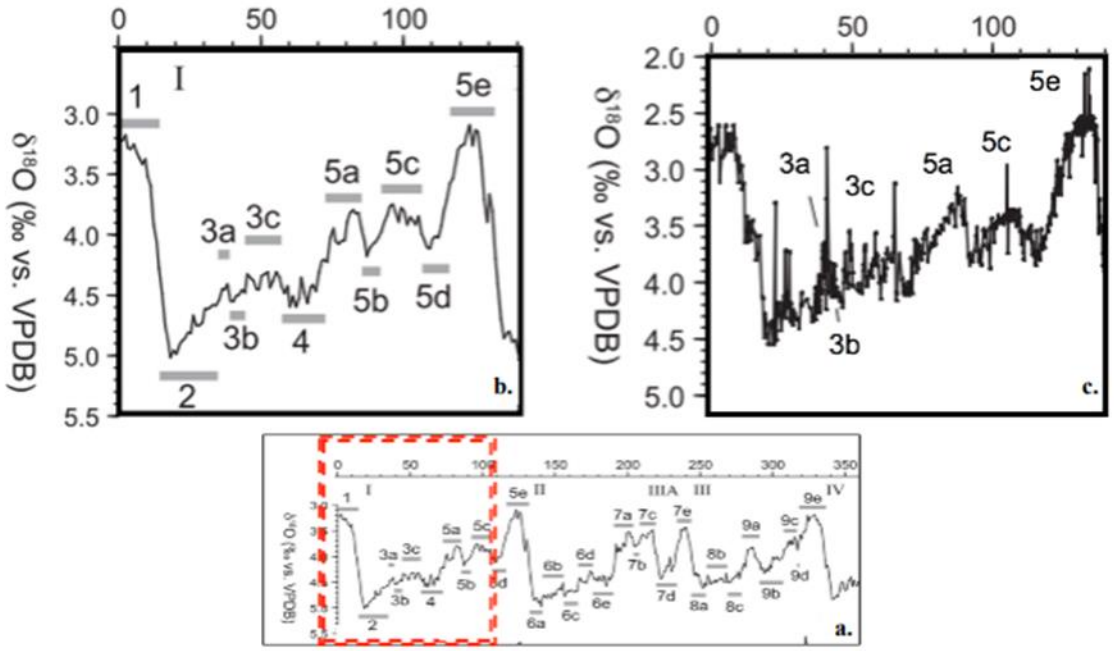

Figure 21. Marine benthic foraminiferal $\delta^{18}O$ data, adapted from Railsback (2015), encompassing marine isotope stages from 140,000 years ago to the present. **a.** Extended $\delta^{18}O$ data displaying marine isotope stages 1-9, starting from Termination IV. **b.** Marine isotope stages relevant to this study (MIS 1-5). **c.** North Atlantic marine record for MIS 1-5.

GIA refers to the Earth's lithosphere's response to the loading and unloading of glaciers as the climate transitions between glacial and interglacial periods (Whitehouse et al., 2021).During the penultimate glaciation (MIS 6, 191-135 ka; Liesecki and Raymo, 2005), the Laurentide Ice Sheet caused a forebulge as mantle material was displaced from the glaciated region to the periphery of the ice sheet (Scott et al., 2010; Stanford et al., 2016). Stanford et al. (2016) studied fluvial, glacial, and estuarine deposits in the Delaware River Basin of New Jersey to model uplift rates following glacier retreat during the middle and late Pleistocene. Their models suggest that the crest of the glacio-isostatic forebulge is located at the southern shore of Delaware Bay, about 200 km south of the late Wisconsinan (approximately 75,000 to 11,000 years ago) glacial limit. Potter and Lambeck (2003) observed that the trend in MIS 5a Caribbean sea-levels aligns with glacio-hydro-isostatic effects and the current non-equilibrium state of Earth's isostasy. They concluded that only by combining multiple ice and Earth model parameter changes can the high gradient in MIS 5a sea-level across the Western North Atlantic be accurately reproduced. A major component of the sea-level gradient is due to the subsidence of the forebulge as the ice sheets retreated and Termination II began (MIS 6-5 transition). This subsidence caused relative sea-level fluctuations to differ from the eustatic sea-level from MIS 6 to MIS 1 (Walcott, 1972; Chappell, 2002; Potter and Lambeck, 2003; Mallinson et al., 2008; Scott et al., 2010; Parham et al., 2013; DeJong et al., 2015; Stanford et al., 2016; Pico et al., 2017).

GIA is also observed in present-day northern North Carolina, including the study area. Mallinson et al. (2008) noted that current GIA in northeastern North Carolina amounts to approximately 26 meters above isostatic equilibrium conditions, with a subsidence rate of about 1 mm/year in response to ice sheet retreat during Termination I (around 20,000 to 10,000 years

ago) (Potter and Lambeck, 2003; Peltier, 2004; Kopp et al., 2015). This highlights the importance of considering isostatic effects when interpreting relative sea-level data and comparing different locations.

4.3 MIS 6 to MIS 5e (150 to120 ka)

Research in southern Virginia indicates that the earliest formation of the Suffolk Shoreline was linked to the erosion of interfluves during the MIS 5 transgression (Oertel and Foyle, 1995; Parham, 2009). As sea-level rose during the transition from MIS 6 to MIS 5 and land elevation subsided, these interfluves evolved into landward-eroding headlands, contributing to the formation of the Suffolk Shoreline. Parham et al. (2013) characterized MIS 5e deposits as shelly laminated mud and shelly sand extending from the Suffolk Shoreline eastward to Pamlico Sound on the Albemarle-Pamlico Peninsula. According to Parham et al. (2013), these MIS 5e deposits are overlain by OSL-dated MIS 5c and 5a deposits.

In this study, the lithofacies associated with MIS 5e, similar to those described by Parham (2013), consist of poorly sorted, strongly coarse-skewed shelly sand that thickens eastward. These deposits are overlain by MIS 5a deposits. Foraminiferal assemblages exhibit low diversity initially, with species diversity increasing upwards in the sequence (Figure 22). Pollen analysis also shows an increase in regional temperatures, indicating conditions warmer than today. Turner et al. (2013) found that conditions in Yukon, northern North America, during MIS 5e and 5a, are recorded by two boreal forest beds separated by a shrub birch tundra. These layers suggest that the MIS 5e and MIS 5a environments were as warm or warmer than present.

As sea levels rose from MIS 6 to MIS 5e, it is likely that the lower Neuse River flooded, resulting in the deposition of estuarine facies, which were subsequently overlain by marine

facies. The increase in foraminifera species diversity and regional temperatures supports this hypothesis.

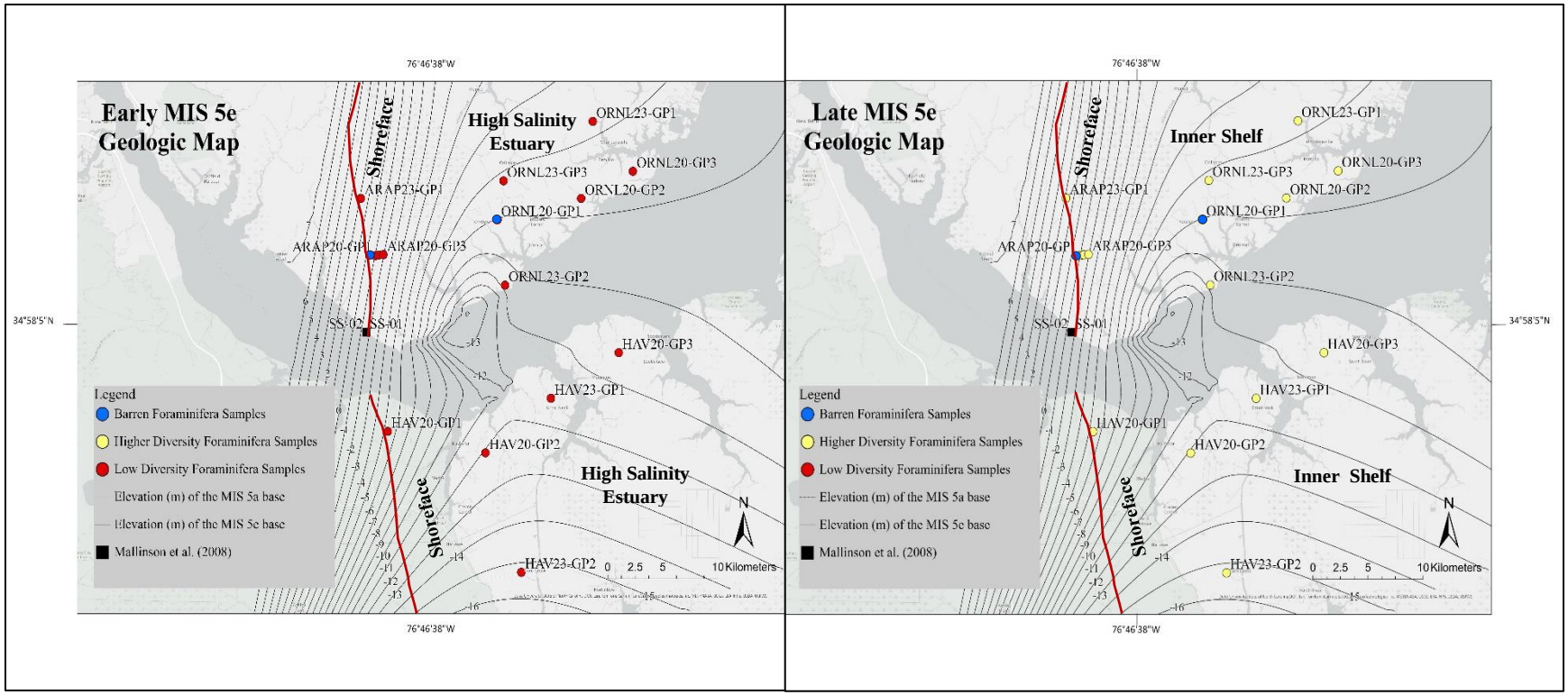

Figure 22. A) Early MIS 5e and B) Late MIS 5e maps showing the structure contour of the MIS 5e basal surface, interpreted paleoenvironments, and foraminifera species diversity increase.

4.4 MIS 5c to MIS 5a (110—70 ka)

Of the five substages of MIS 5, deposits from stage 5a (74 ka – 84 ka) are the most prevalent in coastal Virginia and North Carolina due to glacio-isostatic effects on regional topography (Mallinson et al., 2008; Scott et al., 2010; Parham et al., 2013). MIS 5a relative sea levels were recorded to be between +4 and +10 meters MSL in both North Carolina and Bermuda (Potter and Lambeck, 2004; Mallinson et al., 2008) (Figure 23).

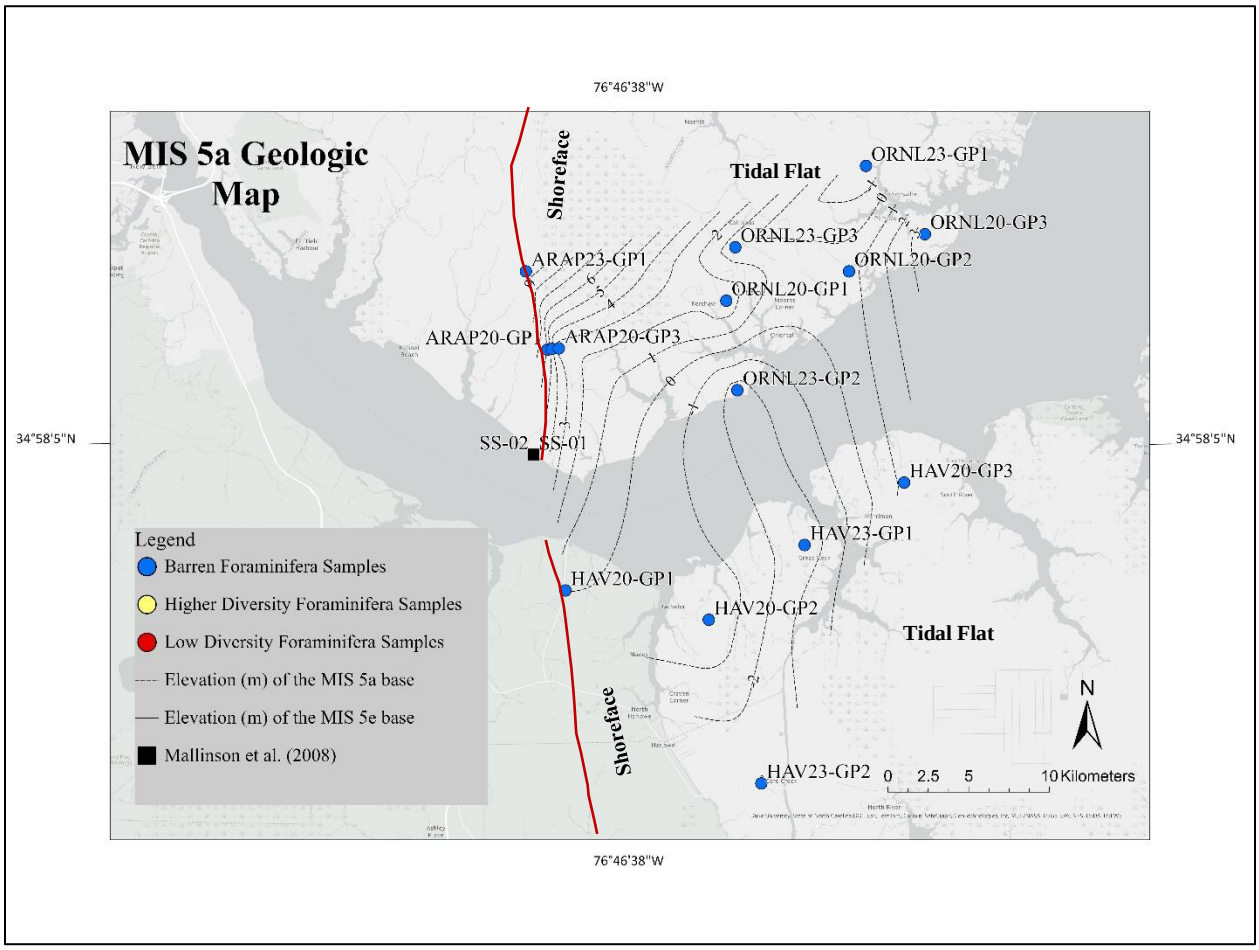

Figure 23. MIS 5a Geologic Map showing structure contour map of the MIS 5a basal surface, interpreted paleoenvironments, and barren foraminifera samples.

Thompson and Goldstein (2005) documented two sea-level highstands that contributed to the formation of the Suffolk Shoreline. Mallinson et al. (2008) identified two geomorphic features interpreted as relict shorelines along the Suffolk Shoreline between the Roanoke River and the Pamlico River. The westernmost ridge possibly represents a mainland-attached shoreline formed during the 84 ka sea-level peak, while the easternmost ridge may correspond to the shoreline formed during the 77 ka sea-level peak. Additionally, Mallinson et al. (2008) yielded an OSL age of approximately 80 ka along the Suffolk Shoreline on the Neuse River (Figure 24). It is likely that the geomorphic features recorded by Mallinson et al. (2008) are the result of the sea-level highstands identified by Thompson and Goldstein (2005) (Parham, 2009). Other dates from shelly substrates east of the scarp also fall within MIS 5a, supporting this timeframe (Cronin et al., 1981; Mixon et al., 1982; Wehmiller et al., 2004; Parham et al., 2009). Following Termination II and the onset of the Sangamon interglacial period (MIS 5), the subsidence of a peripheral forebulge, formed during the Illinoian glacial period (MIS 6), caused a rapid elevation decrease in the Virginia and North Carolina region from about +20 m at 130 ka to around -20 m at 80 ka (Scott et al., 2010).

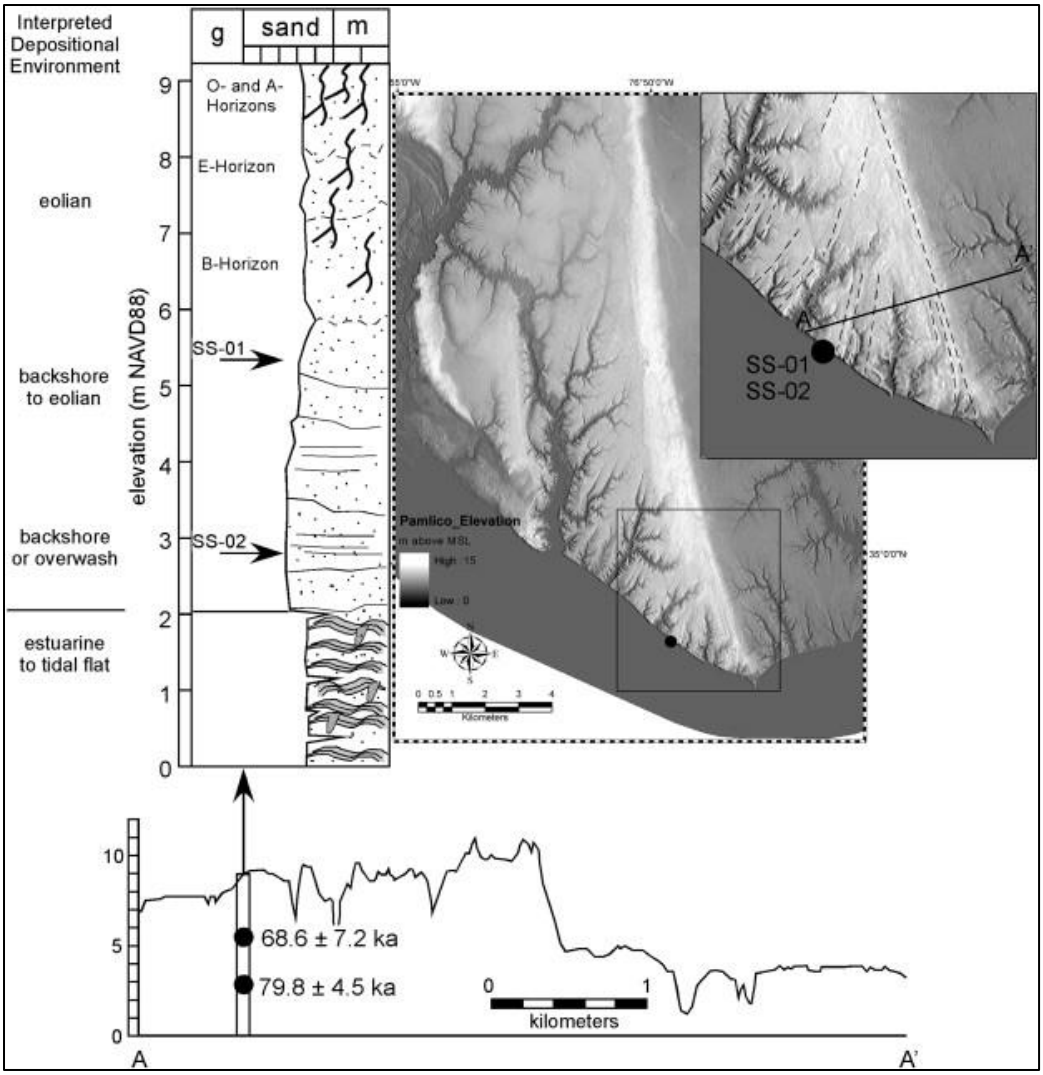

Figure 24. A LiDAR topographic map displays the sample locations from the Suffolk Ridge and the recurve spit/beach ridge morphology (inset, with dashed beach ridges). Additionally, it includes a topographic profile (bottom and A–A′ on the inset map) derived from LiDAR data, along with a stratigraphic column featuring interpretations from the sampled location. Adapted from Mallinson et al. (2008).

Parham et al. (2013) discovered that within interfluve core-hole transects in both the southern and northern parts of northeastern North Carolina, only thin deposits interpreted as MIS 5a are preserved east of the Suffolk Shoreline. These deposits included laminated sand,

laminated mud, sand, and gravelly sand (Figure 25). Parham hypothesized that the minimal occurrence of MIS 5a in these areas is likely due to limited accommodation space and/or subsequent erosion.

In this study, MIS 5a deposits are similarly characterized by burrowed laminated sand, sandy mud, and sand lithofacies, and are generally barren of foraminifera, with the exception of one sample. Depositional shoreface units are visible in the GPR data in Figure 16, corresponding to core ARAP23-GP1 and dated to MIS 5a, supporting the idea that sea level rose to occupy the study area during this time. The apparent tidal bedding and absence of foraminifera suggest that the MIS 5a deposits may represent coastal tidal flat environments.

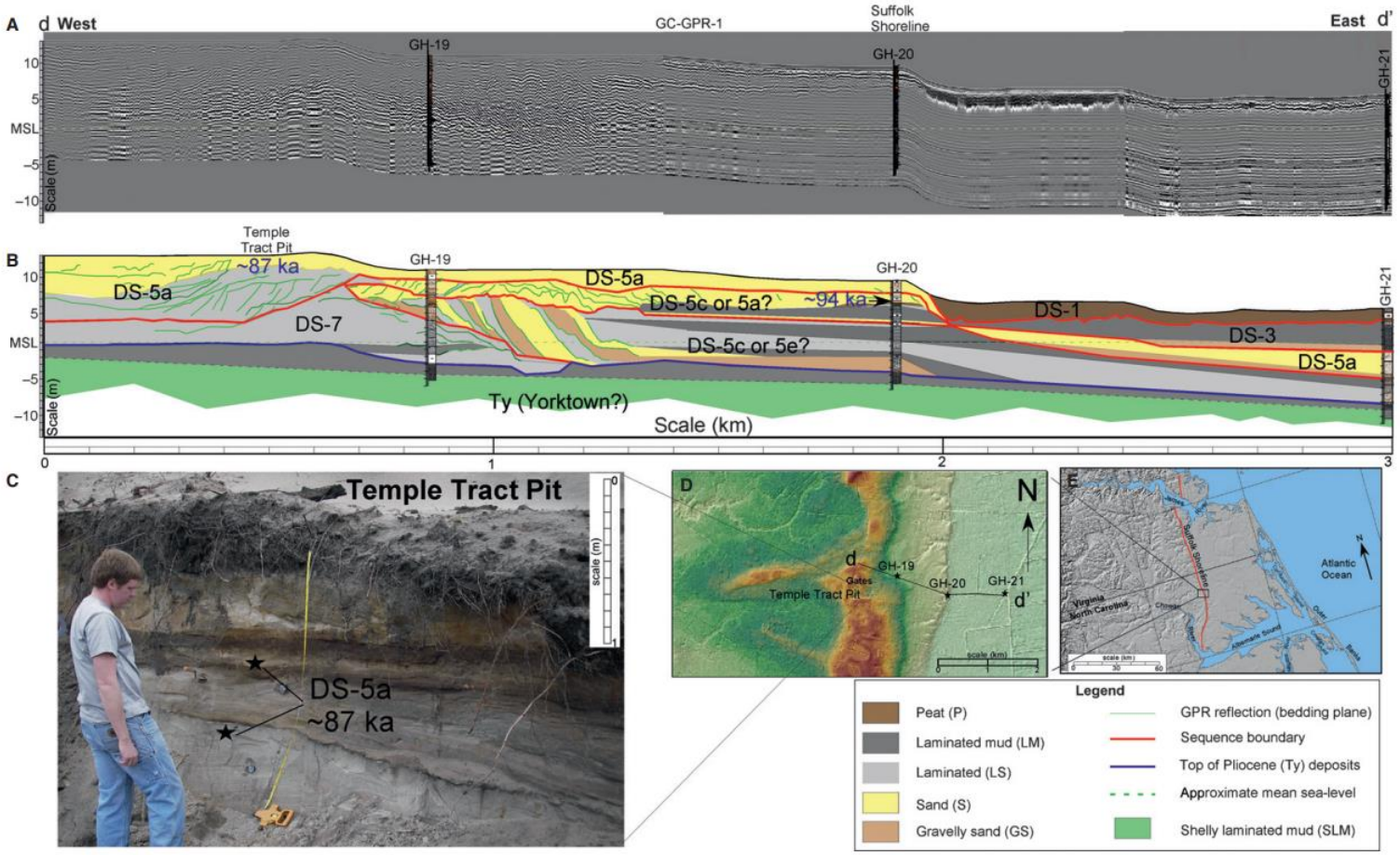

Figure 25. The raw ground penetrating radar (GPR) record (A) spans the Chowan Spit Complex of the Suffolk Shoreline in northeastern North Carolina, corresponding to the d–d' line on the LiDAR map (D). The lower stratigraphic cross-section (B) displays interpreted lithofacies, depositional sequences, and OSL ages. Panel (C) highlights the locations of two OSL samples and their sediment characteristics. From Parham et al. (2013).

4.5 MIS 4 to MIS 3 (70 to 40 ka)

The presence of terrestrial glaciers in North America, specifically the Laurentide Ice Sheet during the Wisconsinan glacial period (approximately 75,000 to 11,000 years ago), significantly influenced regional sea-level fluctuations along the western Atlantic coast through glacio-isostatic adjustment (GIA) (Potter and Lambeck, 2003; Peltier, 2004; Scott et al., 2010) (Figure 26). MIS 4 lies beyond the limits of radiocarbon dating, but there is a consensus that the decline in high-latitude Northern Hemisphere insolation around 70,000 to 80,000 years ago led to a major glacial interval across high-latitude and high-altitude areas of North America (Clark and Lea, 1992). If the initial glacial coverage during MIS 5 was limited to the uplands of the Canadian Arctic, the expansion to a full-fledged North American ice sheet must have been dramatic, given that the interval between MIS 5a and the insolation trough of MIS 4 was only 12,000 years. This rapid growth of the ice sheet may have been associated with more open-water conditions in the Labrador Sea and Baffin Bay, leading to enhanced mass accumulations and a rapid decrease in global sea level (Andrews and Dyke, 2013).

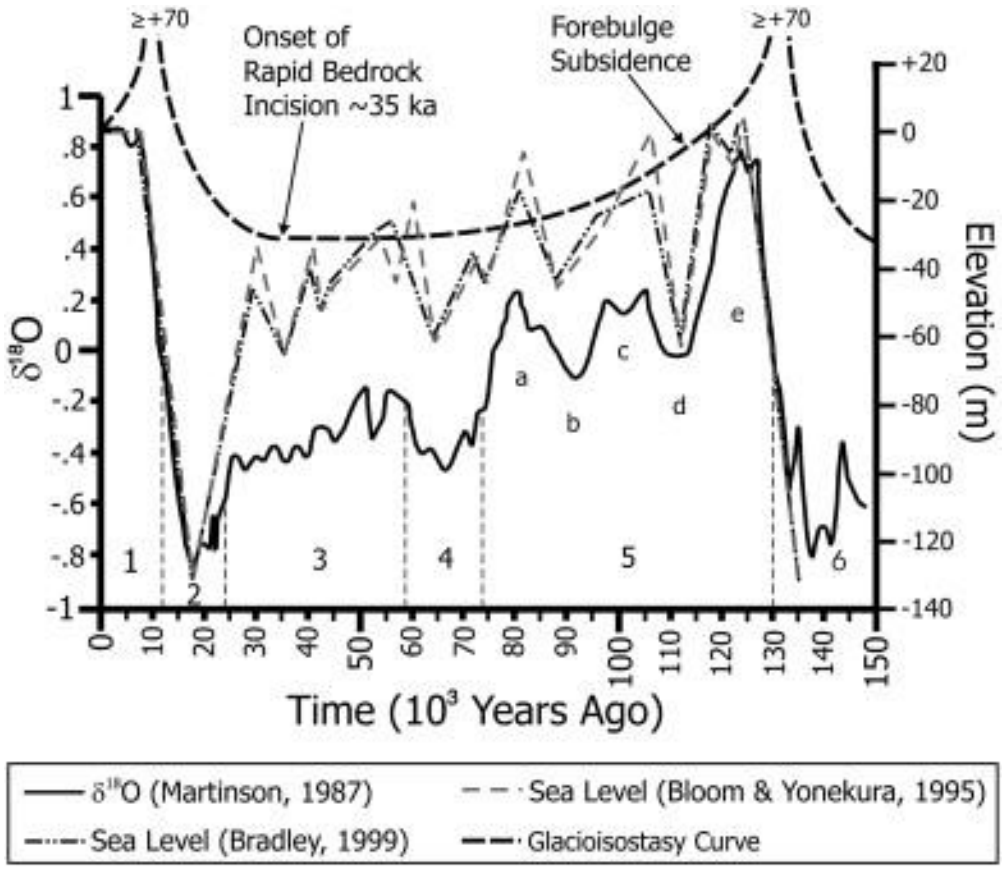

Figure 26. Adapted from Scott (2010), an estimated glacioisostatic curve is depicted alongside the $\delta^{18}O$ SPECMAP composite and eustatic sea-level curves from the Huon Peninsula in Papua New Guinea. Forebulge subsidence during MIS-5 and extending into MIS-3 likely facilitated shoreline deposition in Virginia during MIS-3.

In North Carolina, little is known about MIS 4. The relatively short duration of glaciation during MIS 4 likely did not significantly influence this region isostatically, resulting in a rheological state during MIS 3 similar to that present during late MIS 5 (Parham et al., 2013). Evidence from the inner shelves of Texas (Rodriguez et al., 2000) and New Jersey (Wellner et al., 1993) indicates MIS 3 shorelines at -15 m and -20 m, respectively. However, findings from Mallinson et al. (2008) suggest near-to-present sea levels during MIS 3 in northeast North Carolina. Gudmunson (2022) recovered medium-to-fine-grained sand facies from an interfluve

east of the Yeopim River in the Albemarle Sound, dating to 68.8 ± 5.4 ka. These findings are consistent with mid-to-late MIS 4 and were interpreted as aeolian deposits.. Regression during MIS 4 may have exposed sediment from a shallow MIS 5 marine shoal or shoreface sands south of the Neuse River. As these sand facies became exposed at the land surface, aeolian forces likely reworked the sand into dunes (Burdette and Mallinson, 2008; Parham et al., 2013). Similar data are shown in Figures 20 and 21, where OSL results yielded ages corresponding to MIS 4. The lithofacies associated with these deposits consist of well-sorted, fine-grained sand, barren of foraminifera. This suggests that the sediment south of the river was incised, allowing the exposed sediment to be reworked into dunes.

The stratigraphic and age evidence indicate that during MIS 3, relative sea level was notably higher, estimated to be at least 3 meters above present sea level. Numerous Optically Stimulated Luminescence (OSL) ages obtained from estuarine, paleoshoreline, and marine deposits within the MIS 3 timeframe provide supporting data (Parham, 2009; Burdette, 2006; Scott, 2006; Mallinson et al., 2008; K. Best, pers. comm., 2009). Deposits within the Lynnhaven, Poquosin, and Sedgefield Members of the Tabb Formation in Virginia were laid down during this period (Johnson, 1977). OSL ages from Scott (2006) indicate that sea level was potentially up to approximately 5 meters above present during early MIS 3, covering parts of the Suffolk Shoreline.

During MIS 3, GIA subsidence was at a maximum further north, leading to the formation of coastal deposits such as paleoshorelines and tidal flat deposits in northeastern North Carolina and Virginia. Similarly, several paleo-barrier islands developed on the Pamlico Terrace, prominently observed in the Norfolk Arch area (Parham et al., 2009) (Figure 27). In contrast, the lower Neuse River Basin experienced minimal GIA subsidence, resulting in limited

accommodation space and a lack of MIS 3 deposition. Consequently, no OSL ages corresponding to MIS 3 have been found in the Lower Neuse River Basin.

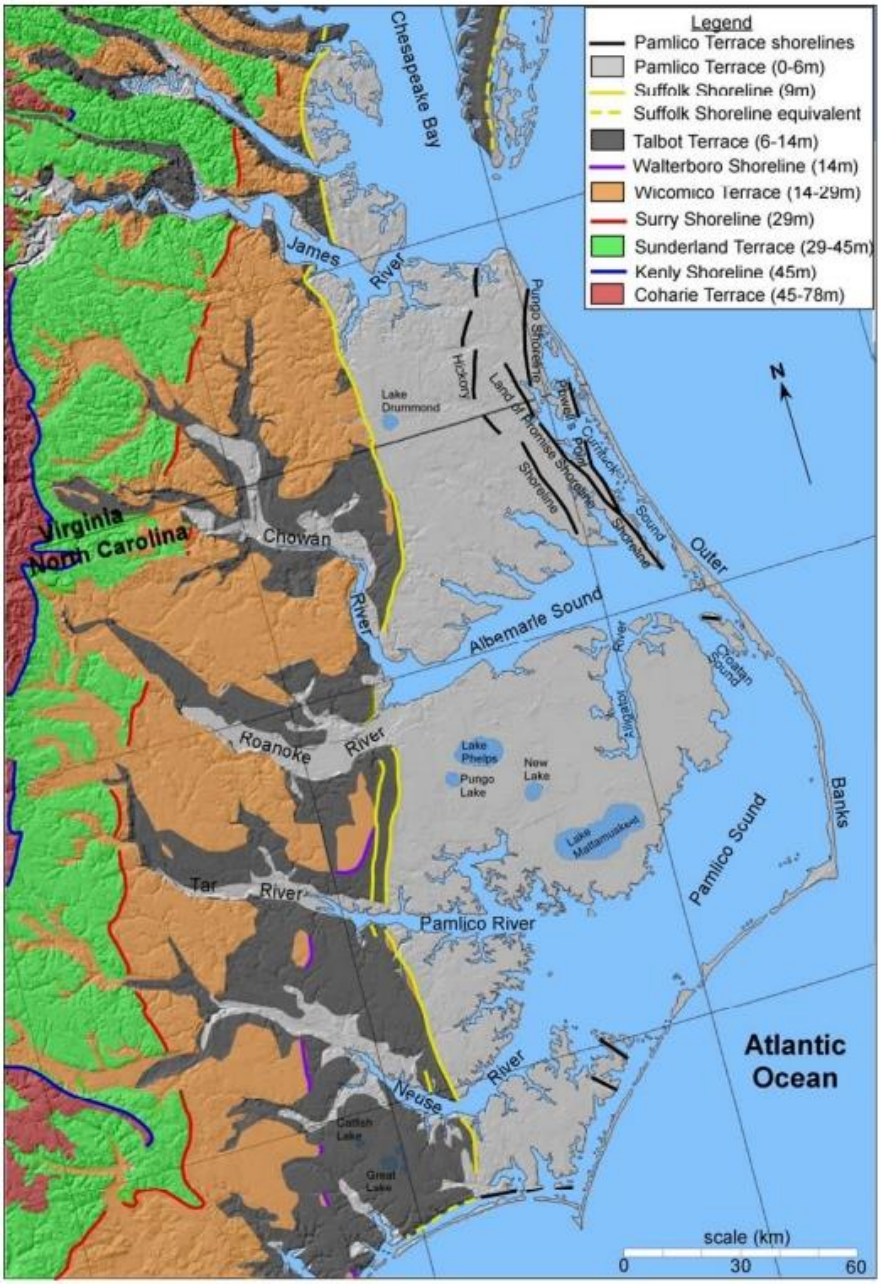

Figure 27. A shaded relief map depicting terraces and paleoshoreline positions in southeastern Virginia and northeastern North Carolina, adapted from Parham et al. (2009).

4.6 Expectations for the Future

The sequence of deposition, the variation in lithofacies, and the nature of unconformities, such as erosional surfaces observed in the cores, provide a historical account of environmental changes during individual sea-level cycles. Given the repetitive nature of sea-level cycles, the future evolution of the coast can be somewhat predictable based on past sea-level events. If sediments indicative of specific environments associated with sea-level highstands appear in older depositional sequences but are absent in the current Holocene sedimentary record, it suggests that these highstand environments may develop in the future with continued sea-level rise and potential disruptions to the barrier-island system by storm processes. For instance, extensive tidal deposits on interfluves are consistently found in Pleistocene depositional sequences within the study area, whereas they are restricted to valley fill in the Holocene section (Sager and Riggs, 1998). Additionally, the high fossil content of most Pleistocene shelly marine deposits, particularly concentrated shell beds, indicates elevated benthic productivity and suggests a more productive aquatic system in response to higher sea levels or increased interaction with marine waters.

The impact of rising sea level on coastal areas is not merely a matter of elevating water levels, but rather involves complex interactions between sedimentary responses and ecosystem dynamics as base level and coastal dynamics change. The influence of increased sea levels during MIS 3 and MIS 5a offers clues about potential future scenarios with continued sea-level rise. The IPCC's Assessment Report (AR6) from 2021 provides short-term predictions of sea-level rise along the east coast of North America, suggesting a rise of approximately 1 meter by the end of the 21st century. Considering ongoing peripheral forebulge subsidence in the region, coastal North Carolina is expected to experience accelerated sea-level rise compared to the North

American East Coast north of New Jersey (approximately Latitude 40°30') (Stanford et al., 2016).

Based on the IPCC AR6 projections, it is anticipated that by the end of the 23rd century, regional sea level could rise by more than 3 meters above current levels, potentially leading to coastal conditions similar to those observed during MIS 3 (Parham et al., 2013). This scenario would transform the coast of North Carolina into a tidally influenced inner shelf environment resembling the modern Georgia Coast (Figure 28). The modern Georgia coast is characterized by a series of short, wide barrier islands extensive tidal flats, coastal wetlands, and complex sediment distribution patterns (Hayes and Michel, 2013) (Figure 29). Seaward of the inlets and central portions of the islands, extensive sand shoal systems are present. The average tidal range is just over six feet, with seasonal spring tides reaching up to ten feet, the highest along the U.S. South Atlantic coast (Henry, 2019). The geological development of the Georgia coast is significantly influenced by the large, cyclical storage capacity of the tidal marshlands behind the barrier islands. The six- to ten-foot tides drive nearshore waters in and out of the sounds through the constricted inlets between the barrier islands (Henry, 2019). Over the past several thousand years, the modern tidal marshlands have formed as Holocene sea-levels gradually rose. Similarly, if sea levels continue to rise, the Lower Neuse River Basin is expected to transition into a tidally influenced inner shelf environment comparable to that of the Georgia coast.

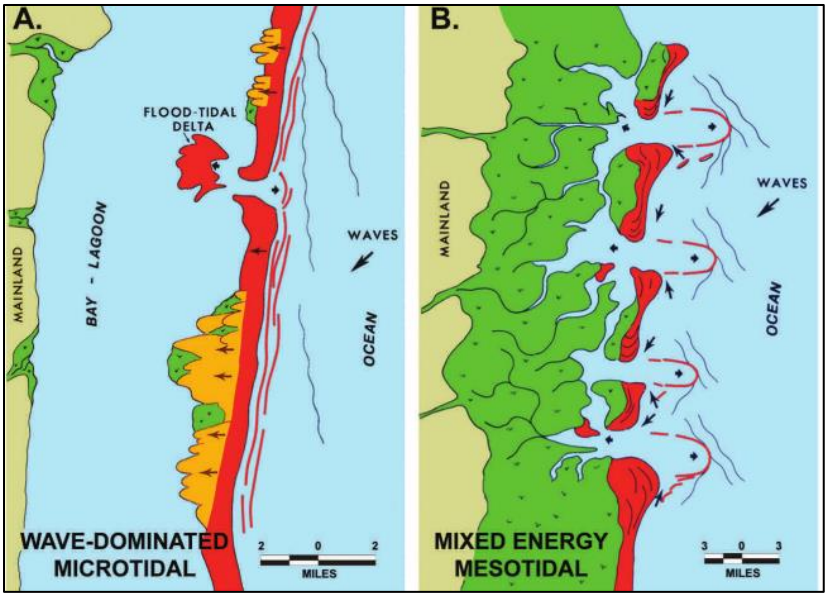

Figure 28. Generalized model of two fundamental types of depositional coasts. Panel A illustrates wave-dominated coasts, typically microtidal with a tidal range less than 6 feet, exemplified by the modern North Carolina Coast. Panel B represents mixed-energy coasts, usually mesotidal with a tidal range of 6-12 feet, showcasing the modern Georgia Coastline. In Panel A, red lines denote nearshore, subtidal wave-formed sand bars, while in Panel B, they indicate sand deposits.

5.0 Conclusions

The shallow stratigraphy of the lower Neuse River east of the Suffolk Shoreline reveals the geomorphic evolution of late Pleistocene paleoenvironments. Stratigraphic sequences, defined by their lithology and chronology, illustrate how the study area responded to sea level during MIS 5 and MIS 4. Geomorphologic interpretations for this study relied on lithologic correlations with surrounding studies, foraminiferal analysis, pollen analysis, geophysical interpretations, and OSL ages to constrain environments and chronology.

These data indicate the presence of multiple paleoenvironments with distinctive facies corresponding to MIS 5e, MIS 5a, and MIS 4. MIS 5e is characterized by shelly sand with increasing foraminiferal species diversity upwards in the sequence . Pollen analysis also shows an increase in regional temperatures, indicating conditions warmer than today. As sea levels rose from MIS 6 to MIS 5e, the lower Neuse River likely flooded, resulting in the deposition of estuarine facies, which were subsequently overlain by marine facies. Transitioning into MIS 5a, the study area experienced a return to highstand conditions. The facies during this period are characterized by burrowed laminated sand, sandy mud, and sand, and barren of foraminifera, indicating coastal tidal flat deposits. Regression during MIS 4 likely led to the incision of the Neuse River channel into MIS 5 marine deposits, exposing sediment from a shallow marine shoal in cores south of the river. As these sand facies were exposed at the land surface, aeolian forces likely reworked the sand into dunes.

References

Abbene, I.J., Culver, S.J., Corbett, D.R., Buzas, M.A., Tully, L.S., 2006. Distribution of foraminifera in Pamlico Sound, North Carolina over the past century. Journal of Foraminiferal Research, v. 36, 136–151.

Andrews, J. T., & Dyke, A. S. 2013. Glaciations | late quaternary in North America. Encyclopedia of Quaternary Science, 245–249. https://doi.org/10.1016/b978-0-444-53643-3.00120-5.

Burdette, K. E. 2006.Chronostratigraphy and geologic framework of the Currituck sand ridges, Currituck County, NC. MS thesis. . Department of Geology, East Carolina University, Greenville, NC, 184 pp.

Burdette, K. E. and Mallinson, D. J. (2008) Geologic framework of the Currituck Sand Ridges, Northeastern North Carolina. Southeast. Geol., 46, 1–15.

Chappell, J., Omura, A., Esat, T., McColloch, M., Pandolfi, J., Ota, Y., and Pillans, B., 1996. Reconciliation of Late Quaternary sea levels derived from coral terraces at Huon Peninsula with deep sea oxygen isotope records: Earth and Planetary Science Letters, v. 141, p. 227–236.

Chua, V. P., and Ming X. 2014, Impacts of Sea-Level Rise on Estuarine Circulation: An Idealized Estuary and San Francisco Bay. Journal of Marine Systems, vol. 139, Elsevier B.V. pp. 58–67.

Clark, P. U., & Lea, P. D. (1992). The last interglacial-glacial transition in North America. Geological Society of America.

Cronin, T. M., Szabo, B. J., Ager, T. A., Hazel, J. E., and Owens, J. P., 1981, Quaternary climates and sea levels of the US Atlantic coastal plain: Science, v. 211, p. 233-240.

Culver, S.J., Buzas, M.A., 1980. Distribution of recent benthic foraminifera off the North American Atlantic coast: Smithsonian Contributions to the Marine Sciences, v.6, 512 p.

Culver, S.J., Farrell, K., Mallinson, D., Horton, B., Willard, D.A., Thieler, E.R., Riggs, S.R., Snyder, S. W., Wehmiller, J.F., Bernhardt, C.E., and Hillier, C., 2008. Micropaleontological record of late Pliocene and Quaternary paleoenvironments in the Northern Albemarle Embayment, North Carolina, U.S.A.: Paleogeography, Paleoceanography, Paleoecology, v. 264, p. 54–77.

Culver, S.J., Farrell, K.M., Mallinson, D.J., Willard, D.A., Horton, B.P., Riggs, S.R., Thieler, E.R., Wehmiller, J.F., Parham, P.R., Moore, J.P. and Snyder, S.W., 2016. Micropaleontologic record of Pliocene and Quaternary paleoenvironments in the southern Albemarle Embayment, North Carolina, USA. Palaeogeography, Palaeoclimatology, Palaeoecology, *457*, pp.360-379.

Davis RB, Webb T. The Contemporary Distribution of Pollen in Eastern North America: A Comparison with the Vegetation. Quaternary Research. 1975;5(3):395-434.

DeJong, B., Bierman, P., Newll, W., Rittenour, T., Mahan, S., Balco, G., Rood, D., 2015. Pleistocene relative sea levels in the Chesapeake Bay region and their implications for the next century: GSA Today, v.25, p. 4–10.

Emiliani, C., 1955. Pleistocene temperatures: Journal of Geology, v. 63, p. 538–578.

Daidu, F., Yuan, W., & Min, L. 2013. Classifications, sedimentary features and facies associations of tidal flats. Journal of Palaeogeography, 2, 66-80.Farrell, K. M., Harris, W. B., Mallinson, D. J., Culver, S. J., Riggs, S. R., Wehmiller, J. F., Lautier, J. C., 2013. Graphic logging for interpreting process-generated stratigraphic sequences and aquifer/reservoir potential: With analog shelf to shoreface examples from the Atlantic coastal plain province, U.S.A.: Journal of Sedimentary Research, v. 83, p.723–745.

Folk, R. L., 1974. Petrology of sedimentary rocks. Hemphill Publishing Co., Austin, TX, p. 182.

Grand Pre, C., Culver, S., Mallinson, D., Farrell, K., Corbett, D., Horton, B., Hillier, C., Riggs, S., Snyder, S., and Buzas, M., 2011. Rapid Holocene coastal change revealed by high-resolution micropaleontological analysis, Pamlico Sound, North Carolina, USA. Quaternary Research, 76(3), pp.319-334.

Gudmunson, E.K., 2022. Defining the Stratigraphic and Paleoenvironmental Record of Rapid Sea-Level Rise During the Late Pleistocene to Holocene in the Albemarle Sound Region of North Carolina. East Carolina University.

Hayes, M. O., & Michel, J. 2013. A tide-swept coast of sand and Marsh: Coastal Geology and ecology of Georgia. Pandion Books, a division of Research Planning, Inc.

Henry, V. 2019 "Geology of the Georgia Coast." New Georgia Encyclopedia, https://www.georgiaencyclopedia.org/articles/science-medicine/geology-of-the-georgia-coast/

IPCC, 2023: Climate Change 2023: Synthesis Report. Contribution of Working Groups I, II and III to the Sixth Assessment Report of the Intergovernmental Panel on Climate Change [Core Writing Team, H. Lee and J. Romero (eds.)]. IPCC, Geneva, Switzerland, pp. 35-115, doi: 10.59327/IPCC/AR6-9789291691647.

Kemp, A.C., Horton, B.P., and Culver, S.J., 2009. Distribution of modern salt-marsh foraminifera in the Albemarle-Pamlico estuarine system of North Carolina, USA: Implications for sea-level research. Marine Micropaleontology 72: 222-238.

Kemp, A.C., Horton, B.P., Culver, S.J., Corbett, D.R., van de Plassche, O., Gehrels, W.R., Douglas, B.C., 2009. The timing and magnitude of recent accelerated sealevel rise (North Carolina, USA). Quaternary Research 71: 9-21.

Komar, P.D., 1998. Beach Processes and Sedimentation. Prentice-Hall. 2nd ed.

Kopp, R. E., Hoerton, B. P., Kemp, A. C., Tebaldi, C., 2015. Past and future sea-level rise along the coast of North Carolina, USA: Climate Change, v. 130.Lindsey, R. 2022. Climate change: Global sea level. NOAA Climate.gov.

Krumbein, W. C.1934. Size frequency distributions of sediments. SEPM Journal of Sedimentary Research, Vol. 4

Lazar, K. B., Mallinson, D. J., & Culver, S. J., 2016. Late Quaternary development of the Croatan Beach ridge complex, Bogue sound, Bogue banks, NC, USA and implications for coastal evolution. Estuarine, Coastal and Shelf Science, 174, 49-64.

Lisiecki, L. E., & Raymo, M. E. 2005. A Pliocene-Pleistocene stack of 57 globally distributed benthic δ^{18}O records. Paleoceanography, 20(1). https://doi.org/10.1029/2004pa001071 Mallinson, D., Riggs, S.R., Thieler, E.R., Foster, D., Culver, S.J., Corbett, D.R., Hoffman, C.W., Wehmiller, J.F., 2005. Late Neogene evolution of the northeastern North Carolina coastal system: filling the northern Albemarle Embayment: Marine Geology, v. 217, p. 97–117.

Mallinson, D., Burdette, K., Mahan, S., and Brook, G., 2008. Optically stimulated luminescence age controls on late Pleistocene and Holocene coastal lithosomes, North Carolina, USA: Quaternary Research, v. 69, p. 97–109.

Mallinson, D., Culver, S., Riggs, S., Thieler, E., Foster, D., Wehmiller, J., Farrell, K., and Pierson, J., 2010. Regional seismic stratigraphy and controls on the Quaternary evolution of the Cape Hatteras region of the Atlantic passive margin, USA. Marine Geology, 268(1-4), pp.16-33.

Masterson, J.P., Fienen, M.N., Thieler, E.R., Gesch, D.B., Gutierrez, B.T. and Plant, N.G. 2014. Effects of sea-level rise on barrier island groundwater system dynamics – ecohydrological implications. Ecohydrol., 7: 1064-1071.

Miller, G.H., Mode, W.N., Wolfe, A.P., Sauer, P.E., Bennike, O., Forman, L.L., Short, S.K., Stafford, T.W., 1999. Stratified interglacial lacustrine sediments from Baffin Island, Arctic Canada: chronology and paleoenvironmental implications. Quaternary Science Reviews 18, 789–810.

Mixon, R. B., Szabo, B. J., and Owens, J. P., 1982, Uranium-series dating of mollusks and corals, and age of Pleistocene deposits, Chesapeake Bay area, Virginia and Maryland: US Geological Survey Professional Paper 1067-E, 18 p.

Mixon, R. B., Berquist Jr., C. R., Newell, W. L., Johnson, G. H., Powars, D. S., Schindler, J. S., Rader, E. K., 1989. Geologic map and generalized cross sections of the coastal plain and adjacent parts of the Piedmont, Virginia: U.S. Geol. Surv. Misc. Invest. Ser., Map I-2033

Munsterman, D., Kerstholt, S., 1996. Sodium polytungstate, a new non-toxic alternative to bromoform in heavy liquid separation: Review of Palaeobotony and Palynology, v. 91, p 417–422.

Murray, J.W., 1969. Recent Foraminifers from the Atlantic Continental Shelf of the United States. Micropaleontology 15: 401-419.

Murray, A. S., Wintle, A. G., 2000. Luminescence of dating of quartz using an improved single-aliquot regenerative dose protocol: Radiation Measurements, v. 32, p. 57–73.

Oertel, G. F. and Foyle, A. M., 1995, Drainage displacement by sea-level fluctuation at the outer margin of the Chesapeake seaway: Journal of Coastal Research, v. 11, p. 583-604.

Parham, P.R., Riggs, S.R., Culver, S.J., Mallinson, D.J., and Wehmiller, J.F., 2007. Quaternary depositional patterns and sea-level fluctuations, northeastern North Carolina: Quaternary Research, v. 67, p. 83–99.

Parham, Peter R., 2009. The late quaternary stratigraphy and geologic history of northeastern North Carolina and southeastern Virginia [Ph.D. thesis]: Greenville, North Carolina, East Carolina University, p. 315.

Parham, P. R., Riggs, S. R., Culver, S. J., Mallinson, D. J., Rink, W. J., and Burdettes, K., 2013. Quaternary coastal lithofacies, sequence development and stratigraphy in a passive margin setting, North Carolina and Virginia, USA: Sedimentology, v. 60, p. 503–547.

Peltier, W. R., 2004. Global glacial isostasy and the surface of the ice-age Earth: the ICE5G (VM2) Model and GRACE: Annual Review of Earth and Planetary Sciences, v. 32, p. 111–149.

Pettijohn, F. J. 1975. Sedimentary rocks. 3rd ed. New York: Harper & Row.

Pisias, N.G., and Moore, T.C.Jr., 1981. The evolution of the Pleistocene climate: A time series approach. Earth and Planetary Science Letters 52, 450–458.

Potter, E., Lambeck, K., 2003. Reconcilliation of sea-level observations in the Western North Atlantic during the last glacial cycle: Earth and Planetary Science Letters, v. 217, p. 171–181.

Riggs, S. R., York, L. L., and Wehmiller, J. H., 1992. Depositional patterns resulting from high-frequency quaternary sea-level fluctuations in northeastern North Carolina: Quaternary coasts of the United States: Marine and lacustrine systems: SEPM special publication. v. 48, p.141–153.

Riggs, S. R. and Ames, D.V., 2003. Drowning the North Carolina coast: sea-level rise and estuarine dynamics: North Carolina Sea Grant Program: North Carolina State University, Raleigh, North Carolina, 152 p.

Robinson, M. M., & McBride, R. A. 2006. Benthic foraminifera from a relict flood tidal delta along the Virginia/north carolina outer banks. Micropaleontology, *52*(1), 67–80.

Rodriguez, A. B., Anderson, J. B., Banfield, L. A., Taviani, M., Abdulah, K., & Snow, J. N. 2000. Identification of A −15 m Wisconsin shoreline on the Texas Inner Continental Shelf. Palaeogeography, Palaeoclimatology, Palaeoecology, 158(1–2), 25–43.

Schnitker, D., 1971. Distribution of foraminifera on the North Carolina continental shelf: Tulane Studies in Geology and Paleontology, v.8.Scott, T.W., Swift, D.P.J., Whittecar, G. R., and Brook, G. A., 2010. Glacioisostatic influences on Virginia's late Pleistocene coastal plain deposits: Geomorphology, v. 116, p. 175–188.

Scott, T.W., Swift, D.J.P., Whittecar, G.R., Brook, G.A., 2010. Glacioisostatic influences on Virginia's Late Pleistocene Coastal Plain Deposits. Geomorphology.

Shmorhun, N., Culver, S., Mallinson, D., Farrell, K., Cressman, A., Grove, A., Howie, L., Lynn, A., Sutton, S., Twarog, M. and Riggs, S.R., 2022. Characterizing Modern and Holocene Barrier-Island Environments with Foraminiferal Assemblages: an Example from a Wave-Dominated, Microtidal Barrier-Island System, North Carolina, USA. Palaios, 37(8), pp.443-470.

Siddal, M., Rohling, E. J., Thompson, W. G., Waelbroech, C., 2008. Marine isotope stage 3 sea level fluctuations: Data synthesis and new outlook: Reviews of Geophysics, v. 46.

Stanford, S.D., Witte, R.W., Braun, D.D., Ridge, J.C., 2016. Quaternary Fluvial History of the Delaware River, New Jersey and Pennsylvania, USA: The Effects of Glaciation, Glacioisostasy, and Eustasy on a Proglacial River System. Geomorphology, vol. 264, Elsevier B.V., pp. 12–28

Stutz M.L., Pilkey O.H., 2011. Open-ocean barrier islands: influence of climatic, oceanographic and depositional settings. J Coast Res 27:207–222.

Thompson, W. G. and Goldstein, S. L., 2005, Open-system coral ages reveal persistant suborbital sea-level cycles: Science, v. 308, p. 401-404.

Turner, D. G., Ward, B. C., Bond, J. D., Jensen, B. J., Froese, D. G., Telka, A. M., Bigelow, N. H. 2013. Middle to Late Pleistocene ice extents, tephrochronology and paleoenvironments of the White River area, southwest Yukon. Quaternary Science Reviews, 75, 59-77.Vance, D. J., Culver, S. J., Corbett, D. R., Buzas, M. A., 2006. Foraminifera in the Albemarle Estuarine System, North Carolina: distribution and recent environmental change. Journal of Foraminiferal Research, v. 36, p.15–33.Ward, L. W., Strickland, G. L., 1985. Outline of Tertiary stratigraphy and depositional history of the U.S. Atlantic Margin. In: Poag, C. W. (Ed.), Geologic Evolution of the United States Atlantic Margin: Van Nostrand Reinhold Co., New York, p. 125–188.

Welcome to North Carolina's Spatial Data Download. North Carolina Spatial Data Download. https://sdd.nc.gov/sdd/

Wehmiller, J.F., Thieler, E.R., Miller, D., Pellerito, V., Bakeman Keeney, V., Riggs, S.R., Culver, S., Mallinson, D., Farrell, K.M., York, L.L., Pierson, J., Parham, P.R., 2010.

Aminostratigraphy of Surface and Subsurface Quaternary Sediments, North Carolina Coastal Plain, USA. Quaternary Geochronology, vol. 5, no. 4, Elsevier Ltd, pp. 459–92.

Wellner, R.W., Ashley, G.M., Sheridan, R.E., 1993. Sheridan Seismic stratigraphic evidence for a submerged middle Wisconsinan barrier: implications for sea-level history. Geology, 21 (1993), pp. 109-112.

Whitehouse, P., Milne, G., Lambeck, K. 2021. Glacial Isostatic Adjustment. In: Fowler, A., Ng, F. (eds) Glaciers and Ice Sheets in the Climate System. Springer Textbooks in Earth Sciences, Geography and Environment. Springer, Cham.

Willard, D.A., Cronin, T.M. and Verardo, S., 2003. Late-Holocene climate and ecosystem history from Chesapeake Bay sediment cores, USA. The Holocene, 13(2), pp.201-214.

Wintle, A. G., Murray, A. S., 2006. A review of quartz optically stimulated luminescence characteristics and their relevance in single-aliquot regenerative dating protocols: Radiation Measurements, v. 41, p. 369–391.

Wolfe, A.P., Frechette, B., Richard, P.J.H., Miller, G.H., Forman, S.L., 2000. Paleoecology of a N90,000-year lacustrine sequence from Fog Lake, Baffin Island, Arctic Canada. Quaternary Science Reviews 19, 1677–1699.

Workman, R. R., 1981, Foraminiferal Assemblages of the Nearshore Inner Continental Shelf, Nags Head and Wilmington Areas, North Carolina, Unpublished Master's Thesis, East Carolina University, Greenville, NC, 161 p.

Zaremba, N., Mallinson, D. J., Leorri, E., Culver, S., Riggs, S., Mulligan, R., and Mitra, S., 2016. Controls on the stratigraphic framework and paleoenvironmental change within a Holocene estuarine system: Pamlico sound, North Carolina, USA: Marine Geology, v. 379, p. 109–123.

Zervas, C. E., 2004, North Carolina bathymetry/topography sea-level rise projcet: determination of sea-level trends: NOAA Technical Report NOS CO-OPS 041, 31 p.

APPENDIX A: GEOPROBE CORE LOCATIONS

Location and depths of cores. Elevation is relative to NAVD88 datum.

Core ID	Longitude	Latitude	Elevation (m)	Penetration (m)
ARAP20-GP1	-76.82305556	35.02527778	7.3	3.7
ARAP20-GP2	-76.82055556	35.02555556	5.2	4.9
ARAP20-GP3	-76.81666667	35.02583333	4.0	4.9
ORNL20-GP1	-76.72361111	35.0475	2.4	3.7
ORNL20-GP2	-76.55527778	35.06083333	0.6	6.1
ORNL20-GP3	-76.61305556	35.07777778	1.5	5.1
HAV20-GP1	-76.81305556	35.91555556	7.0	4.9
HAV20-GP2	-76.73333333	35.90222222	4.3	6.1
HAV20-GP3	-76.62472222	35.96472222	1.8	4.9
ARAP23-GP1	-76.8351	35.0609	12.8	4.9
ORNL23-GP1	-76.6459	35.10881	1.2	3.7
ORNL23-GP2	-76.7174	35.0068	2.7	6.1
ORNL23-GP3	-76.7186	35.07184	2.7	7.3
HAV23-GP1	-76.68	34.93629	2.1	6.1
HAV23-GP2	-76.7041	34.82765	1.8	4.9

APPENDIX B: GRAIN SIZE ANALYSIS

Core Sample	Depth below ground surface (cm)	Sorting Φ	Skewness Φ	Mean Φ	Sediment Type
ORNL 20-GP1	205	0.379	-0.016	2.66	Well Sorted Fine Sand
ORNL 20-GP1	336	0.407	-0.602	2.94	Well Sorted Fine Sand
ORNL 20-GP2	176	0.437	-1.33	3.05	Well Sorted Very Fine Sand
ORNL 20-GP2	270	0.417	-0.793	2.98	Well Sorted Fine Sand
ORNL 20-GP2	428	1.83	-0.971	1.63	Poorly Sorted Medium Sand
ORNL 20-GP2	551	1.29	-0.893	2.08	Poorly Sorted Fine Sand
ORNL 20-GP3	186	0.513	-1.47	2.90	Moderately Well Sorted Fine Sand
ORNL 20-GP3	260	0.465	-1.62	3.27	Well Sorted Very Fine Sand
ORNL 20-GP3	304	0.522	-3.23	2.84	Moderately Well Sorted Fine Sand
ORNL 20-GP3	450	1.53	-1.94	2.68	Poorly Sorted Fine Sand
ORNL 20-GP3	476	0.987	-1.17	2.57	Moderately Sorted Fine Sand
ORNL 20-GP3	546	1.66	-0.802	1.52	Poorly Sorted Medium Sand
ARAP 20-GP1	87-89	0.513	-1.25	2.38	Moderately Well Sorted Fine Sand
ARAP 20-GP1	290	0.697	-1.14	2.37	Moderately Well Sorted Fine Sand
ARAP 20-GP1	330	1.43	-0.190	1.30	Poorly Sorted Medium Sand
ARAP 20-GP2	190	1.31	-0.885	2.15	Poorly Sorted Fine Sand
ARAP 20-GP2	300	1.28	-2.54	2.67	Poorly Sorted Fine Sand
ARAP 20-GP2	470	1.64	-1.35	2.03	Poorly Sorted Fine Sand
ARAP 20-GP3	390	1.87	-1.52	2.17	Poorly Sorted Fine Sand
HAV 20-GP1	294	0.353	-2.00	2.74	Well Sorted Fine Sand

HAV 20-GP2	110	0.838	-0.174	0.86	Moderately Sorted Coarse Sand
HAV 20-GP2	384	0.843	-2.61	2.55	Moderately Sorted Fine Sand
HAV 20-GP2	415	0.999	-1.92	2.36	Moderately Sorted Fine Sand
HAV20-GP2	540	0.907	-2.48	2.46	Moderately Sorted Fine Sand
HAV 20-GP3	276	0.373	-0.904	2.97	Well Sorted Fine Sand
HAV 20-GP3	455	0.361	-0.548	2.90	Well Sorted Fine Sand
ORNL23-GP1	100	0.466	-0.520	2.75	Well Sorted Fine Sand
ORNL23-GP1	222	0.414	-2.25	2.48	Well Sorted Fine Sand
ORNL23-GP1	294	0.418	-1.23	2.79	Well Sorted Fine Sand
ORNL23-GP2	100	0.437	0.317	2.72	Well Sorted Fine Sand
ORNL23-GP2	182	0.702	-4.26	2.84	Moderately Well Sorted Fine Sand
ORNL23-GP2	304	0.350	0.334	2.37	Very Well Sorted Fine Sand
ORNL23-GP2	456	0.455	-0.350	2.17	Well Sorted Fine Sand
ORNL23-GP2	548	0.799	0.400	1.15	Moderately Sorted Medium Sand
ORNL23-GP3	80	0.416	0.379	2.67	Well Sorted Fine Sand
ORNL23-GP3	324	0.569	-1.52	2.79	Moderately Well Sorted Fine Sand
ORNL23-GP3	391	0.743	-2.86	2.70	Moderately Sorted Fine Sand
ORNL23-GP3	476	0.973	-1.95	2.84	Moderately Sorted Fine Sand
ORNL23-GP3	533	1.14	-2.09	2.61	Poorly Sorted Fine Sand
ARAP23-GP1	60	0.434	-0.453	2.41	Well Sorted Fine Sand
ARAP23-GP1	202	0.443	0.003	2.42	Well Sorted Fine Sand
ARAP23- GP1	284	0.431	-0.453	2.31	Well Sorted Fine Sand
ARAP23- GP1	334	0.438	-0.29	2.31	Well Sorted Fine Sand

ARAP23-GP1	446	0.450	-0.748	2.34	Well Sorted Fine Sand
HAV23-GP1	100	0.665	-0.940	2.48	Moderately Well Sorted Fine Sand
HAV23- GP1	222	0.514	-2.04	2.53	Moderately Well Sorted Fine Sand
HAV23-GP1	304	0.478	-2.73	2.66	Well Sorted Fine Sand
HAV23- GP1	446	0.605	-1.61	2.58	Moderately Well Sorted Fine Sand
HAV23-GP1	528	0.481	-0.381	3.12	Well Sorted Very Fine Sand
HAV23- GP1	588	0.867	-1.09	1.89	Moderately Sorted Medium Sand
HAV23- GP2	90	0.782	-0.213	1.83	Moderately Sorted Medium Sand
HAV23-GP2	167	0.699	0.008	2.07	Moderately Well Sorted Fine Sand
HAV23-GP2	207	0.601	-0.423	1.86	Moderately Well Sorted Medium Sand
HAV23-GP2	297	0.373	0.627	2.55	Well Sorted Fine Sand
HAV23-GP2	344	0.601	-2.74	2.55	Moderately Well Sorted Fine Sand
HAV23-GP2	461	0.480	0.419	2.70	Well Sorted Fine Sand

APPENDIX C: CORE LOGS

Key of Symbols


Burrowed Contact


Plant Fragments

Sharp Contact


Shell Pieces


Laminations


Burrows


Root traces

Sample Use

Foram Analysis

Grain Size Analysis

OSL Analysis

Pollen Analysis

Lithofacies Codes

S-org	Fine-grained sand with plant fragments
mS-b-lam	Moderately well sorted, fine-grained sand with mud, burrows, and laminations
S-b	Moderately to well sorted, fine-grained sand with burrows
mS-b	Well to poorly sorted, fine-grained sand with mud and burrows
S	Well to very well sorted, fine-grained sand
mS-lam	Moderately well sorted, fine grained sand with mud and laminations
mS-b-lam-org	Fine-grained sand with mud, burrows, plant fragments, and laminations
mS-org	Fine-grained sand with mud, plant fragments and shell fragments common
mS	Well sorted, fine-grained sand with mud
sM	Mud with moderately to poorly sorted fine-grained sand
sM-b-lam	Mud with poorly sorted fine-grained sand, burrows, and laminations
sM-lam	Mud with moderately sorted, fine to medium-grained sand, and laminations
M	Mud with well sorted very fine-grained sand
sM-b	Mud with poorly sorted medium-grained sand and burrows
sM-rt	Mud with well sorted fine-grained sand, plant fragments common
msG-org	Gravel with poorly sorted coarse sand, broken shells, plant fragments, and mud
mG	Gravel with mud

Arap20-GP1

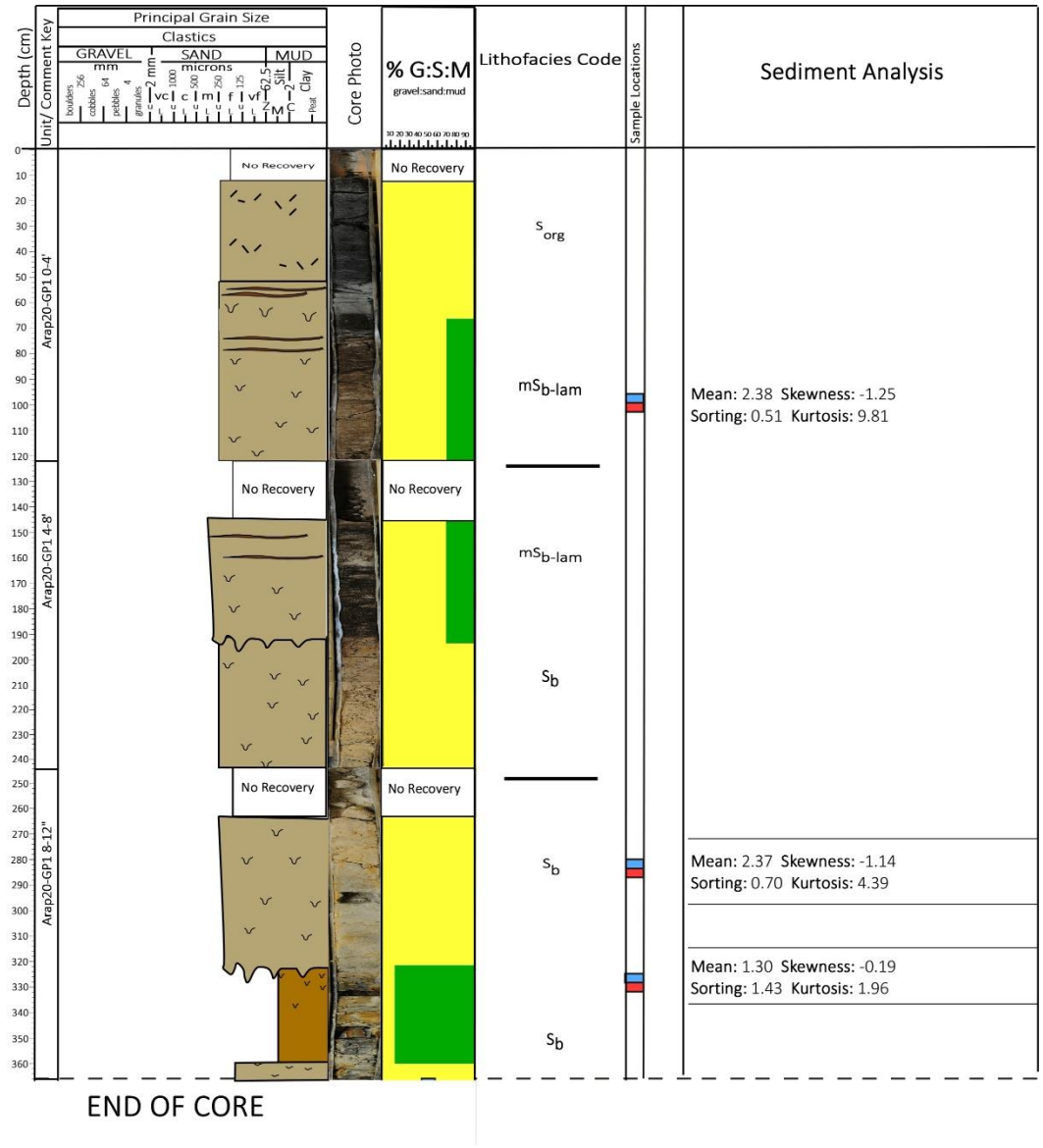
Depth (cm)
Unit/ Comment Key
Principal Grain Size
Clastics
GRAVEL
SAND
MUD
mm
microns
Core Photo
% G:S:M
gravel:sand:mud
Lithofacies Code
Sample Locations
Sediment Analysis
Arap20-GP1 0-4'
Arap20-GP1 4-8'
Arap20-GP1 8-12"
No Recovery
S_{org}
$mS_{b\text{-}lam}$
S_b
Mean: 2.38 Skewness: -1.25
Sorting: 0.51 Kurtosis: 9.81
Mean: 2.37 Skewness: -1.14
Sorting: 0.70 Kurtosis: 4.39
Mean: 1.30 Skewness: -0.19
Sorting: 1.43 Kurtosis: 1.96
END OF CORE

Arap20-GP2

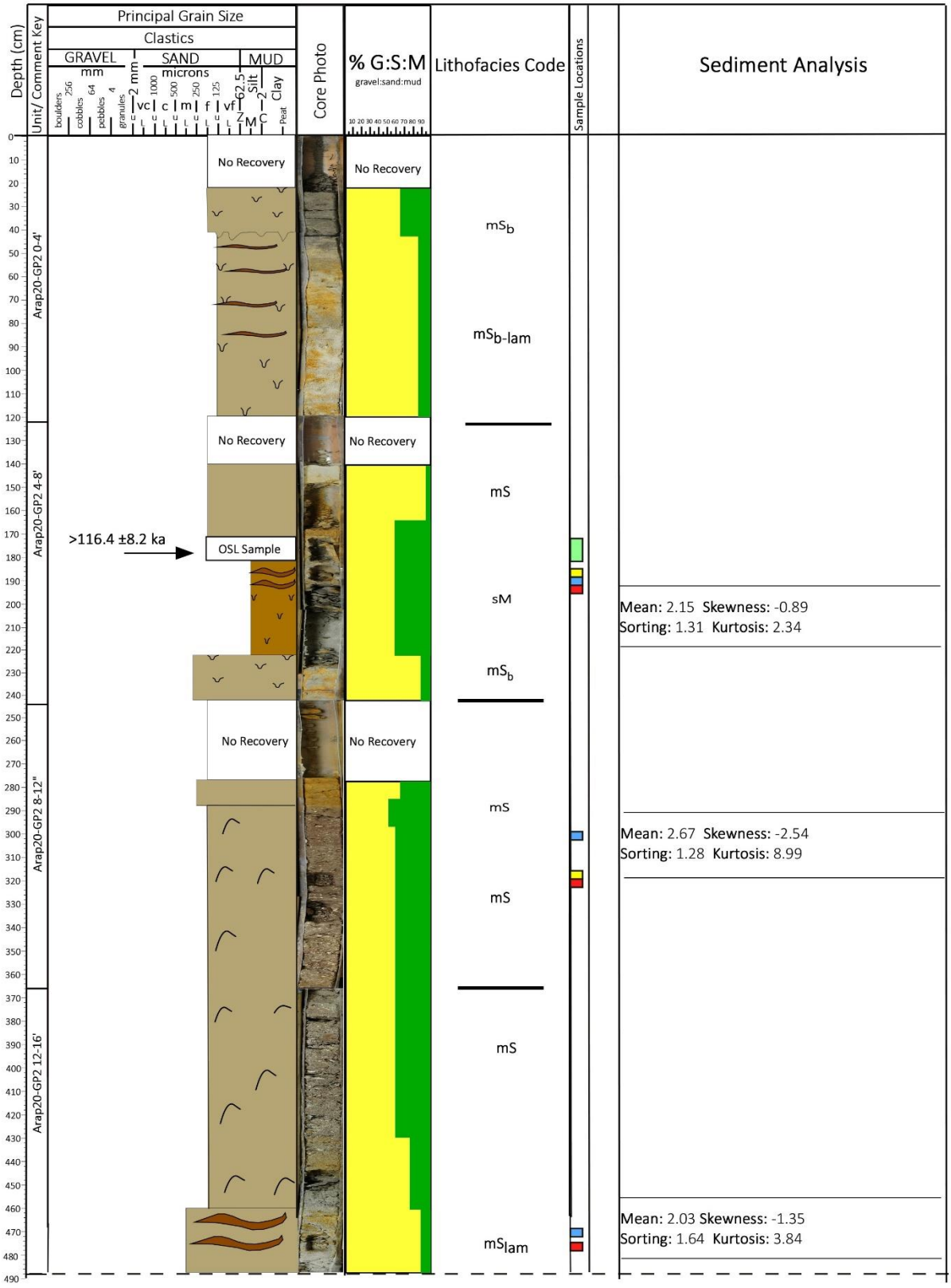

END OF CORE

Arap20-GP3

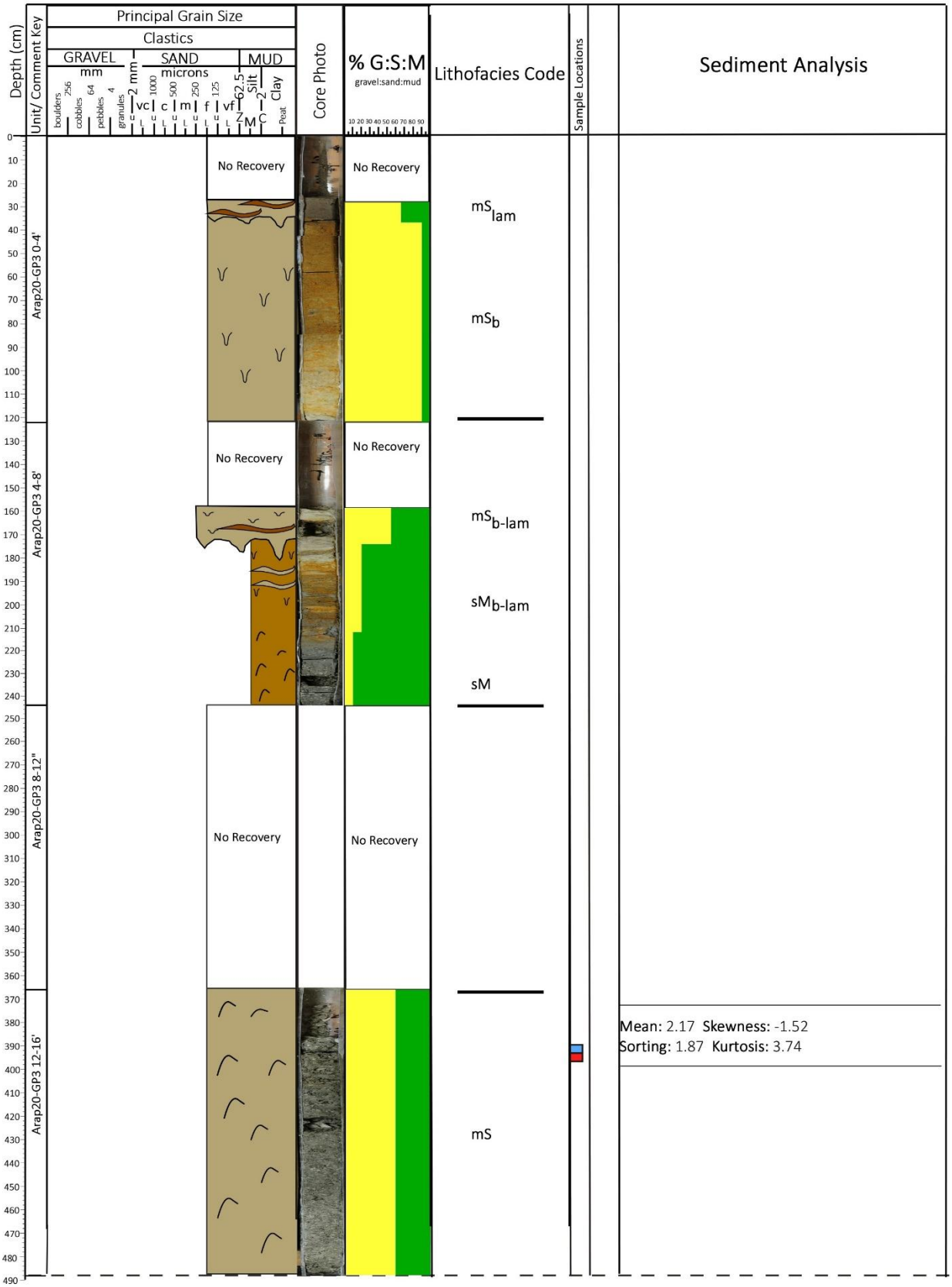

END OF CORE

ORNL20-GP1

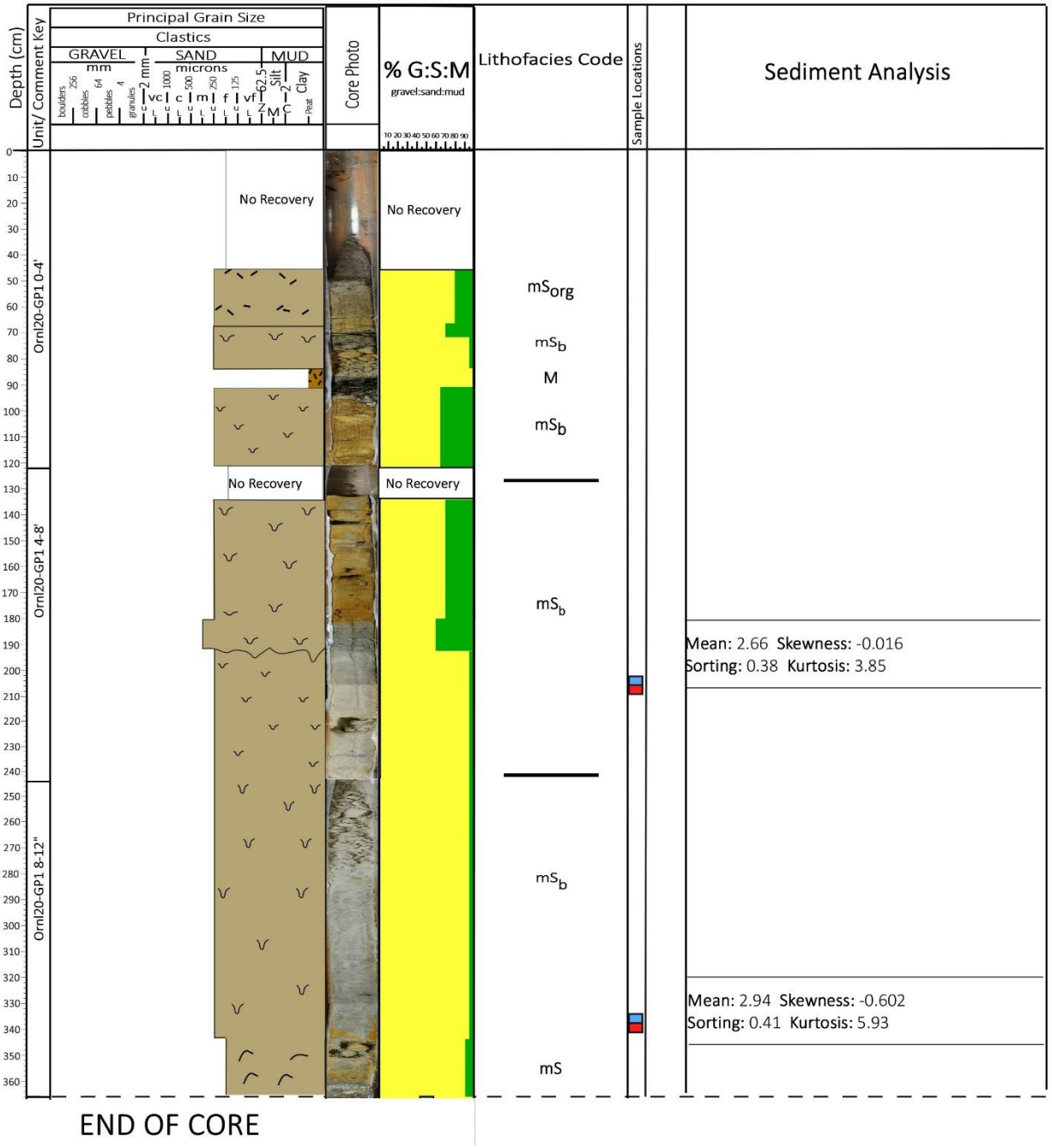
Depth (cm)
Unit/ Comment Key
Principal Grain Size
Clastics
GRAVEL
mm
SAND
microns
MUD
Silt
Clay
Core Photo
% G:S:M
gravel:sand:mud
Lithofacies Code
Sample Locations
Sediment Analysis
Ornl20-GP1 0-4"
Ornl20-GP1 4-8"
Ornl20-GP1 8-12"
No Recovery
No Recovery
No Recovery
mSorg
mSb
M
mSb
mSb
mSb
mS
Mean: 2.66 Skewness: -0.016
Sorting: 0.38 Kurtosis: 3.85
Mean: 2.94 Skewness: -0.602
Sorting: 0.41 Kurtosis: 5.93
END OF CORE

Ornl20-GP2

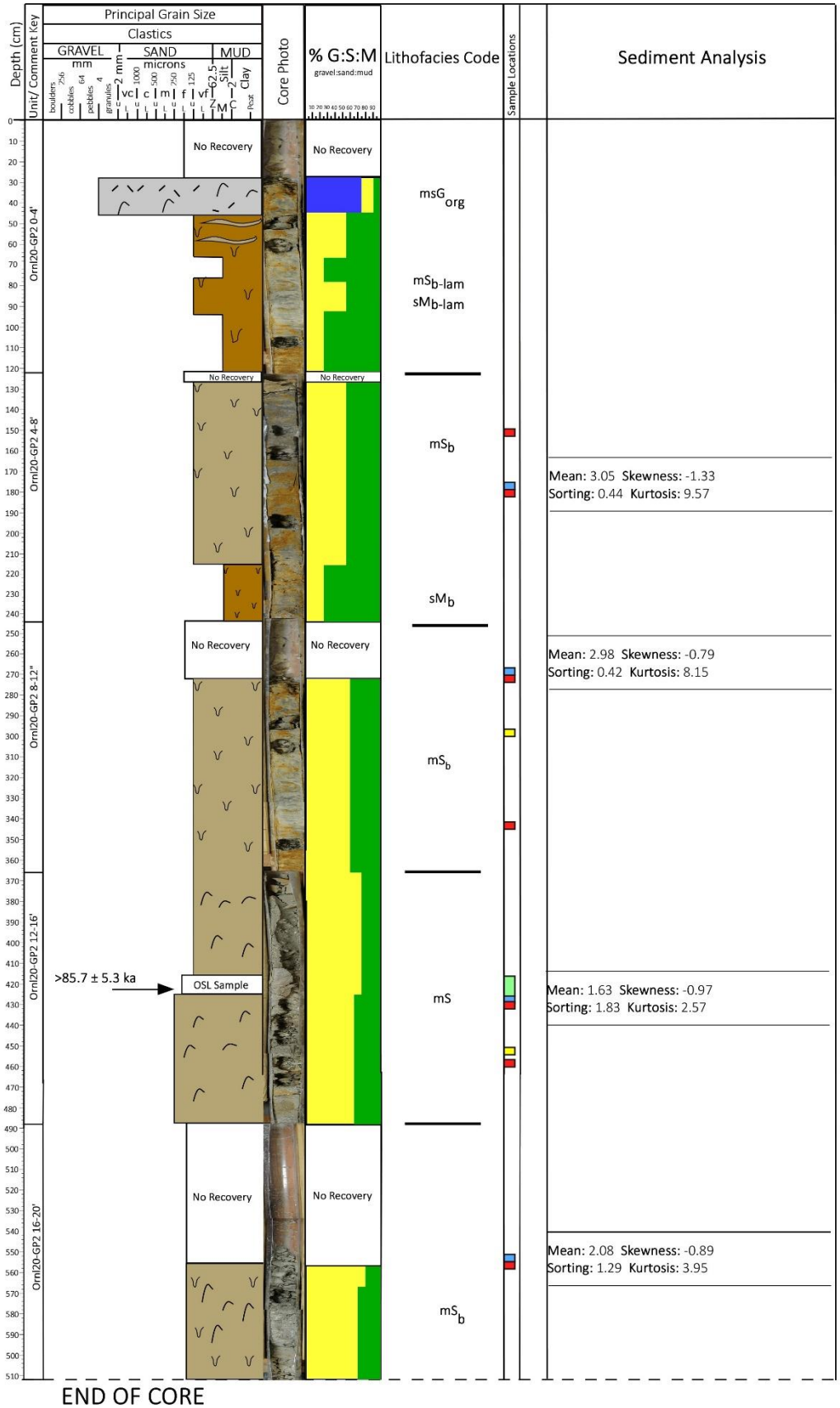
Depth (cm)
Unit/ Comment Key
Principal Grain Size
Clastics
GRAVEL
mm
SAND
microns
MUD
Silt
Clay
Core Photo
% G:S:M
gravel:sand:mud
Lithofacies Code
Sample Locations
Sediment Analysis
Ornl20-GP2 0-4'
Ornl20-GP2 4-8'
Ornl20-GP2 8-12'
Ornl20-GP2 12-16'
Ornl20-GP2 16-20'
No Recovery
msG org
mSb-lam
sMb-lam
mSb
sMb
mS
>85.7 ± 5.3 ka
OSL Sample
Mean: 3.05 Skewness: -1.33
Sorting: 0.44 Kurtosis: 9.57
Mean: 2.98 Skewness: -0.79
Sorting: 0.42 Kurtosis: 8.15
Mean: 1.63 Skewness: -0.97
Sorting: 1.83 Kurtosis: 2.57
Mean: 2.08 Skewness: -0.89
Sorting: 1.29 Kurtosis: 3.95
END OF CORE

Ornl20-GP3

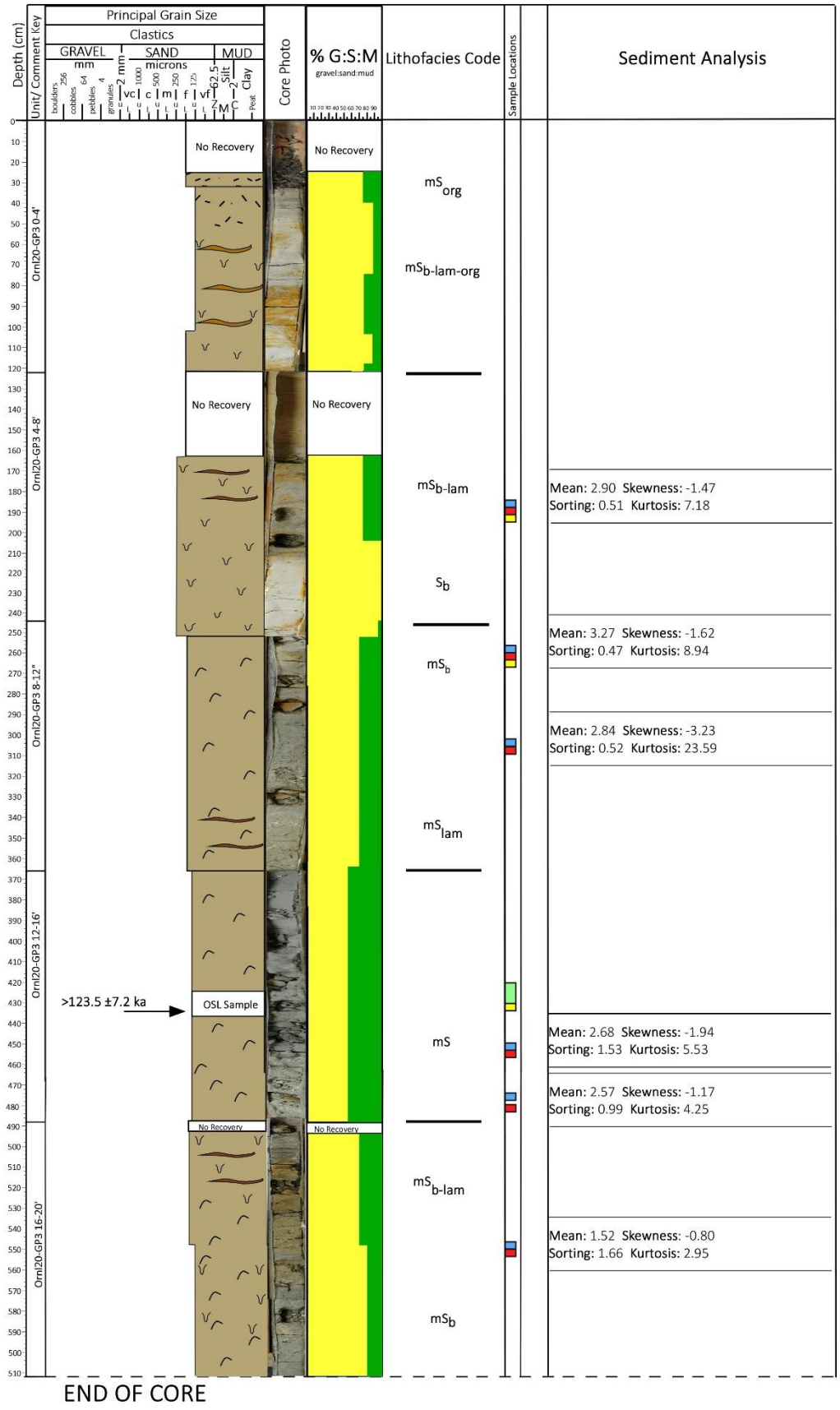
Depth (cm)
Unit/ Comment Key
Principal Grain Size
Clastics
GRAVEL
SAND
MUD
Core Photo
% G:S:M
gravel:sand:mud
Lithofacies Code
Sample Locations
Sediment Analysis
Ornl20-GP3 0-4'
Ornl20-GP3 4-8'
Ornl20-GP3 8-12"
Ornl20-GP3 12-16'
Ornl20-GP3 16-20'
No Recovery
mS org
mS b-lam-org
mS b-lam
S b
mS b
mS lam
mS
mS b-lam
mS b
>123.5 ±7.2 ka
OSL Sample
Mean: 2.90 Skewness: -1.47
Sorting: 0.51 Kurtosis: 7.18
Mean: 3.27 Skewness: -1.62
Sorting: 0.47 Kurtosis: 8.94
Mean: 2.84 Skewness: -3.23
Sorting: 0.52 Kurtosis: 23.59
Mean: 2.68 Skewness: -1.94
Sorting: 1.53 Kurtosis: 5.53
Mean: 2.57 Skewness: -1.17
Sorting: 0.99 Kurtosis: 4.25
Mean: 1.52 Skewness: -0.80
Sorting: 1.66 Kurtosis: 2.95
END OF CORE

Hav20-GP1

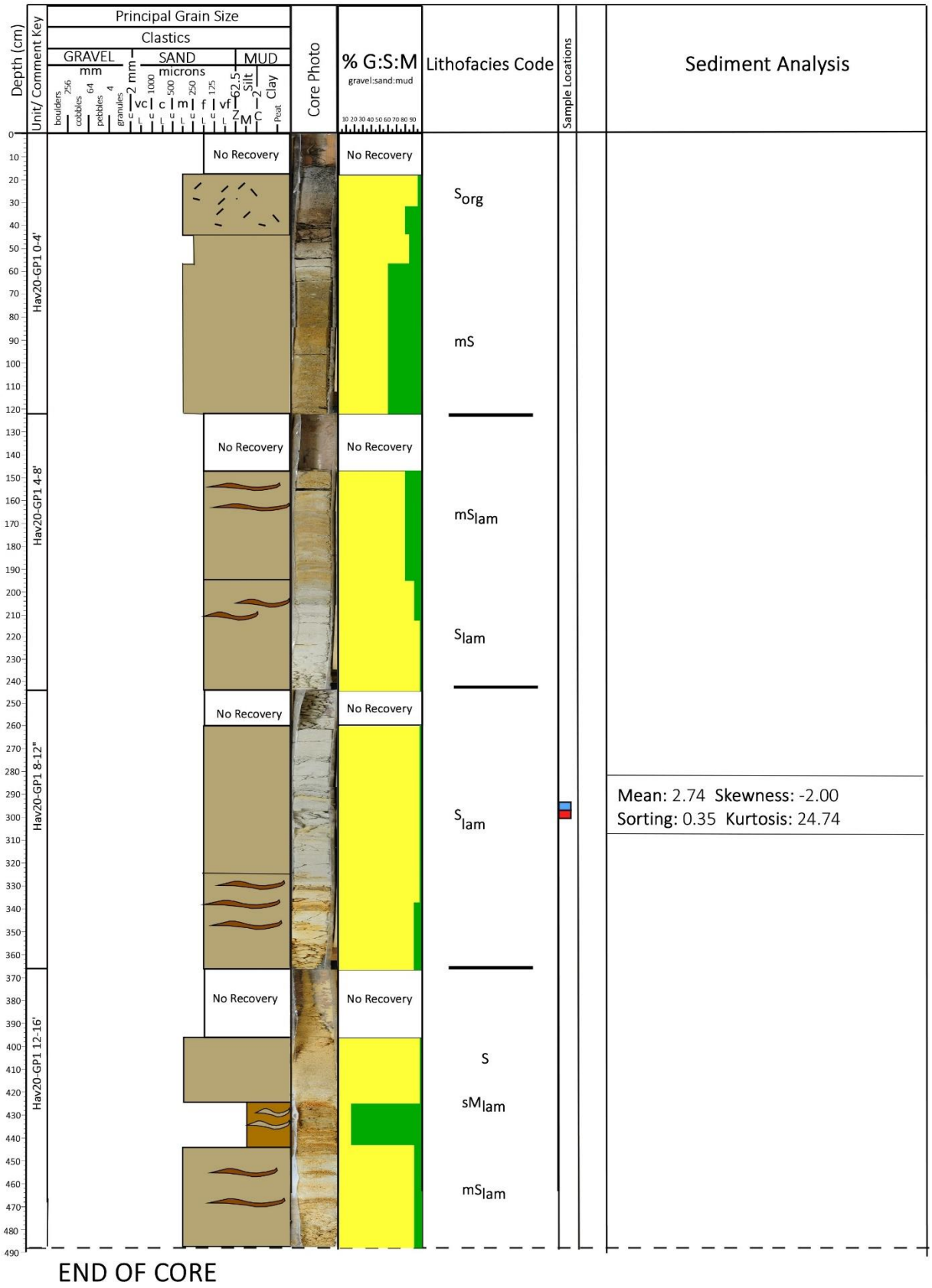
Depth (cm)
Unit/ Comment Key
Principal Grain Size
Clastics
GRAVEL
SAND
MUD
mm
microns
boulders
cobbles
pebbles
granules
vc
c
m
f
vf
Silt
Clay
Peat
Core Photo
% G:S:M
gravel:sand:mud
Lithofacies Code
Sample Locations
Sediment Analysis
Hav20-GP1 0-4'
Hav20-GP1 4-8'
Hav20-GP1 8-12"
Hav20-GP1 12-16'
No Recovery
Sorg
mS
mSlam
Slam
S
sMlam
Mean: 2.74 Skewness: -2.00
Sorting: 0.35 Kurtosis: 24.74
END OF CORE

Hav20-GP2

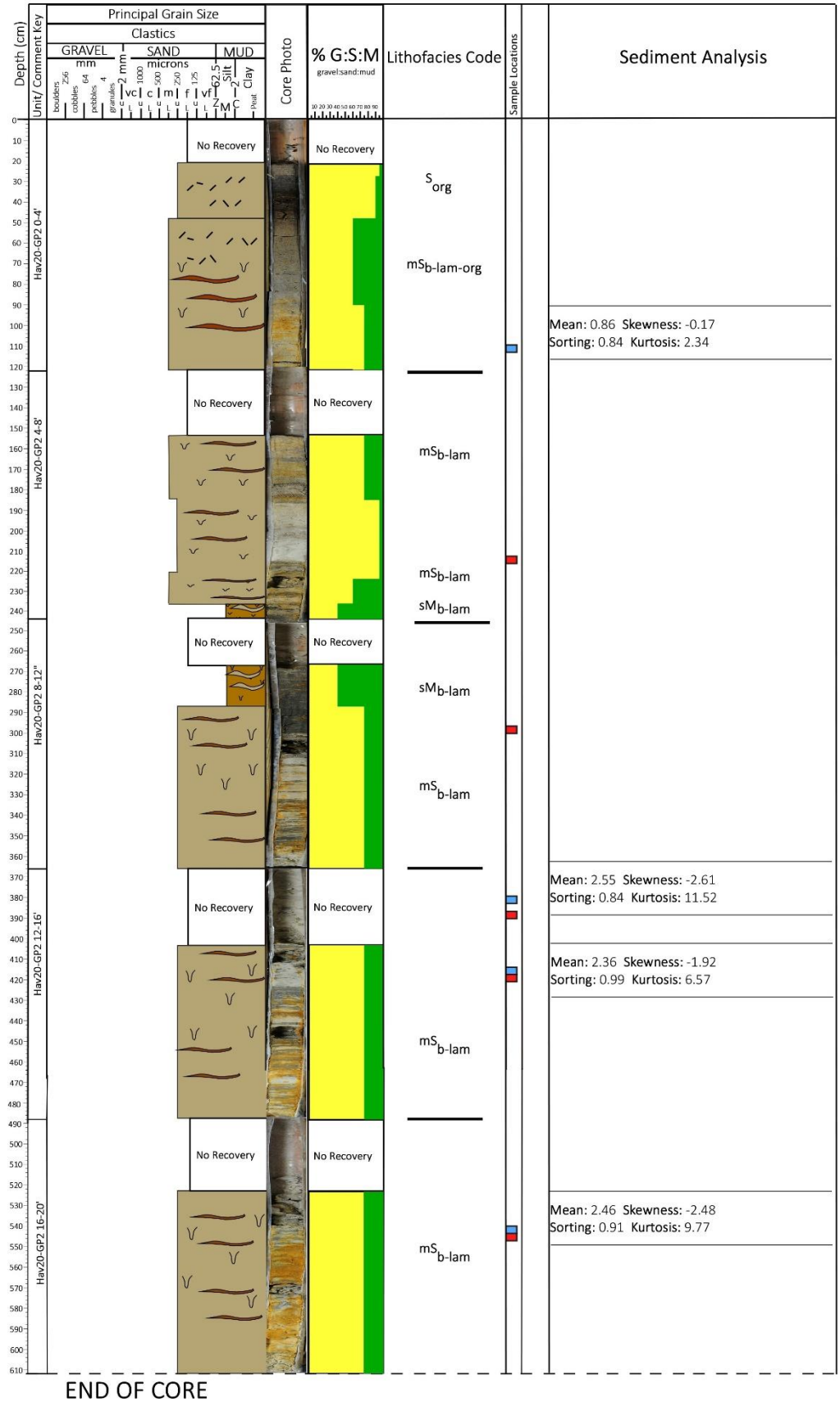
Depth (cm)
Unit/ Comment Key
Principal Grain Size
Clastics
GRAVEL
SAND
MUD
mm
microns
2 mm
Silt
Clay
boulders
cobbles
pebbles
granules
vc
c
m
f
vf
Z
M
C
Peat
Core Photo
% G:S:M
gravel:sand:mud
Lithofacies Code
Sample Locations
Sediment Analysis
Hav20-GP2 0-4'
Hav20-GP2 4-8'
Hav20-GP2 8-12"
Hav20-GP2 12-16'
Hav20-GP2 16-20'
No Recovery
S org
mS b-lam-org
mS b-lam
sM b-lam
Mean: 0.86 Skewness: -0.17
Sorting: 0.84 Kurtosis: 2.34
Mean: 2.55 Skewness: -2.61
Sorting: 0.84 Kurtosis: 11.52
Mean: 2.36 Skewness: -1.92
Sorting: 0.99 Kurtosis: 6.57
Mean: 2.46 Skewness: -2.48
Sorting: 0.91 Kurtosis: 9.77
END OF CORE

Hav20-GP3

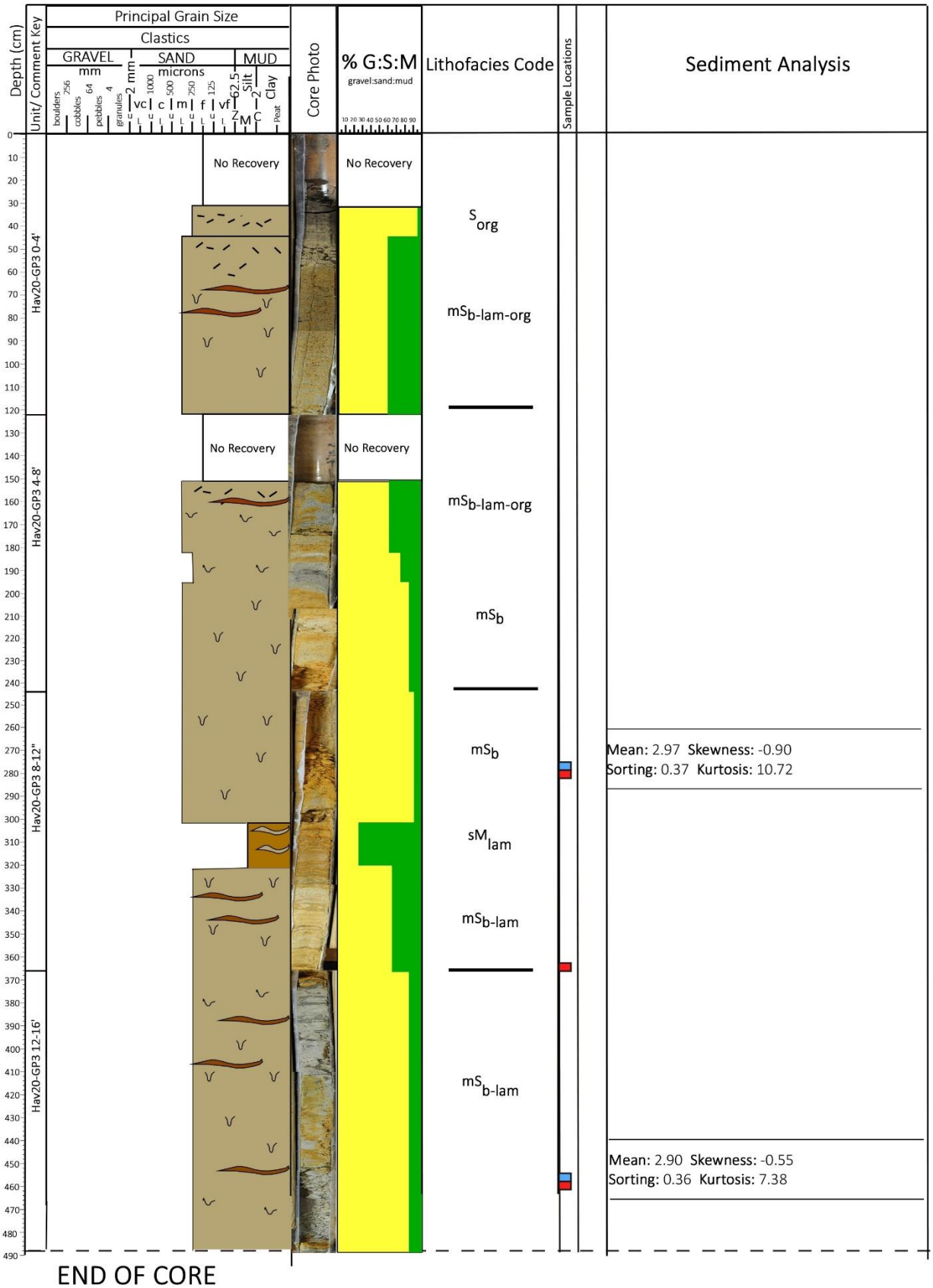
Depth (cm)
Unit/ Comment Key
Principal Grain Size
Clastics
GRAVEL
SAND
MUD
mm
microns
2 mm
boulders
cobbles
pebbles
granules
vc
c
m
f
vf
Silt
Clay
Peat
Core Photo
% G:S:M
gravel:sand:mud
Lithofacies Code
Sample Locations
Sediment Analysis
Hav20-GP3 0-4'
Hav20-GP3 4-8'
Hav20-GP3 8-12"
Hav20-GP3 12-16'
No Recovery
No Recovery
No Recovery
No Recovery
S org
mS b-lam-org
mS b-lam-org
mS b
mS b
sM lam
mS b-lam
mS b-lam
Mean: 2.97 Skewness: -0.90
Sorting: 0.37 Kurtosis: 10.72
Mean: 2.90 Skewness: -0.55
Sorting: 0.36 Kurtosis: 7.38
END OF CORE

Arap23-GP1

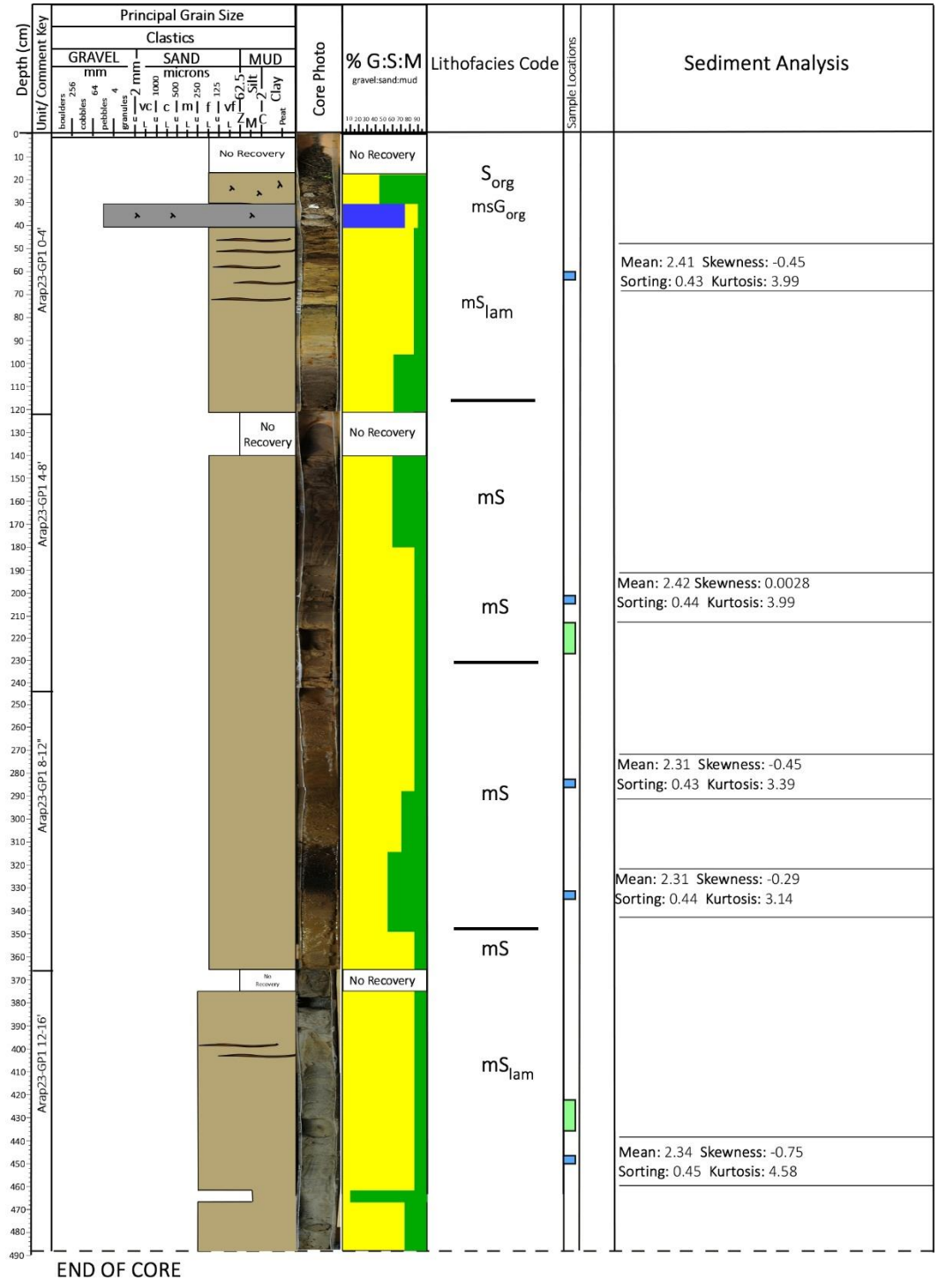
Depth (cm)
Unit/ Comment Key
Principal Grain Size
Clastics
GRAVEL
SAND
MUD
mm
microns
boulders
cobbles
pebbles
granules
vc
c
m
f
vf
Silt
Clay
Peat
Core Photo
% G:S:M
gravel:sand:mud
Lithofacies Code
Sample Locations
Sediment Analysis
Arap23-GP1 0-4'
Arap23-GP1 4-8'
Arap23-GP1 8-12"
Arap23-GP1 12-16'
No Recovery
No Recovery
No Recovery
No Recovery
No Recovery
S_org
msG_org
mS_lam
mS
mS
mS
mS_lam
Mean: 2.41 Skewness: -0.45
Sorting: 0.43 Kurtosis: 3.99
Mean: 2.42 Skewness: 0.0028
Sorting: 0.44 Kurtosis: 3.99
Mean: 2.31 Skewness: -0.45
Sorting: 0.43 Kurtosis: 3.39
Mean: 2.31 Skewness: -0.29
Sorting: 0.44 Kurtosis: 3.14
Mean: 2.34 Skewness: -0.75
Sorting: 0.45 Kurtosis: 4.58
END OF CORE

Ornl23-GP1

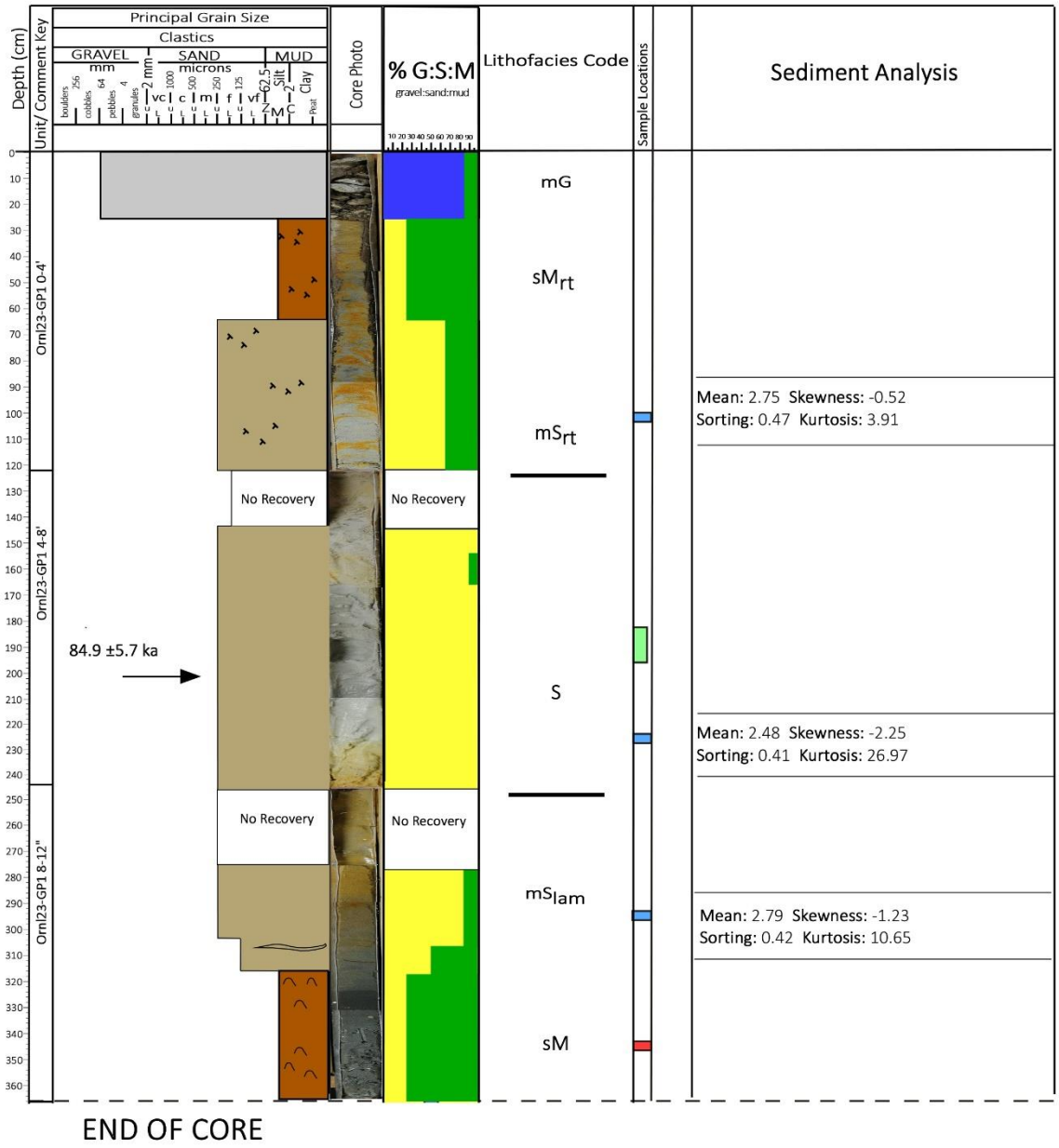
Depth (cm)
Unit/ Comment Key
Principal Grain Size
Clastics
GRAVEL
mm
SAND
microns
MUD
Core Photo
% G:S:M
gravel:sand:mud
Lithofacies Code
Sample Locations
Sediment Analysis
Ornl23-GP1 0-4'
Ornl23-GP1 4-8'
Ornl23-GP1 8-12"
No Recovery
No Recovery
No Recovery
No Recovery
84.9 ±5.7 ka
mG
sMrt
mSrt
S
mSlam
sM
Mean: 2.75 Skewness: -0.52
Sorting: 0.47 Kurtosis: 3.91
Mean: 2.48 Skewness: -2.25
Sorting: 0.41 Kurtosis: 26.97
Mean: 2.79 Skewness: -1.23
Sorting: 0.42 Kurtosis: 10.65
END OF CORE

Ornl23-GP2

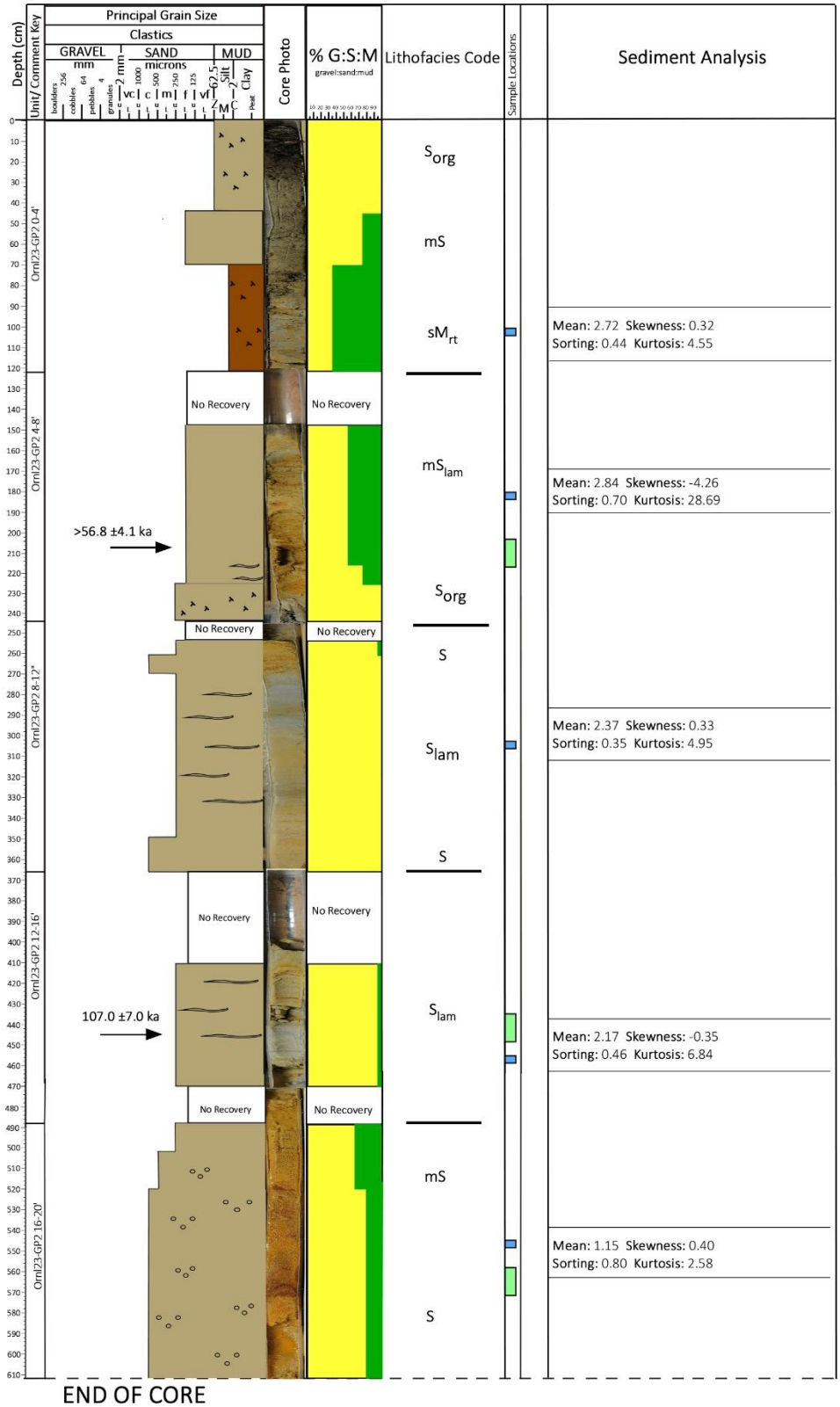
Depth (cm)
Unit/ Comment Key
Principal Grain Size
Clastics
GRAVEL
SAND
MUD
mm
microns
boulders
cobbles
pebbles
granules
vc
c
m
f
vf
Silt
Clay
Peat
Core Photo
% G:S:M
gravel:sand:mud
Lithofacies Code
Sample Locations
Sediment Analysis
Ornl23-GP2 0-4'
Ornl23-GP2 4-8'
Ornl23-GP2 8-12'
Ornl23-GP2 12-16'
Ornl23-GP2 16-20'
No Recovery
>56.8 ±4.1 ka
107.0 ±7.0 ka
Sorg
mS
sMrt
mSlam
Slam
S
Mean: 2.72 Skewness: 0.32
Sorting: 0.44 Kurtosis: 4.55
Mean: 2.84 Skewness: -4.26
Sorting: 0.70 Kurtosis: 28.69
Mean: 2.37 Skewness: 0.33
Sorting: 0.35 Kurtosis: 4.95
Mean: 2.17 Skewness: -0.35
Sorting: 0.46 Kurtosis: 6.84
Mean: 1.15 Skewness: 0.40
Sorting: 0.80 Kurtosis: 2.58
END OF CORE

Ornl23-GP3

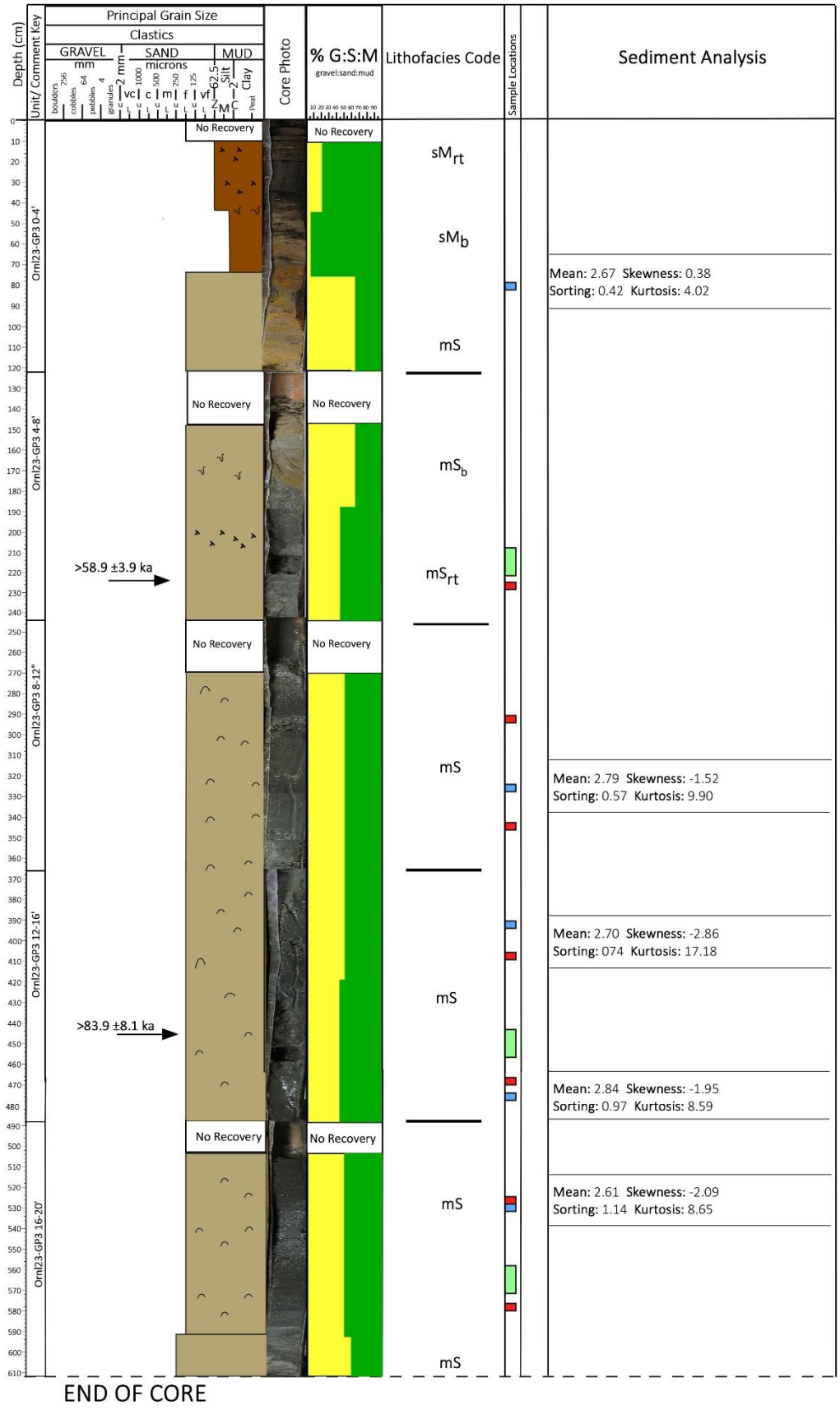
Depth (cm)
Unit/ Comment Key
Principal Grain Size
Clastics
GRAVEL
SAND
MUD
mm
microns
2 mm
Silt
Clay
Core Photo
% G:S:M
gravel:sand:mud
Lithofacies Code
Sample Locations
Sediment Analysis
Ornl23-GP3 0-4'
Ornl23-GP3 4-8'
Ornl23-GP3 8-12"
Ornl23-GP3 12-16'
Ornl23-GP3 16-20'
No Recovery
sMrt
sMb
mS
mSb
mSrt
>58.9 ±3.9 ka
>83.9 ±8.1 ka
Mean: 2.67 Skewness: 0.38
Sorting: 0.42 Kurtosis: 4.02
Mean: 2.79 Skewness: -1.52
Sorting: 0.57 Kurtosis: 9.90
Mean: 2.70 Skewness: -2.86
Sorting: 074 Kurtosis: 17.18
Mean: 2.84 Skewness: -1.95
Sorting: 0.97 Kurtosis: 8.59
Mean: 2.61 Skewness: -2.09
Sorting: 1.14 Kurtosis: 8.65
END OF CORE

Hav23-GP1

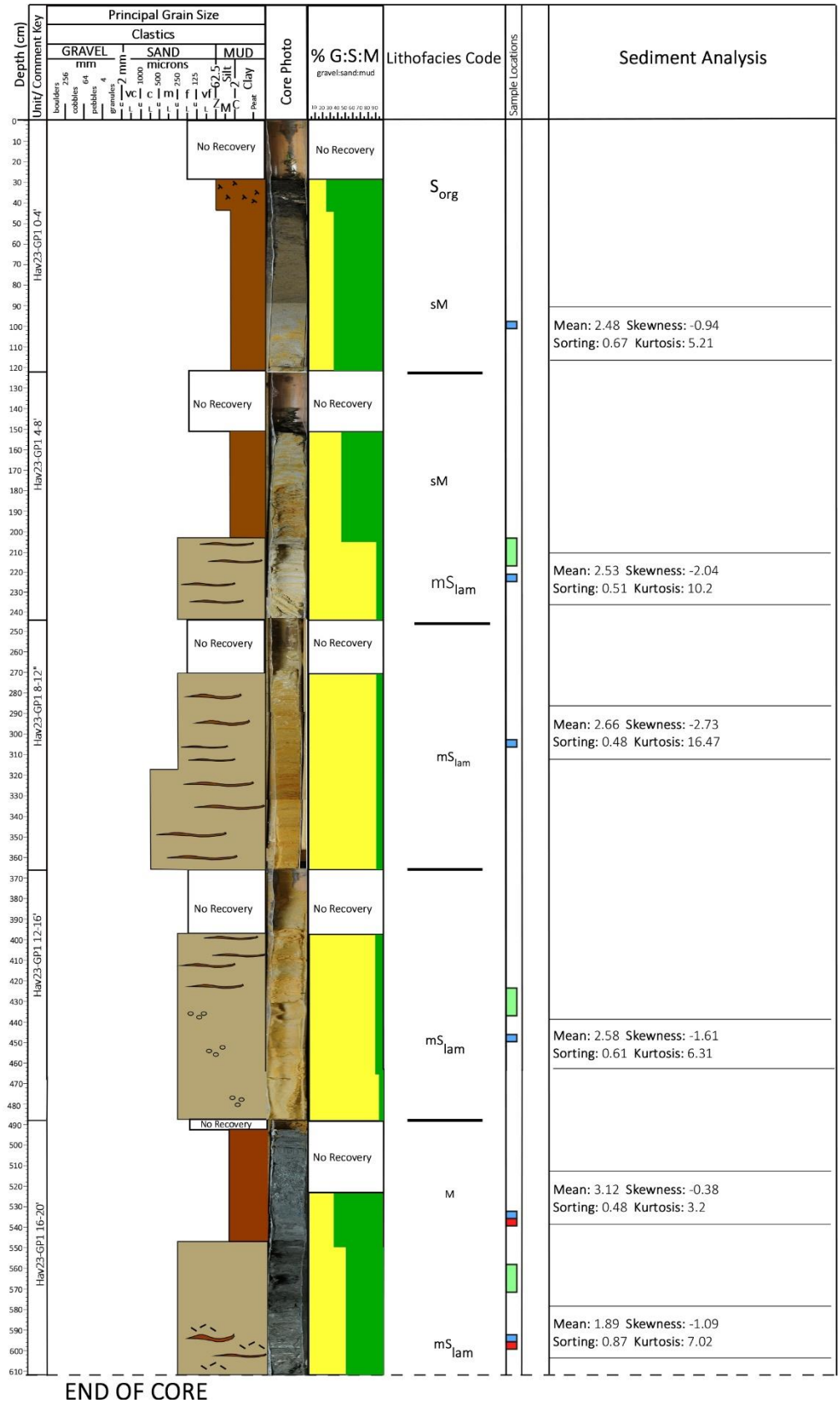

END OF CORE

Hav23-GP2

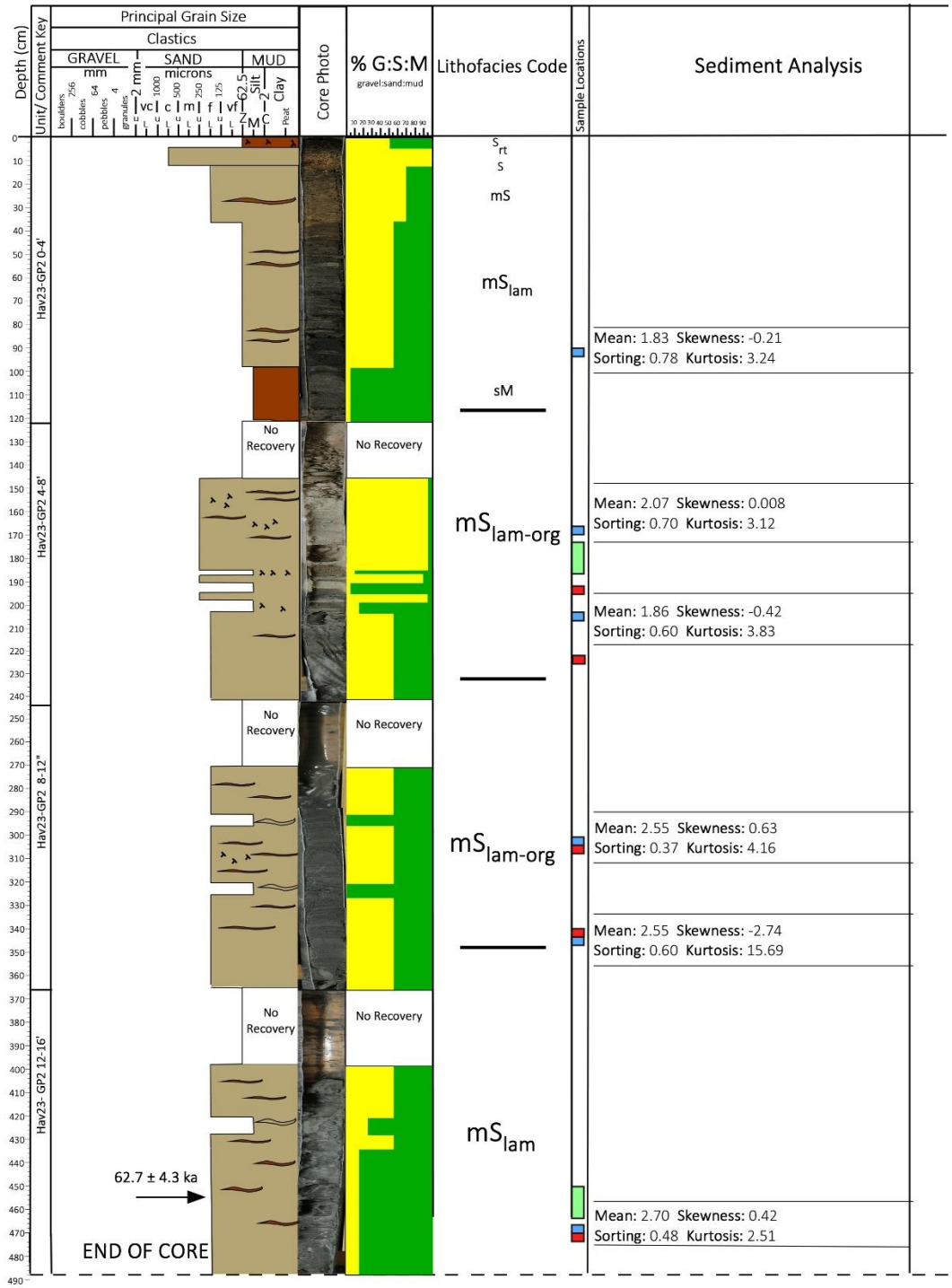
Depth (cm)
Unit/ Comment Key
Principal Grain Size
Clastics
GRAVEL
SAND
MUD
mm
microns
Silt
Clay
Peat
Core Photo
% G:S:M
gravel:sand:mud
Lithofacies Code
Sample Locations
Sediment Analysis
Hav23-GP2 0-4'
Hav23-GP2 4-8'
Hav23-GP2 8-12"
Hav23- GP2 12-16'
No Recovery
mS
mS lam
sM
mS lam-org
62.7 ± 4.3 ka
END OF CORE
Mean: 1.83 Skewness: -0.21
Sorting: 0.78 Kurtosis: 3.24
Mean: 2.07 Skewness: 0.008
Sorting: 0.70 Kurtosis: 3.12
Mean: 1.86 Skewness: -0.42
Sorting: 0.60 Kurtosis: 3.83
Mean: 2.55 Skewness: 0.63
Sorting: 0.37 Kurtosis: 4.16
Mean: 2.55 Skewness: -2.74
Sorting: 0.60 Kurtosis: 15.69
Mean: 2.70 Skewness: 0.42
Sorting: 0.48 Kurtosis: 2.51

APPENDIX D: FORAMINFERAL CENSUS DATA (RELATIVE PERCENT)

Sample	Depth	*Ammonia parkinsoniana*	*Ammonia tepida*	*Buccella inusitata*	*Buliminella elegantissima*	*Cassidulina* sp.	*Cibicides* sp.	*Elphidium excavatum*	*Elphidium gunteri*	*Elphidium mexicanum*	*Elphidium* sp.	*Elphidium translucens*	*Fursenkoinia fusiformis*	*Hanzawaia strattoni*	*Nonionella atlantica*	*Quinqueloculina jugosa*	*Quinqueloculina seminula*	*Rosalina* sp.	Total Foraminifera Picked
Arap20-GP2	320 cm	12 (11.7)	3 (2.9)	1 (0.97)	1 (0.97)	1 (0.97)		80 (77.7)		4 (3.9)			1 (0.97)						103
Arap20-GP2	478 cm	25 (27.2)						58 (63)	1 (1.1)	8 (8.7)									92
Arap20-GP3	393 cm	7 (7.1)	3 (3.03)			1 (1.01)		85 (85.9)		2 (2.02)					1 (1.01)				99
ORNL20-GP2	430 cm	20 (17.9)		2 (1.8)				74 (66.1)	1 (0.9)	7 (6.3)				2 (1.8)	3 (2.7)			3 (2.7)	112
ORNL20-GP2	460 cm	25 (27.2)						49 (53.3)	1 (1.1)	8 (8.7)				1 (1.1)	5 (5.4)		3 (3.3)		92
ORNL20-GP2	555 cm	20 (21.7)						72 (78.3)											92
ORNL20-GP3	264 cm	3 (25)						8 (66.7)		1 (8.3)									12
ORNL20-GP3	308 cm	31 (29.2)	3 (2.8)					55 (51.9)		17 (16)									106
ORNL20-GP3	456 cm	16 (18.8)		1 (1.2)				64 (75.3)		1 (1.2)				1 (1.2)	1 (1.2)			1 (1.2)	85
ORNL20-GP3	480 cm	10 (20.4)						38 (77.6)		1 (2.04)									49
ORNL20-GP3	550 cm	2 (1.9)						101 (98.1)											103
HAV23-GP1	598 cm	12 (13.04)						53 (57.6)	2 (2.2)	3 (3.3)				5 (5.4)		3 (3.3)	14 (15.2)		92
ORNL23-GP1	344 cm	23 (22.5)	1 (0.98)	1 (0.98)			1 (0.98)	63 (61.8)		11 (10.8)					1 (0.98)			1 (0.98)	102
ORNL23-GP3	294 cm	15 (15.2)	2 (2.02)	1 (1.01)				53 (53.5)		24 (24.2)	2 (2.02)	2 (2.02)							99
ORNL23-GP3	344 cm	21 (21.4)	1 (1.02)					53 (54.1)		22 (22.4)		1 (1.02)							98
ORNL23-GP3	406 cm	22 (23.4)	2 (2.1)					54 (57.4)		14 (14.9)					2 (2.1)				94
ORNL23-GP3	466 cm	6 (6.5)						87 (93.5)											93
ORNL23-GP3	523 cm	20 (17.5)						94 (82.5)											114
ORNL23-GP3	579 cm	1 (5.9)						16 (94.1)											17

APPENDIX E: POLLEN DATA

Sample	Summary of analogs (SCD≤0.15) from marine surface sample database	Est MAT from terrestrial surface samples in Whitmore dataset (˚C)	closest SCD from Whitmore dataset	Arboreal pollen (%)	Non-arboreal pollen (%)	Comments/interpretations: warmer = orange; similar to modern = green; cooler = blue	Age
ARAP20-GP2 190 cm	Ten closest analogs are from Chesapeake, but there are a number of Gulf Coast sites that also have SCD ≤ 0.15. All three of the ARAP samples have 40-50% pine, 24-35% oak. Lots of sweetgum and hickory - typical mid-Atlantic assemblage.	11.16134524	0.41386072	86.9	11.4	**Based on combination of marine analogs and estimates from Whitmore dataset, this is the warmest of the three samples from this core - possibly warmer than today, based on similarity to Gulf Coast assemblages.**	**MIS 5e**
ARAP20-GP2 314 cm	Closest analogs (≤0.15) are almost exclusively from Chesapeake, with only a couple GC sites.	10.73808333	0.38522412	88.6	9.6	**Similar to modern conditions - intermediate between other two samples from this core.**	**early MIS 5e**
ARAP20-GP2 466 cm	Closest analogs are almost exclusively from Chesapeake, MD sites - a couple from OBX surface samples.	8.997690476	0.44172185	87.1	10.3	**Modern to slightly cooler than modern temperatures, based on lack of close analogs from the Gulf Coast.**	**early MIS 5e/6**
ORNL20-GP2 294 cm	Closest analogs are primarily from the GC samples and WHOI sites in FL and the Carolinas; 56% pine, 30% oak.	11.6599881	0.40846141	92.1	5.7	**Modern to warmer than modern conditions, based on analogs from Florida and the Gulf Coast.**	**MIS 5a**
ORNL20-GP2 451 cm	Mix of sites from Chesapeake to Florida and the GC sites; 59% pine and 18% oak; 3.5% Tsuga (hemlock).	10.12377824	0.55183521	93.6	3.3	**Cooler than sample above based on existence of modern analogs as far north as Chesapeake and the presence of hemlock. Likely near modern conditions.**	**MIS 5a**
ORNL20-GP3 182 cm	Mix of sites from Chesapeake to Florida and the GC sites. 53% pine, 28% oak.	10.81971429	0.46917315	91.4	6.4	**Modern to slightly warmer than modern conditions.**	**MIS 5a**
ORNL20-GP3 264 cm	Primarily sites in Chesapeake region - extending as far north as NJ and some in OBX. A couple GC sites. 48% pine, 33% oak.	10.09004762	0.42959027	92.3	5.0	**Probably cooler than today but warmer than underlying sample.**	**MIS 5a**
ORNL20-GP3 426 cm	Some Chesapeake, many NC - FL and GC; strong dominance of pine (61%) and also 5% Tsuga (hemlock); analogs driven by pine and oak abundance. Nyssa (tupelo) and Cupressaceae (cypress) present (totaling 4% together).	10.97330952	0.57384492	95.3	1.9	**Modern hemlock distribution in the east is primarily limited to the Piedmont and Appalachians. The closest coastal occurrence of hemlock is in mid-New Jersey, so these likely represent cooler than modern conditions. May have forested wetlands nearby, based on occurence of cypress and tupelo pollen.**	**MIS 5e**

APPENDIX F: OPTICALLY STIMULATED LUMINESCENCE DATA

OSL age estimates for each sample.

Sample	Sample ID	Sample Depth (m)	Dose (Gy)	Dose Rate (Gy/ka)	Age (ka)	Interpreted MIS
OSL 1	HAV23-GP1	2.02 to 2.12	74.2 ± 4.6	1.086 ± 0.026	68.3 ± 4.5	4
OSL 2	HAV23-GP1	4.26 to 4.36	73.1 ± 4.9	1.030 ± 0.027	71.0 ± 5.1	4
OSL 3	HAV23-GP1	5.58 to 5.66	>95.1 ± 5.5	1.259 ± 0.034	>75.6 ± 4.8	5e
OSL 5	ORNL23-GP1	1.82 to 1.92	80.1 ± 4.9	0.944 ± 0.028	84.9 ± 5.7	5a
OSL 6	ORNL23-GP2	2.02 to 2.12	>101.1 ± 7.0	1.782 ± 0.042	> 56.8 ± 4.1	5a
OSL 7	ORNL23-GP2	4.36 to 4.46	43.6 ± 2.6	0.407 ± 0.012	107.0 ± 7.0	5d
OSL 8	ORNL23-GP3	2.09 to 2.19	>107.5 ± 6.6	1.827 ± 0.045	>58.9 ± 3.9	5e
OSL 9	ORNL23-GP3	4.46 to 4.56	>133 ± 12	1.581 ± 0.041	>83.9 ± 8.1	5e
OSL 13	ORNL-20-GP2	4.16 to 4.66	82.6 ± 4.2	0.963 ± 0.036	85.7 ± 5.3	5a
OSL 14	ARAP-20-GP2	1.72 to 1.82	227 ± 14	1.949 ± 0.074	116.4 ± 8.2	5e
OSL 15	ORNL-20-GP3	4.26 to 4.36	179.4 ± 9.8	1.282 ± 0.049	123.5 ± 7.2	5e

APPENDIX G: SEDIMENT STATISTICS

Sample	Weight% Gravel	Weight% Sand	Weight% Mud
ORNL23-GP3 16-20' 45 cm	0.95	29.71	9.99
ORNL23-GP2 4-8' 60 cm	0.47	30.61	17.74
ORNL23-GP3 0-4' 80 cm	0	19.91	17.64
ORNL23-GP2 0-4' 100 cm	0	13.1	14.09
ORNL23-GP2 8-12' 60 cm	0	53.13	15.51
HAV23-GP2 12-16' 95 cm	0	20.59	15.63
ORNL23-GP1 0-4' 100 cm	0	32.9	20.31
HAV23-GP2 8-12' 53 cm	0	31.16	17.27
HAV23-GP1 0-4' 100 cm	0	17.47	35.2
HAV23- GP2 0-4' 90 cm	0	14.9	19.76
ARAP23- GP1 8-12' 90 cm	0	46.35	9.32
HAV23-GP1 16-20' 40 cm	0	6.66	37.36